BEHAVIOR OF WEAKLY CEMENTED SOIL SLOPES UNDER STATIC AND SEISMIC LOADING CONDITIONS

Nicholas Sitar, G. Wayne Clough,
and Robert G. Bachus

John A. Blume Earthquake Engineering Center
Department of Civil Engineering
Stanford University

USGS CONTRACT NO. 14-08-0001-16836
Supported by the EARTHQUAKE HAZARDS REDUCTION PROGRAM

OPEN-FILE NO. 81-52

U.S. Geological Survey
OPEN FILE REPORT

BEHAVIOR OF WEAKLY CEMENTED SOIL SLOPES UNDER STATIC AND SEISMIC LOADING CONDITIONS

By

Nicholas Sitar, G. Wayne Clough, and Robert C. Bachus

Prepared For

United States Geological Survey
Department of the Interior

FINAL REPORT

Contract No. USGS-14-08-0001-16836

June, 1980

PREFACE

This report describes research carried out under the sponsorship of the United States Geological Survey, Contract No. USGS 16836, covering the period March, 1978 to October, 1979. It is directed towards the question of response to seismic loading of slopes formed in weakly cemented sands and silts, and the behavior of these materials under static and dynamic loading.

Numerous individuals assisted in the work. Drs. T. L. Youd and G. F. Wieczorek and Mr. E. L. Harp of the United States Geological Survey provided valuable advice and insights relative to their extensive experiences in the area of slope behavior under seismic loading. Professors H. Shah and H. Krawinkler of Stanford gave assistance with the structural dynamics aspects of the problem. Mr. J. Crosby of Jo Crosby Associates provided data on cemented sands from his files. Finally, and not least, Mr. Abdulaziz Alfi and Nader Shafii-Rad performed a number of key tests. To all these colleagues the authors express their appreciation.

ABSTRACT

Large surface and near surface deposits of weakly cemented soils occur in various geologic environments. These materials are typically composed of sand or silt size particles and can have unconfined compressive strengths from slightly greater than zero up to 690 kN/m^2. After failure in an unconfined test, a weakly cemented soil exhibits brittle response and loses most, if not, all of its strength. In spite of their relatively low strength, however, vertical to near vertical slopes of heights in excess of 100 m are found in these materials. Examples may be found in the marine terrace sands along the Pacific Coast of California and Oregon, the windlaid ash deposits in central America, and the loess soils in the central United States and along the Yellow River in China.

Failure of a steep slope in cemented soil during a seismic event is usually spectacular because, if the strength of the soil is exceeded near the face of the slope, it collapses and cascades downward. Observations of such failures have been made in numerous cases, and loss of life and property is substantial where populated areas are involved. Interestingly, however, little is known about the cemented soils. This study represents an initial part of a comprehensive investigation of slope behavior in cemented soils, and it is directed toward: (1) documenting of the behavior of natural slopes in weakly cemented soils, (2) defining the engineering response of weakly cemented soils under static and dynamic loading, (3) establishing the stress conditions in steep slopes during static and dynamic loading, and (4) developing guidelines for evaluation of seismic stability of slopes in cemented soils.

To achieve these objectives, field observations of slope behavior in the weakly cemented soils have been conducted in Guatemala and in California, along the Pacific Coast, between San Francisco and Santa Cruz. A laboratory testing program of over 200 static and dynamic tests on artificially and naturally cemented sands was carried out, and static and dynamic finite element analyses of idealized vertical slopes in linear elastic material were performed.

The results of the field studies show that failure in a cemented soil slope initiates by tensile splitting in the upper part of the slope. The failure then progresses either by toppling of blocks in the upper part of the slope or by shear failure in the lower part of the slope. The likelihood of the tensile fracturing phenomenon is supported by the fact that the dynamic tensile strength of cemented soil decreases as a result of cyclic loading.

The finite element analyses indicate that the magnitude of the dynamic stresses in a slope is a function of both the size of the earthquake as well as the degree of matching between the natural period of the slope and the dominant period of the earthquake. The analyses are also used to develop nondimensionalized charts for evaluation of slope stability of vertical slopes in cemented soil.

TABLE OF CONTENTS

LIST OF FIGURES

LIST OF TABLES

CHAPTER I

Introduction

Weakly cemented soils can be identified either as rocks or as soils, depending on the observers' training and experience. In this report, weakly cemented soils are defined as naturally occurring, cemented, granular deposits with measurable unconfined compressive strength less than 690 kN/m^2. Typically, in unconfined compression or at low confining pressures the weakly cemented soils exhibit very brittle behavior. At failure the soil commonly disintegrates into individual grains and rapidly loses strength. A characteristic of deposits of cemented soil is their ability to stand in surprisingly high, vertical or almost vertical slopes. Near the slope faces the confining pressures are low and the brittle failure can lead to sudden, catastrophic landslides during seismic events.

The weakly cemented soils occur in various geologic environments. They include deposits of loess, volcanic ash, dune sands, and marine beach sands. Nearly vertical slopes in deposits of loess in China are up to 90 meters in height (Lutton, 1969). In Nebraska, natural slopes in loess deposits reach 16 meters at an angle of 76 degrees. In Mississippi, benches in roadcuts are normally 4.5 meters high at an angle of 80 degrees. Similarly, almost vertical natural slopes reach up to 100 meters in deposits of weakly cemented volcanic ash in Guatemala and it is standard practice to make vertical roadcuts as much as 30 meters high. In California and Oregon, vertical or nearly vertical slopes in coastal cliffs of weakly cemented sand reach up to 180 meters in height.

During the 1920 earthquake in China, large landslides developed

in deep deposits of loess. Entire villages were buried by the moving soil and topography was significantly altered (Close and McCormick, 1922). In the 1906 and 1957 San Francisco earthquakes landslides occurred in the weakly cemented sands along cliffs overlooking the Pacific Ocean. The coastal highway and railroad were destroyed in several places by these landslides in 1906 (Figure 1-1a). The highway was disrupted again in 1957 and subsequently abandoned. One of the landslides during an after-shock of the 1906 earthquake was described by R. Crandall (in Lawson and others, 1908);

> On April 25, the writer was on the edge of the cliffs near Wood's Gulch. About 3 p.m. of that day there was a shock with an intensity estimated to be between VI and VII. At that time the cliffs shook like so much gelatine, and it was necessary to hold on to prevent falling. On the north side of the canyon, hundred of tons of earth fell even with the slightest shock.

In 1976, an earthquake in Guatemala caused thousands of landslides in the deposits of weakly cemented volcanic ash. Although a number of people died directly in the landslides, the major impact of the landsliding was on lifelines--roads and railroads. Every major highway and railroad line was disrupted, delaying deliveries of needed medical supplies which contributed to a large death toll. Two typical landslides are shown in Figure 1-2.

The loss of life and economic impact of the landsliding in weakly cemented soils caused by seismic events has been enormous. In California and Guatemala, increasing economic and population pressures result in continuing development above and below the steep slopes in the cemented soils (Figure 1-1b). Yet until now surprisingly little research has been directed at important engineering questions related to their past or future performance. For example, little is known either about how to

Figure 1-1a FAILURE OF CEMENTED SOIL SLOPES IN THE 1906 SAN FRANCISCO EARTHQUAKE [AFTER YOUD AND HOOSE (1978)]

Figure 1-1b CEMENTED SOIL SLOPES IN DALY CITY SHOWING URBAN DEVELOPMENT.

Figure 1-2 SLOPE FAILURES IN CEMENTED SOIL SLOPES IN GUATEMALA TRIGGERED BY 1976 EARTHQUAKE (TYPICAL OF HUNDREDS WHICH OCCURRED).

properly sample the weakly cemented soils or about their stress-strain characteristics. Conventional geotechnical sampling techniques often result in destruction of the cementation. As a consequence, sufficient quantities of high quality samples for laboratory testing are difficult to obtain and good information about the stress-strain behavior is rare.

In addition, not much is known about how to evaluate the stability of slopes in the weakly cemented soils under static and dynamic loading. Field observations of the types of failures in the loess soils (Lutton, 1969) and in the volcanic ash indicate that tensile splitting is an important mechanism involved in the slope failures. Therefore, application of conventional slip circle type of stability analysis is inadequate and some other approach to slope stability analyses in the weakly cemented soils is needed.

The research now in progress at Stanford University is aimed at improving the state-of-the-art of knowledge concerning the behavior and design of slopes in cemented soils. Specifically, the long range objectives are: (1) formulating a model for the behavior of cemented soils under static and dynamic loading; (2) developing proper methods of sampling and testing of cemented soils so as to minimize disturbance effects; and, (3) developing a procedure for the analysis of cemented soil slopes subjected to dynamic loading.

Because of the large scope of needed work the research program was divided into several phases. The first phase of the research is described in this report. It comprises about one and a half years of work in the following areas:

1) Documentation and preliminary analyses of the behavior of natural slopes in the weakly cemented soils in

Guatemala and California;

2) Preliminary static laboratory testing of weakly cemented sands from deposits around the San Francisco Bay Area;

3) Static and dynamic laboratory testing of artificially cemented sands; and

4) Static and dynamic finite element analyses of idealized slopes in the weakly cemented soils.

The work performed for this report concentrated mainly on the weakly cemented sands which are abundant in California, and the San Francisco Bay Area. They present a natural choice for the initial studies because of convenience in access and the fact that historical evidence of behavior during seismic events is available.

CHAPTER II

Weakly Cemented Sands--Background and Field Observations

2.1 Introduction

Sand deposits form in many geologic environments. In California, Quarternary marine terrace deposits and Tertiary marine and dune deposits of weakly cemented sand are found along most of the Pacific Coast, on the San Francisco Penninsula, and in the Los Angeles Basin. The presence of cementation in these sands manifests itself in their ability to stand in very steep slopes. The steep slopes and the overall appearance of the sands give the impression that they are cemented into hard rocks. It is often surprising to find out that one can dig by hand into the sands which form vertical cliffs of 50 meters or higher. Small fragments of the weakly cemented sand can commonly be crushed in the palm of a hand.

Since the usual angle of repose for uncemented sands is about 30 degrees, it is apparent that the presence of small amounts of cementation has a significant effect on the slope formation and stability of the sands. Yet, the cementation is barely mentioned in literature (Lawson and others, 1908; Bonilla, 1959; Cleveland, 1975; Sullivan, 1975) and its effect on the engineering properties of the sands is largely unknown.

In this chapter background information on cementation and structure of cemented soils and observations of natural slope characteristics in the weakly cemented sands are presented.

2.2 Cementing Agents and Cementation

The effect of cementing agents in sedimentary deposits is to bind individual grains together. The presence of the cementing agents in detrital sedimentary rocks is well recognized in geologic literature,

although the descriptions of the types and characteristics of individual cement types are usually brief and qualitative. Any mention of cementation, and especially weak cementation, in soil mechanics literature is rare.

According to Krynine and Judd (1957) the most common cements found in sedimentary rocks are: silica or sileceous cement; calcium carbonate or calcareous cement; clay or argillaceous cement; and iron-bearing minerals or ferruginous cement. The cement may be either present in the soil at the time of deposition, precipitate from percolating groundwater, or may be formed by weathering of minerals present in the soil mass. The degree of binding action depends on factors such as the amount and type of cementing agent, water content, groundwater movement, and weathering.

Silica cement is the strongest and also the most resistant to weathering and water action. Clay cement is strong and brittle when dry but can change into a weak, ductile material when wetted. Carbonate cement is resistant to moisture content fluctuations but may be leached and weakened by acidic groundwater.

Two other processes, mechanical interlocking of grains, and capillary tension, can produce effects similar to that of cementing agents. Mechanical interlocking occurs in soils composed of angular particles such as wind laid volcanic ash or dune sand. Capillary tension serves to increase the effective stresses in the soil. It is most prominent in partially dried, fine silty soils.

2.3 Structure of Cemented Soils

Cemented soils can be divided on the basis of their structure into void bound and contact bound (Figure 2-1; Sowers and Sowers, 1970). In the contact bound structure the individual particles are cemented at the

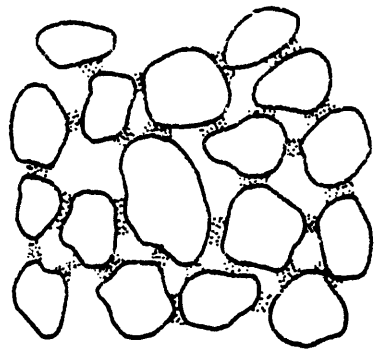

CONTACT-BOUND

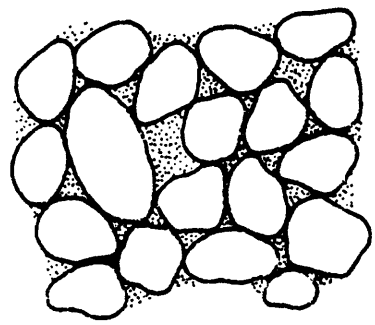

VOID-BOUND

Figure 2-1 TYPES OF CEMENTED SOIL STRUCTURES (AFTER SOWERS AND SOWERS, 1970).

points of contact and the voids are open. The void bound structure has the voids filled by smaller particles and the cementing agents.

Void bound structure is more stable than the contact bound structure and it is characteristic of soils containing high percentage of silt and clay size particles. Contact bound structure is found in soils with predominantly sand size or greater than sand size particles. Open work gravel is an extreme example of this type of soil. The contact bound structure can lose strength suddenly if the bonds between the particles are broken. The sudden loss of strength is a result of rearrangement of individual particles as they move into a dense configuration. The weakly cemented sands described in this report exhibit predominantly the contact bound structure.

2.4.1 Slopes in Volcanic Ash Soils in Guatemala

Two of the authors,Clough and Sitar, first observed the behavior of slopes in weakly cemented soils during separate visits to Guatemala, in February and September of 1976 respectively. The purpose of these visits was to study slope failures which occurred during a magnitude 7.5 earthquake in February of 1976. These studies were later followed by an investigation of slope behavior in weakly cemented sands in California. The slopes in both the volcanic ash and the sand, are characteristically very steep and the modes of failure are quite similar.

The volcanic ash soils in Guatemala are Pleistocene in age and are composed of layers of volcanic glass fragments. The grain size ranges from coarse gravel to very fine silt from bed to bed, but within the individual beds it appears to be quite uniform. The thickness of the beds varies from a few centimeters to several meters. Distinct paleosoil horizons representing periods of weathering often separate the ash beds.

The paleosoils are characterized by reddish brown color and contain varying amounts of adobe clay. Surprisingly, the underlying ash beds do not show effects of weathering. The volcanic glass particles are angular with sharp edges and free of surficial coating or alteration. Thus, the apparent cementation seems to be cause by a mechanical interlocking of the individual particles.

The strength of this apparent cementation is very low. The soil can be easily excavated by hand even at the base of the highest observed roadcuts. Block sampling of the soil by hand appears to be the only way of obtaining undisturbed samples and even then it is difficult to keep the samples from breaking up.

The slopes in the volcanic ash soils can be divided into two groups depending on whether or not they are covered by vegetation. The vegetated slopes reach heights of several hundred meters and are often steeper than 45 degrees. The nonvegetated slopes occur in areas of active stream erosion and stand at angles between 70 degrees and vertical. Their height can reach over 100 meters. Roadcuts, which can also be included in this category, are routinely cut at 80 degrees or steeper, and reach up to 30 meters in height.

One of the most common types of slope failure in the volcanic ash during the 1976 earthquake was shallow sliding on the vegetated slopes. The sliding usually occurred along planes approximately sub-parallel to the slope surfaces and involved the upper 2 to 3 meters of soil. The general appearance of these slides was similar to sliding that can be observed in piles of cohesionless sand. It seems that the bonds between the particles in the landslide masses were destroyed early during the shaking, and the soil in the slide mass then behaved basically

as a cohesionless material.

Along the nonvegetated slopes, the failures appear to have occurred by toppling of narrow, 2 to 3 meters thick, blocks of soil. Sets of tension cracks running parallel to the crest line of the slope were commonly observed. The mechanism of this type of failure is explained in detail later. Interestingly, the toppling type failures observed in roadcuts south of Guatemala City were always associated with faults running through the strata. Although no offset as a result of the most recent earthquake was observable in these faults, their presence may have provided planes of weakness aiding the slope failures. Toppling failures which occurred on steep slopes along streams within Guatemala City were not investigated in sufficient detail to determine the factors controlling the occurrence of the sliding. However, Harp (Harp and others, 1978) suggests that they were caused by variations in lithology.

In retrospect, it seems remarkable that given the very weak nature of the soil, the toppling failures in the very steep and vertical slopes were relatively localized and not more pervasive.

2.4.2 Slopes in Weakly Cemented Sand in California

Field trips to outcrops along the beaches between Santa Cruz and San Francisco, and the site of Stanford Linear Accelerator (SLAC) were conducted in order to gather information about the properties of the weakly cemented sands and to define the most common types of slope failures in them.

Slopes in the weakly cemented sands along the Pacific beaches are often vertical or nearly vertical and reach 30 to 50 meters in height. In the area between Lake Merced and Mussel Rock on the San Francisco Penninsula, the slopes in the weakly cemented sands of the Merced

Formation are over 150 meters high at angles locally exceeding 40 degrees. Cuts made in the weakly cemented sands during construction at SLAC stood at slopes steeper than 60 degrees and were up to 15 meters high. In the Los Angeles Basin, deep excavations in weakly cemented sands reached depths in excess of 30 meters with very little movement (Maljian and Van Beveren, 1974).

The grain size of the sands in the San Francisco Bay area changes from locality to locality and ranges from fine silty sand to coarse grained sand. However, individual beds are quite uniform in grain size. For example, the weakly cemented sand from a site in Pacifica has a uniformity coefficient of 1.7 (Figure 2-2). The sand grains are composed mainly of quartz and feldspar. Cementing agents are clays, carbonates, and minor gypsum and iron oxides. Weathering usually penetrates to a depth of 10 meters from the surface and weathered sand can be identified by its tan to light brown color. Unweathered sand is gray. No appreciable difference in the strength characteristics of the sand due to weathering was found during a geotechnical exploration program at SLAC (Dames & Moore, 1972).

With the exception of three large deep seated landslide complexes with special characteristics, recently occurring slope failures in the weakly cemented sands immediately south of San Francisco appear to be primarily shallow, involving only the outer 2 to 3 meters of material. This seems also to be the case for seismic loading conditions based on photographs obtained after the 1906 and 1957 earthquakes (see Fig. 1-1a). The vertical or nearly vertical slopes generally fail by separation of a narrow block of soil along the essentially vertical tension crack at the top of the slope and subsequent shearing of material at the base of

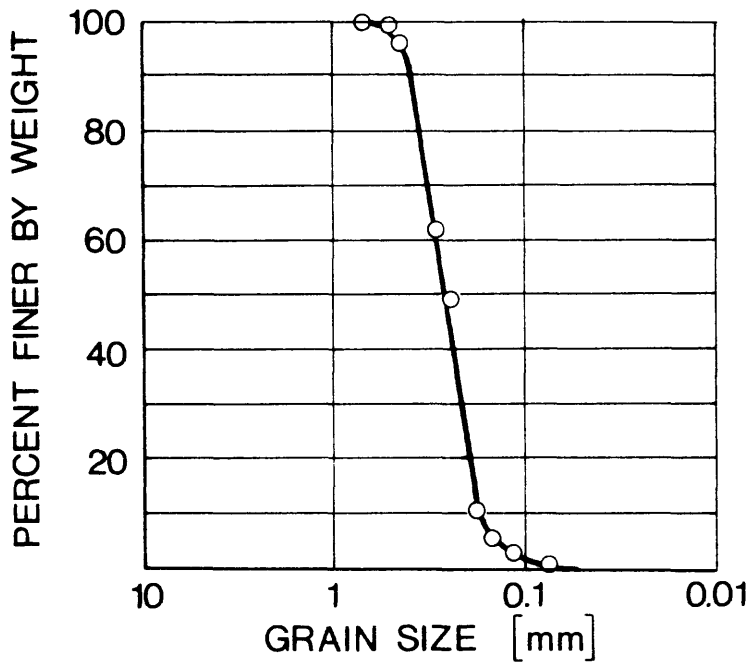

Figure 2-2 GRAIN SIZE DISTRIBUTION CURVE FOR WEAKLY CEMENTED SAND FROM PACIFICA.

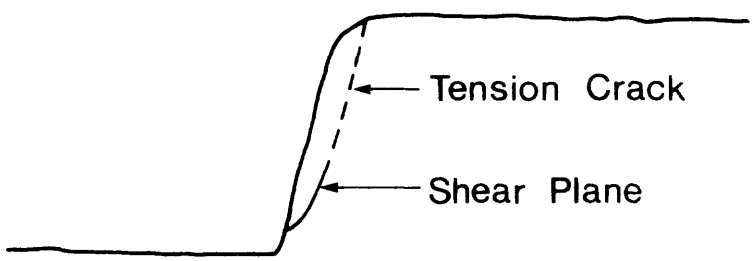

Figure 2-3 SCHEMATIC DIAGRAM OF A TOPPLING FAILURE

the block (Figure 2-3). Lutton (1969) reports the same mechanism of failure in slopes of Loess and Hutchinson (1971) has documented this type of slope failure for the bluffs in deposits of chalk in England.

Presence of the zones of tension in the upper part of very steep slopes can be demonstrated using numerical solutions (Figure 2-4). The conditions leading to failure under static loading are likely caused by erosion of toe support which increases the tensile stress in the slope to the point of failure. Similarly earthquake loading can lead to increased tensile stresses and possible failure. After the 1906 earthquake, extensive toppling type failures were reported in the cliffs of weakly cemented sand from Cape Mendocino to Point San Pedro, and in the Santa Cruz Mountains (Lawson and others, 1908). Interestingly, no failures of this type were reported after the 1957 earthquake.

On more gentle slopes in cemented sand the mode of failure is shallow sliding of disintegrated soil. The slip planes are subparallel to the slope surfaces and the soil fails in shear. The chief cause of these slope failures appears to be toe erosion under static loading and inertia forces under earthquake loading. Numerous landslides of this type also occurred during the 1906 and 1957 earthquakes in the sands of the Merced Formation between Lake Merced and Mussel Rock.

Two of the deep seated landslides observed along the Pacific Coast are in the Merced Formation. One of these is located directly astride the San Andreas Fault, and the other is in a zone identified as a potential fault in Wood's Gulch north of the San Andreas Fault. The cementation seems to be destroyed in these areas probably due to shearing along the faults. Thus the deep seated landsliding north of the San Andreas appears to occur in loose essentially uncemented material and

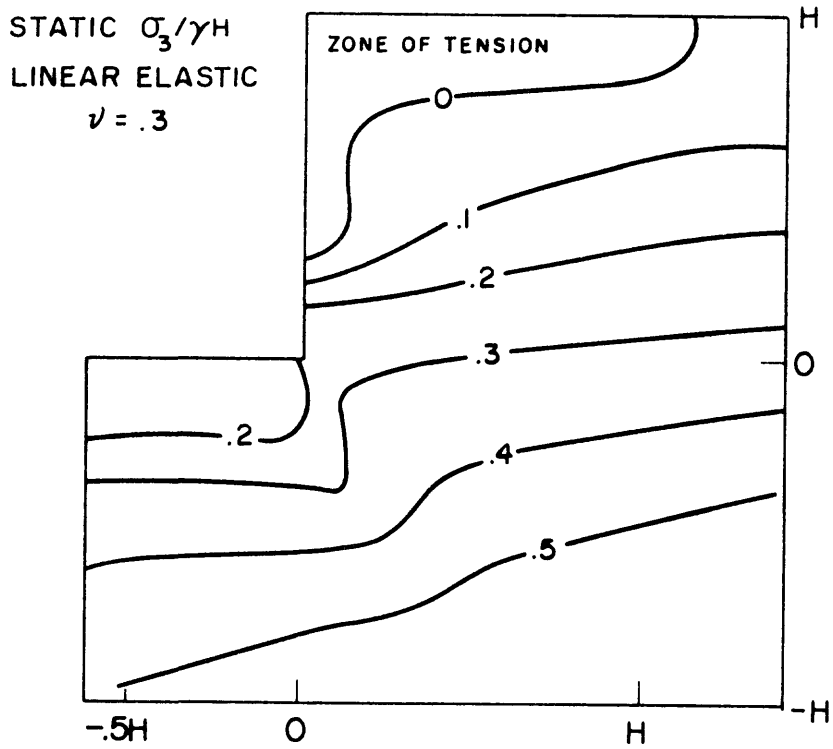

Figure 2-4 DISTRIBUTION OF MINOR PRINCIPAL STRESS IN A VERTICAL SLOPE IN A LINEAR ELASTIC MEDIUM

presents an entirely different situation than that of a weakly cemented sand.

A conspicuous difference in the intensity of landsliding between the coastal bluffs to the north and the coastal bluffs to the south of Mussel Rock was noted during both the 1906 and the 1957 earthquakes. The landsliding to the north of Mussel Rock and especially in the sands of the Merced Formation was extensive. To the south of Mussel Rock very few landslides were noted after the 1906 earthquake (Lawson and others, 1908) and none after the 1957 earthquake. Lawson concluded that the difference in response of the bluffs was due to lithologic differences between the geologic units north and south of the San Andreas Fault. However, the lithology on both sides of the fault appears to be quite similar. The Late Tertiary marine sands of the Merced Formation to the north of Mussel Rock and the Pleistocene marine terrace deposits south of Mussel Rock are of similar geologic origin, the grain sizes appear to be in the same range, and the cementing agents, clays and carbonates, are the same. However, significant differences exist in the geometry of the slopes, the bedding orientations, and in the position of the bluffs with respect to the fault. The bluffs in the Merced Formation are about 180 meters high at their highest point and the bedding has an apparent dip of 70 to 80 degrees at the slope face. The slopes are generally inclined at angles of 40 to 45 degrees to the horizontal. In contrast, the marine terrace deposits to the south of Mussel Rock are essentially horizontally bedded and overlain in many areas by fresh water clay layers. The height of the bluffs is about 50 meters, and the bluff faces slope at angles between 70 degrees and vertical. In the Merced Formation north of the fault, failures can occur entirely within one weaker bed, whereas

in the marine terrace deposits south of the fault the failures have to cut through strata of different strengths. The one deep-seated failure which was observed south of the fault cut across an upper recent clay layer and through a lower mass of cemented sand. The upper clay was apparently deposited in a fresh water pond or lake which once existed at the site. The slope failure was structurally controlled by a stiff shale layer which dips towards the Pacific Ocean at about 20-30° and underlies the cemented sand. Conditions in this area appear to be an exception to the general stratigraphy along the coast.

There is also a significant difference in the distance from the San Andreas Fault to the coast bluffs north and south of the San Andreas Fault. Along the section of the coast from Mussel Rock to Cape Mendocino the fault is essentially parallel to the shore and the distance varies between 0 and 5 km. To the south of the Mussel Rock the distance between the fault and the shore increases rapidly and reaches more than 10 km near Half Moon Bay. Thus, the increased attenuation of the earthquake motions coupled with a different slope height, slope geometry, and bedding orientation may have been the reason for a lower incidence of landslides reported along the coast south of Mussel Rock.

2.5 Summary

Cemented sands are characterized by their ability to stand in very steep natural slopes. They usually exhibit a contact bound structure and the most common cementing agents are silica, clays, carbonates, and iron oxides.

Two types of slope failures caused by earthquake shaking were found characteristic of cemented sands: (1) toppling failures caused by initial tensile failure at the top of very steep or vertical slopes;

and (2) shallow shear failures along planes essentially subparallel to the slope surfaces on more gentle slopes (less than about 45 degrees). These types of failure are quite similar to those observed in the volcanic ash soils in Guatemala.

CHAPTER III

Weakly Cemented Sands--Strength and Stress-Strain Behavior

3.1 Introduction

Prior to initiation of this study, in 1977, the data on the stress-strain and strength characteristics of cemented soils published in the geotechnical literature were almost entirely the product of research into the properties of cement treated soils (Mitchell, 1976). Only recently, first information on the behavior of naturally occurring weakly cemented sands has been published by Salomone and others (1978) and Saxena and Lastrico (1978). The reasons for this apparent lack of interest in the properties of weakly cemented soils are not clear. However, it seems that the relatively undisturbed samples for laboratory testing are difficult to obtain in these soils, and that conventional geotechnical design would usually tend to be conservative and neglect the presence of cementation.

For this investigation a two-pronged approach was undertaken towards experimenting with cemented soils. The properties of naturally occurring cemented sands in the Bay Area were to be determined by testing undisturbed block samples. However, because of the difficulty in obtaining these samples, and the likelihood that natural variability in cementation would obscure data trends, it was decided to also fabricate artificially cemented samples in a controlled manner which would model the natural soils. Both the natural and artificially cemented sands would be tested under static and dynamic loadings. At the time of this writing, the testing of the artificially cemented sands is much more advanced than that for the naturally cemented sands. The preliminary results for the naturally cemented sands are presented first however, to establish a base

for the behavior of cemented soils. The results for the artificially cemented sands are presented in Chapter V.

3.2 Field Site Description

The field studies for this project were to involve sampling, evaluating natural slope processes, and performing in-situ tests using the self-boring pressuremeter. With this in mind, a survey was made of possible sites in the Bay Area where all the objectives could be achieved, and three were selected for intensive study. Two of the sites are on the coast of Pacific Ocean, one about one-half mile south of the San Andreas Fault, in Pacifica, and one about one-half mile north of the San Andreas Fault, near Daly City. These two sites are especially interesting in that steep bluffs of cemented soils are present in both areas. Historically, those north of the fault have collapsed spectacularly during both the 1907 and 1957 earthquakes, while those south of the fault have been relatively stable. The third site is located on the Stanford campus at the Linear Accelerator (SLAC). In this case, deposits of cemented soils are being exposed by excavations for an extension of the accelerator. This site is especially convenient for equipment trials and as a nearby source of fresh block samples.

Two distinctly different cemented soils are found at SLAC; both were sampled and tested in the laboratory. One has an average unconfined compressive strength of about 2600 kN/m^2 (377 psi) which is significantly greater than the 690 kN/m^2 (100 psi) upper limit used to define weakly cemented soils in this study. The second soil sampled at SLAC is very much weaker than the first. Its surface can be easily scraped by a light pressure and it has an unconfined compressive strength of about 50 kN/m^2 (7 psi). Both the weak and strong soils at the SLAC

site stand in vertical cuts of up to 15 m (50 ft).

Three different types of material were found in the bluffs of the field study site near Pacifica. The base of the bluffs is formed by a weak sandstone which is overlain by a deposit of weakly cemented clean sand reaching up to 30 m (100 ft) in thickness. Capping this sequence is a 5 to 10 m (15-33 ft) thick sand stratum with about 20% clay and silt sized particles. This upper layer is stronger than the weakly cemented sand below it.

The soils at the second site on the Pacific Coast north of the San Andreas fault appear to be more uniform than those south of the fault. However, no sampling has been done as of this writing.

3.3 Sampling in Weakly Cemented Soils

Standard geotechnical sampling techniques appear likely to result in sample disturbance in weakly cemented sands. For example, during a geotechnical investigation at SLAC samples were obtained using the Modified California Sampler, which is hammered into the ground by a 140 lb falling weight. Unconfined compression tests performed on these samples gave strengths ranging from near zero to 3500 kN/m^2 (Dames & Moore, 1972). The near zero strength of samples from certain localities caused enough concern that 1.8 meter diameter exploration shafts were drilled to allow a closer inspection. In all cases, the sand was found to be sufficiently well cemented to safely stand unsupported in the shafts. Thus, the near zero unconfined compressive strength of the samples was evidently caused by sample disturbance.

Lastrico and Saxena (1978) reported testing several different sampling bits in order to obtain undisturbed samples in variably cemented sand. They used 76 mm ID Pitcher Sampler, 150 mm ID Denison Sampler, and

75 mm, 100 mm, and 15 mm Denison Sampler with sawtooth and carbide or diamond bits. "Optimum recovery" was achieved using the 76 mm ID Denison Sampler with carbide and diamond bits. However, disturbance of the samples apparently still was a problem.

Alternatives to downhole sampling are few. One is to use in-situ testing apparatus in order to obtain the stress-strain characteristics of the material. This avenue is being pursued in another phase of this research effort. The other is to cut block samples by hand from trenches or slope exposures in the field and then carefully trim them in the laboratory for testing. This is a time-consuming but necessary process, and for all cases reported herein, samples for laboratory testing were obtained by block sampling. The block samples of the stronger soil from SLAC were cut using a radial power saw with a carbide tipped blade (Alfi, 1978). The blocks were then cut again in the laboratory and the final test specimens were hand trimmed. In the weaker soil at SLAC hand tools were sufficient to obtain the block samples and extreme care was required to transport the blocks to the laboratory without disturbance. The test samples were trimmed into cylindrical shape by careful scraping of larger blocks.

In Pacifica, block samples were obtained by digging with hand tools at the slope face and also from a trench dug by backhoe. Again, the samples were very highly susceptible to disturbance and had to be carefully handled through the process of sampling, transporting them to the laboratory, and shaping into test specimens. In general, after an initial learning period satisfactory results were obtained, but even so two or three specimens would have to be trimmed to obtain one good one for testing.

3.4 Engineering Characteristics--Laboratory Test Results

3.4.1 Strongly Cemented Sand from SLAC

The strongly cemented sands at SLAC are a part of a sequence of Late Tertiary sandstones, siltstones, and claystones which were most probably deposited in a shallow marine environment and were later tectonically folded and faulted. They are thickly bedded with relatively indistinct bedding planes even though the amount and strength of cementation appears to be controlled by the bedding. Fractures and joints are common with occasional slickensides.

Alfi (1978) conducted a laboratory testing program aimed primarily at determining the strength and stress-strain characteristics of the strongly cemented sand and at establishing how these characteristics are affected by variations of density, moisture content, void ratio, and amount of cementation. In addition, petrographic examinations of thin sections and scanning electron microscope analyses were used to describe the soil fabric and to identify the cementing agents and their distribution.

Grain size analyses on the test specimens show that the sand is fairly uniform, silty, and grading from fine to very fine. The median grain size is about 14 mm and the uniformity coefficient is 3.4 (Alfi, 1978; Table 3-1). Individual sand grains are angular to subangular and are composed mainly of quartz, chert, and feldspar (Figure 3-1). In thin sections, the sand grains can be observed to be closely packed with interpenetrative grain to grain contacts in which the projections on the surface of one grain match the depressions in the surface of its neighbor (see Figure 3-1). The cementation is provided mainly by a fine grained matrix of hydrous silicates--clays and hydrated micas, smaller amounts of

Table 3-1

PHYSICAL PROPERTIES OF THE STRONGLY CEMENTED SAND FROM SLAC (ALFI, 1978)

	RANGE	AVERAGE
Dry Unit Weight (kN/m^3)	17.1-18.5	17.6
Natural Moisture Content (%)	8.9-11.5	10.0
Void Ratio	0.40-0.52	0.48
Porosity (%)	29-34	32
Saturation (%)	44-56	56
Grain Size, D_{50} (mm)	-	0.14

Figure 3-1 PHOTOMICROGRAPH OF THE STRONGLY CEMENTED SAND. (GRAIN IN THE CENTER IS ABOUT .1 MM ACROSS.)

silica cement, carbonates, and iron oxides. Pressure solution and corresponding welding of quartz grains at points of contact is also present and contributes to the cementation. The close packing of the sand grains and the fact that the pore spaces are filled by the fine grained matrix are reflected in a low void ratio ranging from 0.4 to 0.52 and a low porosity of 28.8 to 34.2 percent.

Strength Characteristics The strength characteristics of the strongly cemented sand were determined from unconfined compression and drained triaxial compression tests on 36 undisturbed samples and 9 reconstituted samples. Of the undisturbed samples, 24 were tested at natural water content, 4 were soaked in water for two days, 4 were soaked for four days, and one for seven days. Three samples were oven dried before testing. The reconstituted samples were compacted to the in-situ density at natural water content. Five of them were tested at the natural water content and four were oven dried.

A typical set of stress-strain curves obtained from the triaxial compression tests on undisturbed samples at natural water content is presented in Figure 3-2. As apparent from this plot the stress-strain response of the strongly cemented sand is characterized by a relatively brittle behavior in the range of confining pressures from 0 to 414 kN/m^2 (60 psi) used in the testing program. The peak strength of the soil is provided by a combination of cementation and intergranular friction. The frictional component seems to dominate the peak strength response of the strongly cemented sand and is reflected by the increase in the peak shear strength of the soil with increasing confining pressure. Mohr failure envelopes plotted in Figure 3-3 show that the angle of internal friction, ϕ, is about 48 degrees for the undisturbed strongly cemented

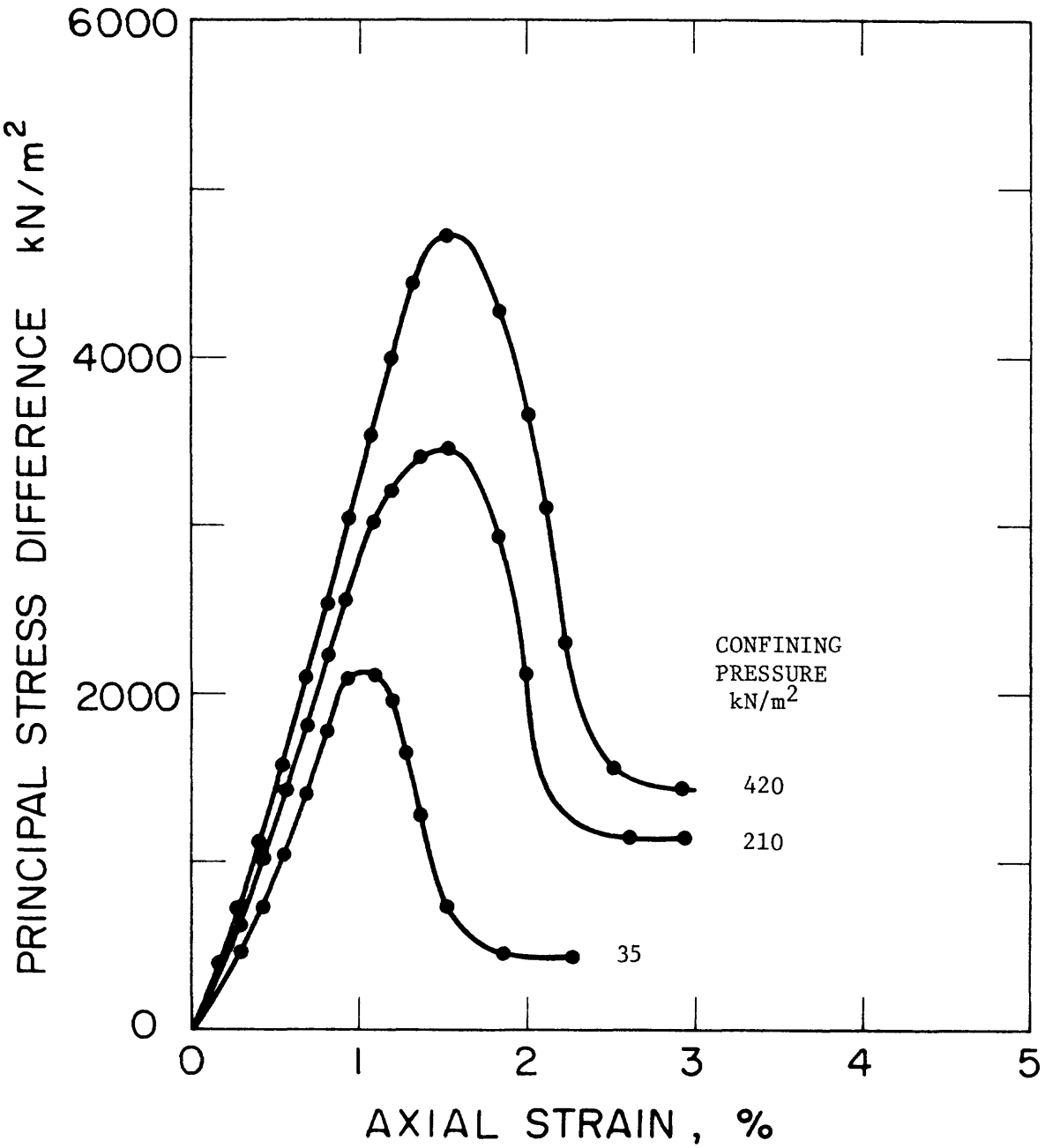

Figure 3-2 STRESS-STRAIN CURVES FOR STRONGLY CEMENTED SAND, SLAC SITE.

sand at natural moisture content. This angle is somewhat larger than would be normally expected of dense sands which typically have an angle of internal friction of 38 to 44 degrees. Before attempting to explain the reasons for the unusually high friction angle, ϕ, it should be noted that the friction angle determined from tests on undisturbed, soaked samples (Figure 3-3) is also 48°, and that the oven dry samples have an even higher angle of internal friction of 62 degrees. The high value of ϕ for oven dry undisturbed samples is based on only three data points. However, this finding is supported by the results obtained from tests on the reconstituted samples (Figure 3-4). These show that the oven dry reconstituted sand yields a friction angle of 58 degrees. The reconstituted sand at the natural moisture content of 10% showed a friction angle of 41 degrees, a value consistent with that often quoted for uncemented sand.

The relatively high friction angle determined for the sand at the natural moisture content is apparently due to its high density and the interpenetrative grain to grain contacts. For uncemented dense sand, the friction angle is known to be a function of its basic frictional characteristics and its tendency to expand when sheared. The work done against the expansion contributes to increasing the recovered friction angle. The high density and interpenetrative grain to grain contacts of the cemented sand would obviously contribute a significant expansion component and produce a high friction angle.

The explanation of the causes for increased friction angle and cohesion due to oven drying of the soil is not readily apparent. However, since both the reconstituted and undisturbed soil samples show similar strength characteristics when oven dried, the causes should be the same

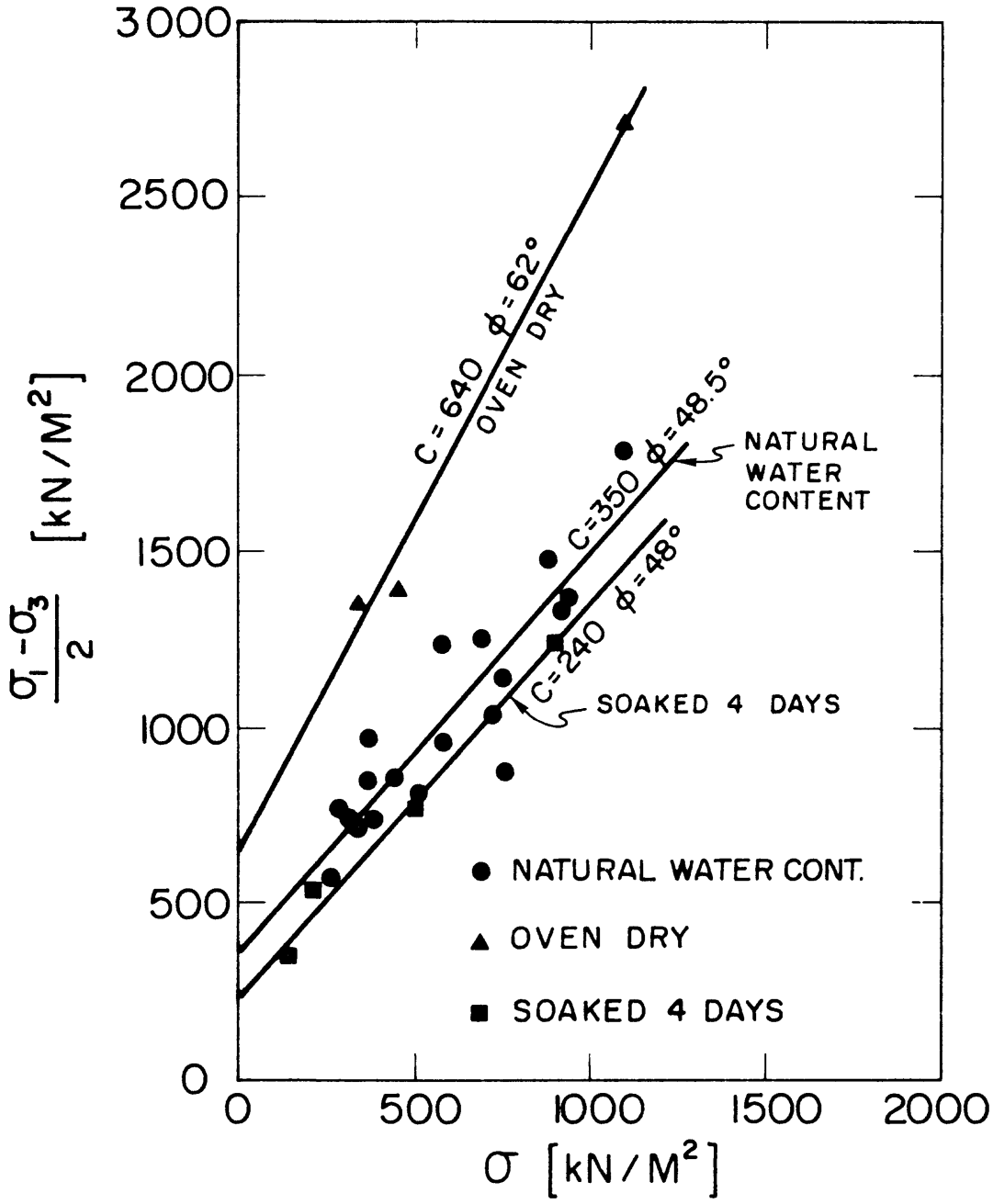

Figure 3-3 DRAINED STRENGTH ENVELOPES FOR STRONGLY CEMENTED SAND, SLAC SITE.

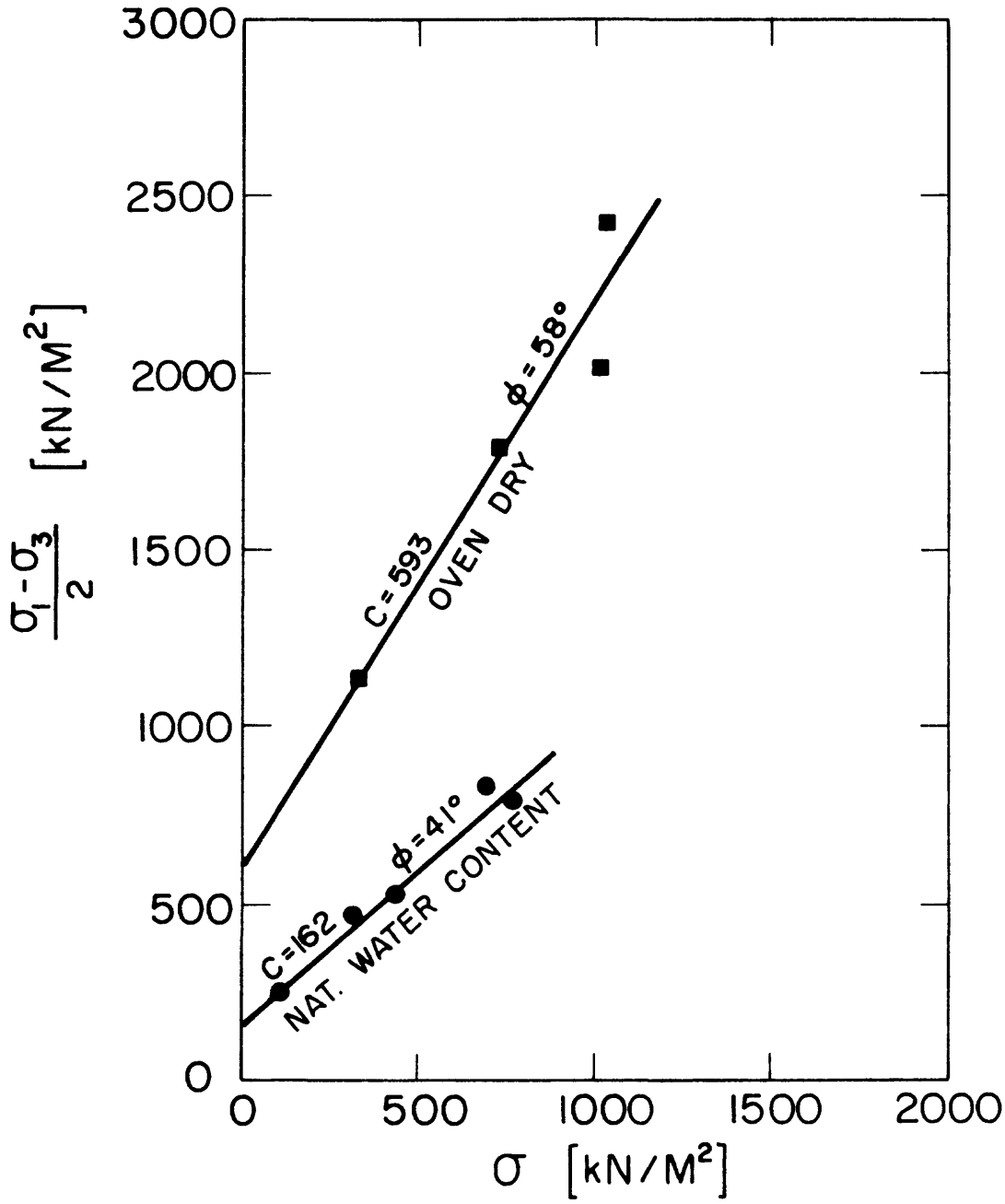

Figure 3-4 STRENGTH ENVELOPES FOR REMOLDED STRONGLY CEMENTED SAND, SLAC SITE.

in both cases (Table 3-2). The simplest explanation is that oven drying results in increased strength and stiffness of the clays and hydrated micas thus increasing the strength of the cementing bonds. Also the water still remaining in micropores and adsorbed on the silt and clay sized particles of the matrix is most probably in a state of tension, thus providing higher intergranular forces and increased friction.

In summary, the results of the laboratory tests show that the peak friction angle of the strongly cemented sand is not significantly affected by soaking (see Figure 3-3, Table 3-2) although the cohesion intercept and the unconfined compressive strength decreases due to soaking. Oven drying on the other hand causes significant increases in both the peak friction angle and cohesion. This means that the strength of the cementing agents is affected by the moisture content and supports the conclusions of microscopic observations that clays and hydrous mica minerals are important cementing agents in the strongly cemented sands. The tests on the reconstituted samples at natural moisture content show that natural fabric of the soil and original cementing bonds are an important component of strength of the naturally occurring material and that this strength cannot be recovered once the original soil fabric is altered.

Stiffness The stiffness of a material refers to the slope of its stress-strain relationship. For a soil, the stress-strain response is nonlinear and no singular slope exists to define the stiffness over the entire stress range. As can be seen in Figure 3-1, the stress-strain curves for the strongly cemented soil show three distinct regimes of behavior. Upon initial loading, the curve is concave upwards showing increasing stiffness with increasing strain. This is followed by an almost linear position which then yields to a concave downwards segment

Table 3-2

STRENGTH CHARACTERISTICS OF STRONGLY CEMENTED SAND (FROM ALFI, 1978)

SAMPLE CONDITION	NUMBER OF SAMPLES	ϕ_{PEAK} DEGREES	COHESION KN/M^2
Undisturbed,Nat. Water Content	24	48.5	350
Undisturbed, Soaked 2 days	4	47	340
Undisturbed, Soaked 4 days	4	48	240
Undisturbed Oven dry	3	62	640
Reconstituted, Nat. Water Content	5	41	162
Reconstituted, Oven dry	4	58	593

until failure occurs.

For purposes of describing an average stiffness for the stress-strain curve, a tangent modulus, E_t, was calculated at 50% of the ultimate strength for each test result. Values of E_t, normalized by dividing by the atmospheric pressure, p_a, are plotted against the confining pressure, σ_3, used in each test, also normalized by p_a in Figure 3-5. The scales used for the variables are logarithmic, following a format often used for uncemented soils (see Wong and Duncan, 1974). Typically, the relationship between log (E_t/p_a) and log (σ_3/p_a) is linear for uncemented soils, yielding the functional relationship.

$$E_t = Kp_a\left(\frac{\sigma_3}{p_a}\right)^n \qquad (3.1)$$

in which K is the intercept at a value of $\sigma_3/p_a = 1.0$ and "n" is the slope of the straight line. Mitchell (1976) has also demonstrated that artificially cemented soils yield results consistent with Equation (3.1). Examination of Figure 3.5 shows the cemented soils tested for this work to also obey this rule.

The data in Figure 3-5 show the following trends:

1) The oven dry specimens yield the highest modulus values.
2) The remoulded specimens tested at their natural moisture content have the lowest modulus values.
3) Soaking reduces the modulus relative to the case where the moisture content remains at its natural value.
4) The data for undisturbed samples at the natural moisture content and that for remoulded samples at the natural moisture content follow straight lines.

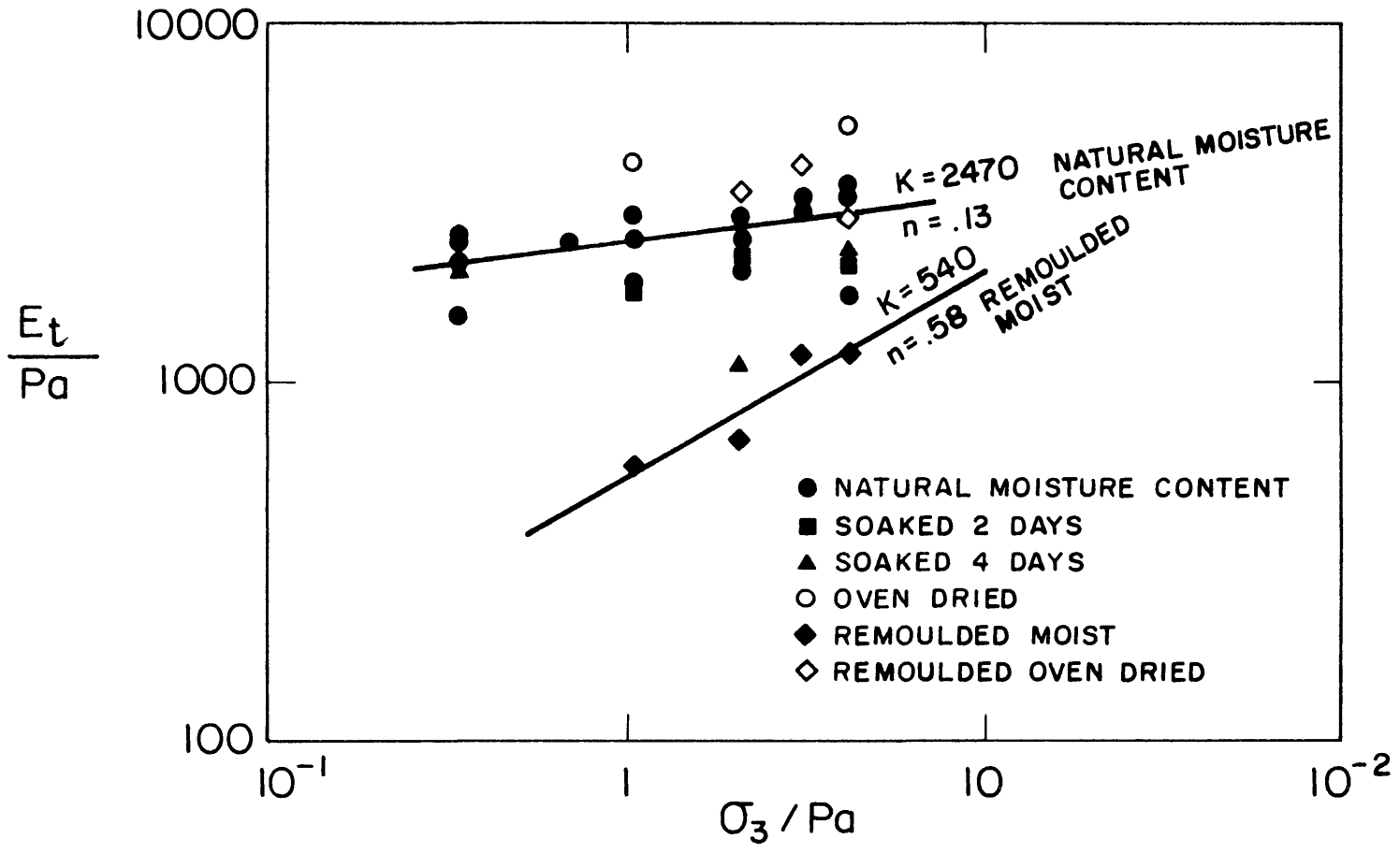

Figure 3-5 SECANT MODULUS VALUES AT FAILURE FOR STRONGLY CEMENTED SANDS, SLAC SITE.

In the case of the undisturbed soil, the straight line fitted to the data yields a K of 2470 and an "n" of 0.13. These values are consistent with those reported for artificially cemented soils by Mitchell (1976). The remolded soil data yields a "K" of 540 and an "n" of 0.58, values in line with those reported by Wong and Duncan (1974) for dense uncemented sands.

These results show that the stiffness of a strong cemented soil is much greater than that of an uncemented soil. However, the evidence shows that the stiffness of the naturally cemented soil follows behavior trends similar to those observed on artificially cemented soils.

3.4.2 Weakly Cemented Sands from the SLAC and Pacifica Test Sites

The weakly cemented sands from the SLAC and Pacifica test sites have many similar characteristics. In Table 3.3 the basic physical properties are compared, and it can be seen that the unit weights, void ratios, porosities and median grain sizes are essentially the same. Only the water contents and degrees of saturation are different, with the water content and degree of saturation higher at the SLAC site than at the Pacifica site. These differences are however more a function of the seasons when sampling was done than an actual disparity between average conditions. Sampling at SLAC was done during and shortly after the rainy season while the sampling at Pacifica was performed in the summer months.

In comparison to the strongly cemented sand at SLAC, the weakly cemented sands have a lower average density (16.6 kN/m^2 vs. 17.6 kN/m^2) and a higher void ratio (0.56 vs. 0.47). Also, the weakly cemented soils have a considerably smaller amount of fine grained (silt and clay) sized soil particles. For the strongly cemented soil, 24% by weight is

Table 3-3

PHYSICAL PROPERTIES OF WEAKLY CEMENTED
SANDS FROM SLAC AND PACIFICA SITES

	SLAC		PACIFICA	
	Range	Avg.	Range	Avg.
Dry Unit Weight (kN/m^3)	16.0 - 17.0	16.5	16.0 - 17.4	16.7
Natural Water Content (%)	10.0 - 19.0	14.0	3.8 - 4.3	4.0
Void Ratio	0.52- 0.62	0.57	0.49- 0.62	0.56
Porosity (%)	34 - 38	36	33 - 38	15
Saturation (%)	29 - 96	61	18 - 23	20
Grain Size, D_{50} (mm)	-	0.24	-	0.26

finer than 0.1 mm while only 1 to 2% by weight is finer than 0.1 mm for the weakly cemented sands. This helps explain the difference in cementation of the three soils. The strongly cemented sand is more tightly packed and has its void spaces more filled by the fine fraction of soil particles than the weakly cemented soils. Also, the fine fraction in the strongly cemented soil provides a positive cementing component through capillary tension and the presence of clays and hydrous mica.

Strength Characteristics A total of eight and seven drained triaxial tests were performed on the samples from SLAC and Pacifica respectively. Volume changes were measured only in the case of the Pacifica samples by a special apparatus devised to measure the amount of air expelled during shear. Typical stress-strain curves for SLAC are presented in Figure 3-6, and for Pacifica in Figure 3-7. The stress-strain curves generally show a peak at about two percent axial strain and drop off to a residual value by an axial strain of two to four percent for low confining pressures and six to eight percent for higher confining pressures. There is an increase in the peak strength as confining pressure increases, indicating a significant frictional component of behavior.

For the Pacifica data there is a very distinct transition in shape of the stress-strain curve after failure as confining pressure increases. A similar, but less distinct response can be observed for the SLAC data. At low confining pressures the stress-strain curve drops sharply after peaking, but at higher confining pressures the drop is more gradual until a point is reached where a rather steep drop occurs. For the Pacifica soils, and presumably also for the SLAC soils, this point corresponds to the axial strain at which the sample ceases to expand in

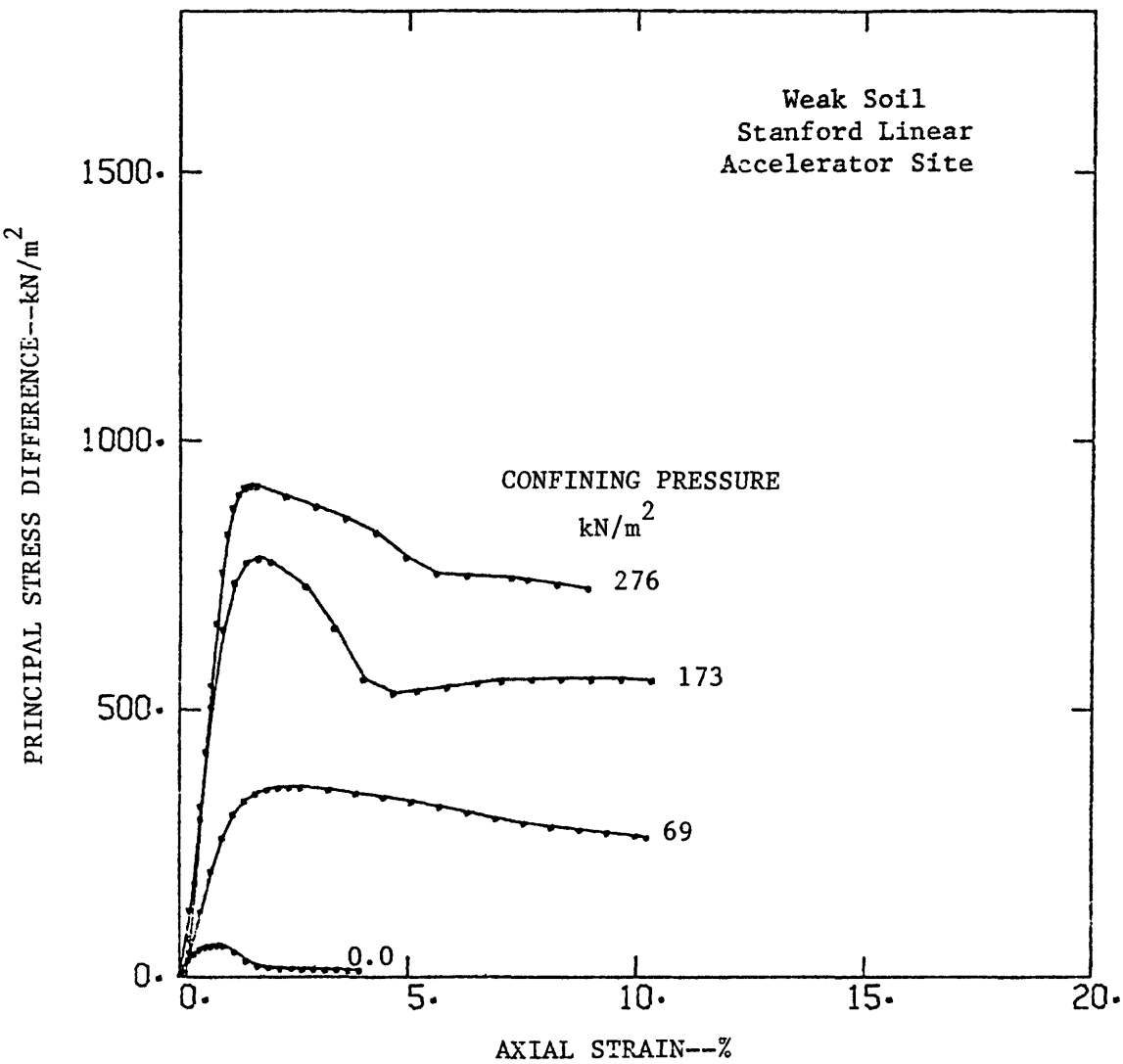

Figure 3-6 TYPICAL TRIAXIAL COMPRESSION STRESS-STRAIN CURVES FOR WEAKLY CEMENTED SOIL AT STANFORD LINEAR ACCELERATOR SITE.

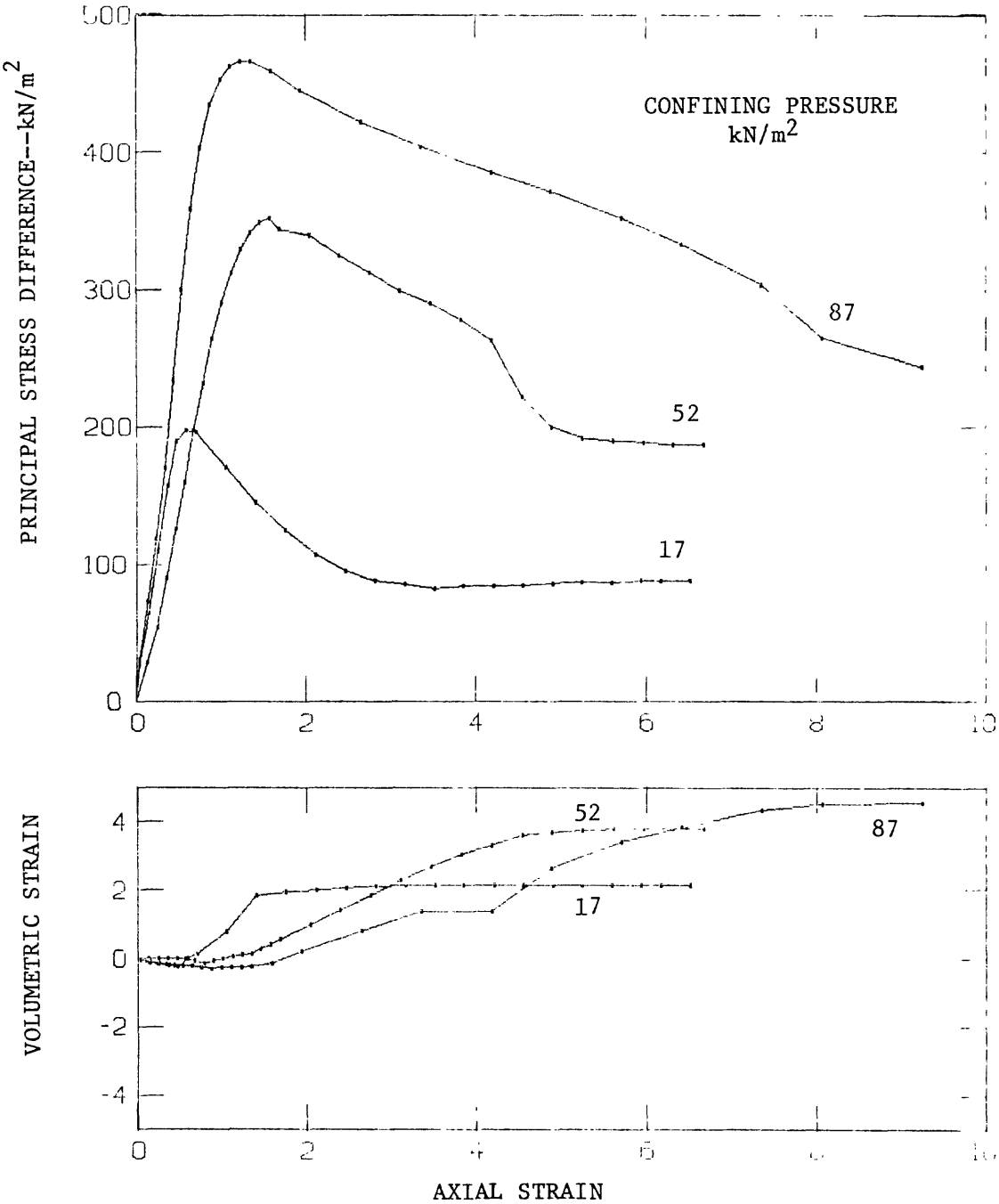

Figure 3-7 TYPICAL STRESS-STRAIN CURVES FOR WEAKLY CEMENTED SAND, PACIFICA SITE.

volume. This type of behavior is observed repeatedly in the test results for the artificially cemented samples (see Chapter 5). It appears that the shape of the curves are dictated by the following phenomena:

1. The first peak corresponds to the mobilization of the cementation bonds and their rupture.
2. The gradual descent limb at higher confining pressures represents the mobilization of the strength of the sand through the basic friction mechanism and the energy expended in work against volumetric expansion.
3. The subsequent sharp drop occurring as volumetric expansion ceases is due to the fact that less work is required to shear the soil after this point.

Further comment will be made on this behavior in Chapter V.

Mohr envelopes based on peak strength values for the Pacifica and SLAC weakly cemented sands are shown in Figure 3-8. The results are very close, with the SLAC sand yielding a slightly higher friction angle and lower cohesion or concentration than the Pacifica sand. The friction angles of the two sands, 38 and 40 degrees, and the cohesion intercepts, 40 and 16 kN/m^2, are well below the strength parameters of the strongly cemented sand at SLAC, ϕ = 48 degrees and cohesion = 350 kN/m^2. Residual friction angles for the sands range from 37 to 40 degrees, values not greatly different than those prior to failure.

Stiffness In Figure 3-9 the tangent modulus at 50% strength mobilization, E_t, is plotted against confining pressure, σ_3. Both parameters are normalized by dividing by atmospheric pressure, p_a and plotted on log scales. Also shown is the trend line for the strongly cemented soil from SLAC tested at its natural moisture content. As

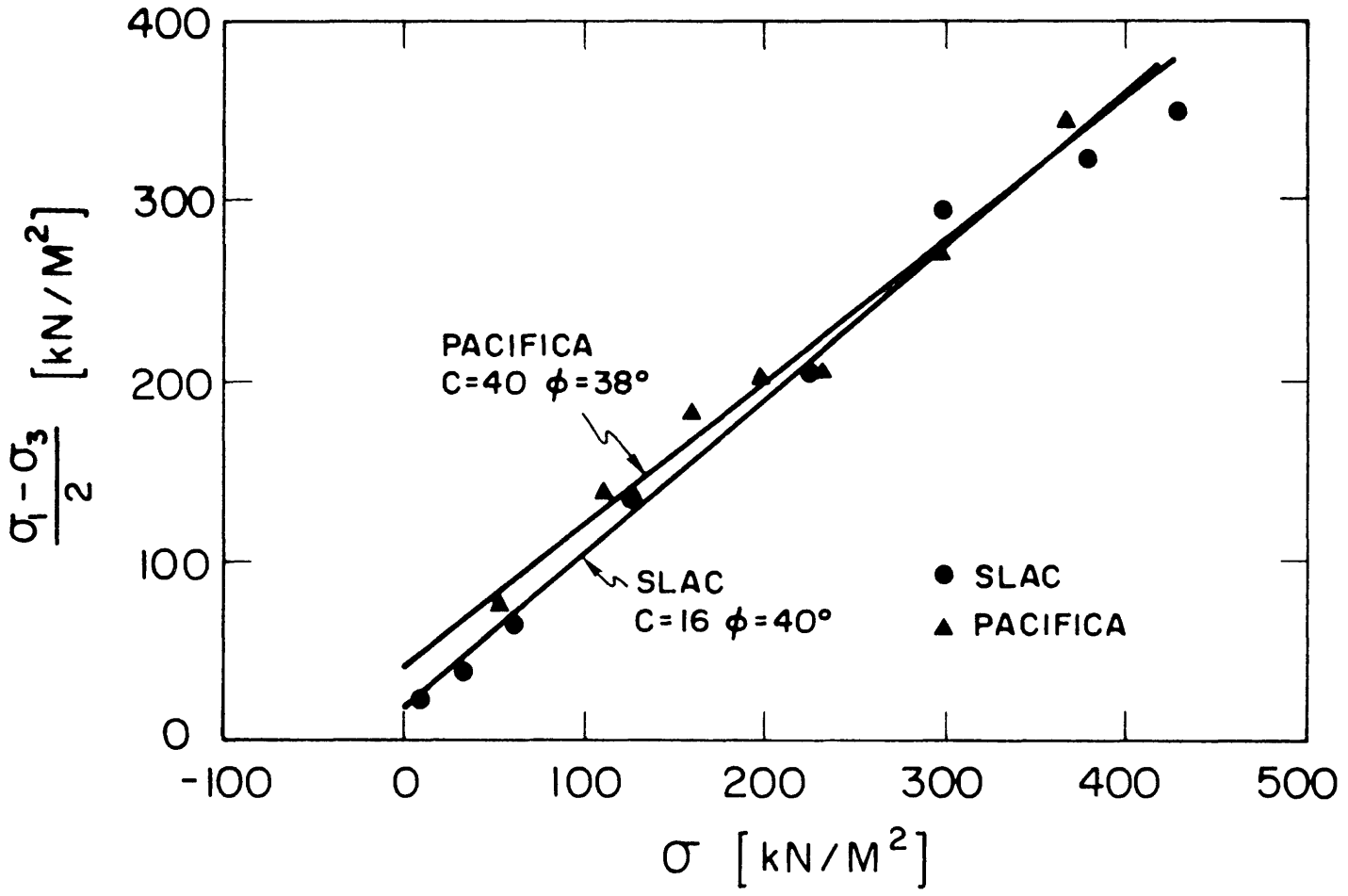

Figure 3-8 FAILURE ENVELOPES FOR WEAKLY CEMENTED SANDS AT THE SLAC AND PACIFICA SITES.

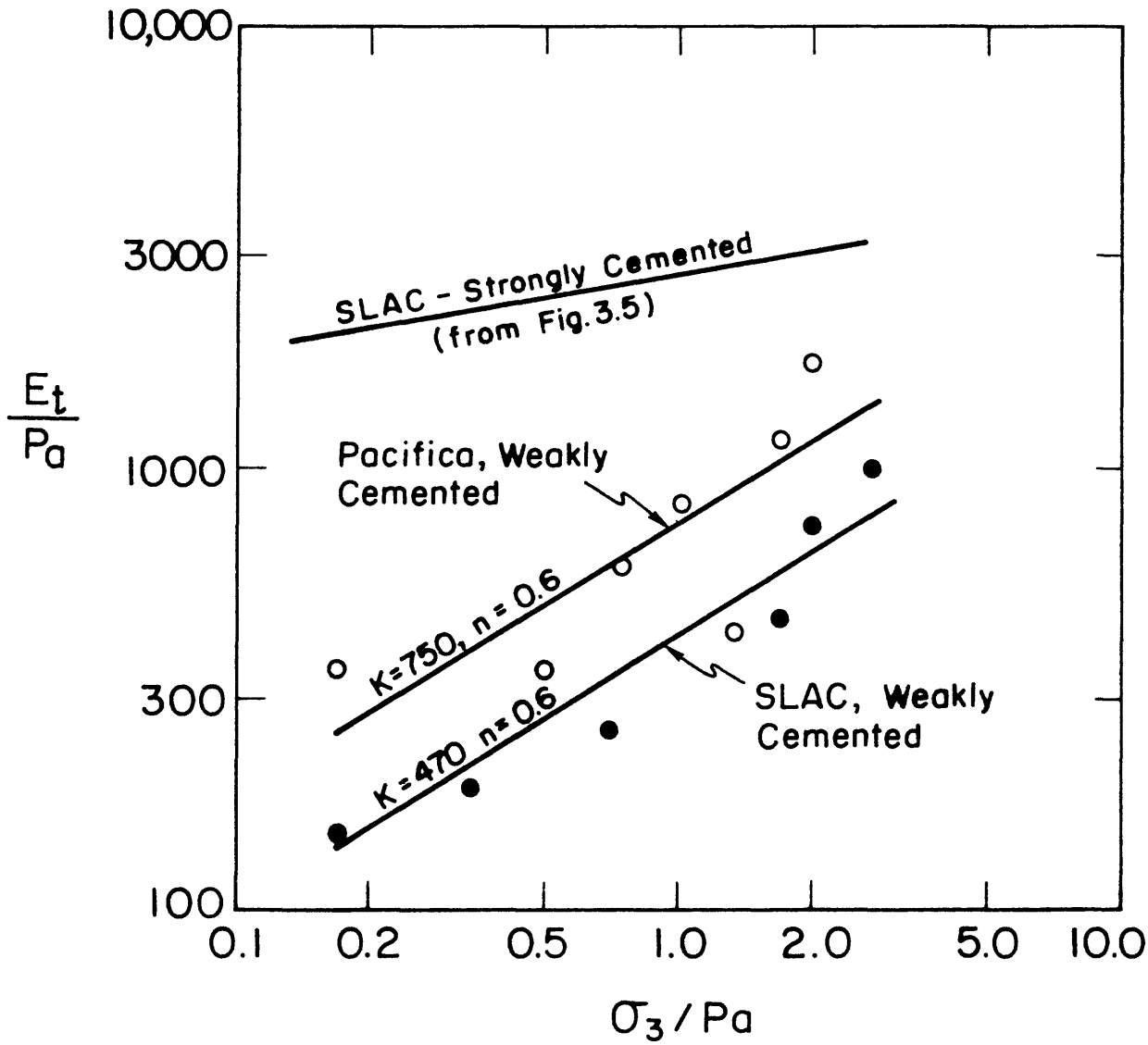

Figure 3-9 SECANT MODULUS VALUES AT FAILURE FOR WEAKLY CEMENTED SANDS FROM SLAC AND PACIFICA SITES.

with the strongly cemented soil, there appears to be a reasonable straight line fit between E_t/p_a and σ_3/p_a for both the SLAC and Pacifica soils. The weakly cemented sands obviously yield much lower modulus values than the strongly cemented sand, with the SLAC samples giving lower values than the Pacifica samples. The straight line relationships from Figure 3-9 are defined by the following equations:

$$\text{SLAC Weakly Cemented Sand} \qquad E_t = 420\ p_a \left(\frac{\sigma_3}{p_a}\right)^{0.6} \tag{2}$$

$$\text{Pacifica Weakly Cemented Sand} \qquad E_t = 750\ p_a \left(\frac{\sigma_3}{p_a}\right)^{0.6} \tag{3}$$

Modulus values for both of these sands are consistent with those usually associated with dense, uncemented sands. The fact that the modulus values for Pacifica sands are higher than those for the SLAC sands, may be due to any of several reasons. First, because the stress-strain curves for the SLAC samples are not as consistent as those from Pacifica, it may be presumed that some disturbance of the SLAC soils occurred, reducing the modulus values. Alternatively, the differences may be real, reflecting differences in cementation agents or the fact that the average moisture content of the SLAC samples was greater than that of the Pacifica samples.

3.5 Summary

This chapter presents all of the information developed during the sampling and testing of three naturally cemented sands from the San Francisco Bay area. Two of the sands were located at the site of the Stanford Linear Accelerator (SLAC), while the third was found along the Pacific Coast on the north side of the City of Pacifica, California.

Of the two sands from the SLAC site, one is strongly cemented, yielding unconfined compressive strengths of greater than 700 kN/m^2 (100 psi) while the other is weakly cemented with unconfined strengths of about 50 kN/m^2 (7 psi). The sand from the Pacifica site has physical properties and strengths very close to those of the weakly cemented sand at SLAC.

The test results show that the strengths of all of the cemented sands basically yield straight line failure envelopes in the compressive stress region. The friction angles for the cemented sands are essentially the same as those one would expect for dense, uncemented sands, with the value for the strongly cemented sand at 48° and that for the weakly cemented sands from 38° to 40°. The high friction angle for the strongly cemented sand appears to be due to a significant degree of interparticle penetration, an effect seen in thin sections of the soil. Naturally, the cohesion intercept of the Mohr failure envelope is greater for the strongly cemented sand than for the weakly cemented sands. This is in part due to the fact that the strongly cemented sand contains 20% fines, an important cementing agent not present in the weakly cemented soils.

The modulus values of each of the cemented soils increases with confining pressure in the nature of a frictional material. As expected, the moduli of the strongly cemented sand are considerably above those of the weakly cemented sands. Values for the weakly cemented sands are only slightly above or about equal to those expected for an uncemented, dense sand.

CHAPTER IV

Testing of Artificially Cemented Sands Materials and Testing Procedures

4.1 Introduction

In the previous chapter it was noted that there are few published data on the static or dynamic stress-strain behavior or strength of weakly cemented sands. The objectives of the laboratory testing program on artificially cemented soils were to develop an understanding of the behavior of weakly cemented sands under loading conditions and strain levels commensurate with the problem of defining response of slopes in these materials.

As noted previously in Chapter III, it was decided to test artificially cemented samples because of the difficulty of obtaining samples of naturally cemented soils and the natural variability in these materials. By creating artificially cemented specimens in the laboratory, close control can be exerted on the density, cementation level, grain size water content of the material. Effects of variations in each of these parameters can also be studied by changing one at a time, a situation unlikely to be achieved by changing sites in the field. Of course, the key to obtaining meaningful results using the artificially cemented soils lies in using a mix of sand and cementing agent which produces a material response like that of the naturally cemented soil. For this reason, considerable attention was given to the question of mix design.

4.2 Artificial Mix Design

The artificially cemented sand used in the study was designed to

meet the following criteria: (1) it had to be weakly cemented yet strong enough to withstand handling during test preparation; (2) it had to be inexpensive and easy to prepare; (3) its properties had to be reproducible; and (4) it had to be similar to naturally occurring materials.

The sand component of the mix consisted of equal parts of Monterey Lapis Lustre #20 and #30. The grain size distribution curve is shown in Figure 4-1 together with the curve for Pacifica Sand for comparison. The median grain size diameter of the lab sand is about .58 mm; the minimum void ratio is .58 and the maximum is .85.

Two cementing agents, wax and Portland Cement, were considered for the work. Korbin and Brekke (1975) successfully used a sand-wax mixture to model the time dependent behavior of a weak rock mass. The sand-wax mixture was easy to prepare and its properties could be reproduced. However, because the sand grains were entirely coated by wax, the angle of internal friction could be as low as 11.5 degrees. Also, the material was susceptible to creep under load.

The use of Portland Cement presents a different set of problems in that the strength of a sand-cement mixture depends on the length of curing, moisture content during curing, temperature fluctuations during curing, homogeneity of the final mix, the uniformity and degree of compaction, and the elapsed time between adding water and compaction (Mitchell, 1977). However, there are important advantages to mixing cement with sand, namely: the angle of internal friction of the mix, 30 to 45, degrees, fits in the range observed in cemented sands; the cement is much less susceptible to creep than wax; the cement provides bond only at the points of contact between sand grains which results in a contact bound structure; and, strength can be varied over a wide range.

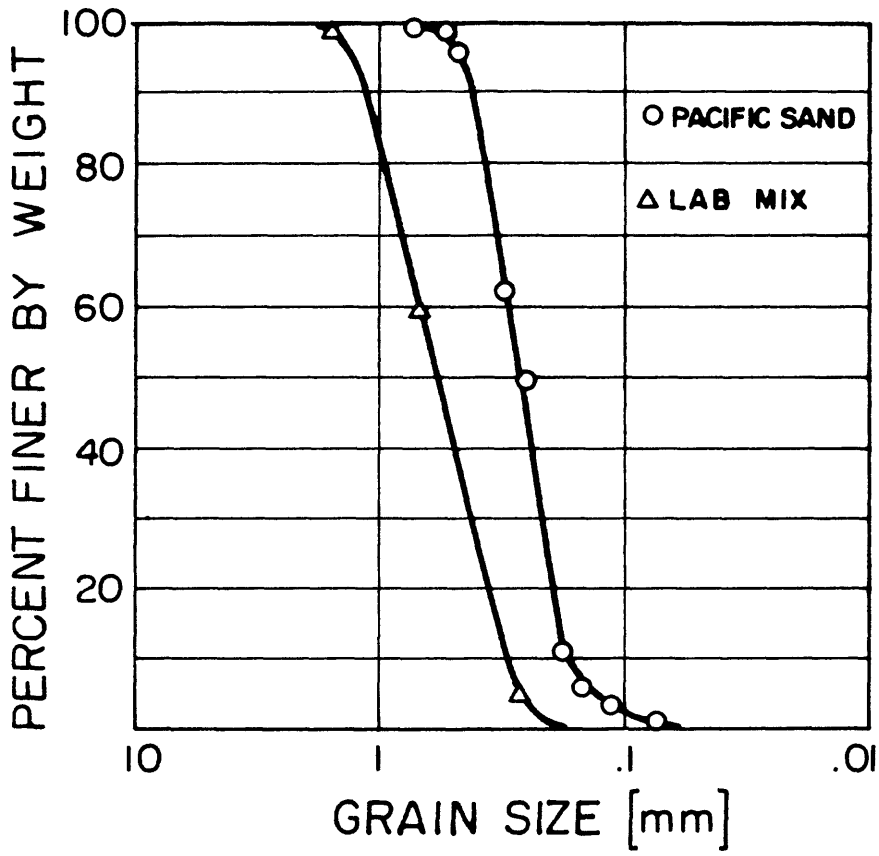

Figure 4-1 GRAIN SIZE DISTRIBUTION CURVES FOR THE LAB MIX AND PACIFICA SAND.

Therefore, the Portland Cement was selected as the cementing agent for this work.

The variables affecting the ultimate strength of the mixture were accounted for as follows:

1. Compaction--the samples were compacted in layers of constant thickness to assure uniform density of the samples.
2. Mixing Water Content--the water content of the mix was kept at 8 percent. This value was chosen because it created a mixture which was easy to handle and the moisture distribution in the sample during and after curing remained relatively uniform.
3. Cement Content--2 percent or 4 percent cement by weight of the sample was used. These cement contents gave compressive strengths in the desired range.
4. Curing Time--the strength of the cement bond increases with time. A total of 28 unconfined compression tests were performed on samples ranging from 3 to 28 days in age to determine the variation of the strength with time. The results of these tests are summarized in Figure 4-2. The unconfined compressive strength of the material increased rapidly during the first 10 days of curing, gaining about 80 percent of its 28 day strength. On the basis of the above information it was decided to use 14 day old samples for this investigation. This allowed samples to be prepared without too long a wait for curing and got them out of the period where rapid changes in strength were occurring. Sets of samples were prepared on a daily basis so that after the initial 14 day period samples could be tested daily.

The final mix compositions and their basic properties are given in Table 4-1.

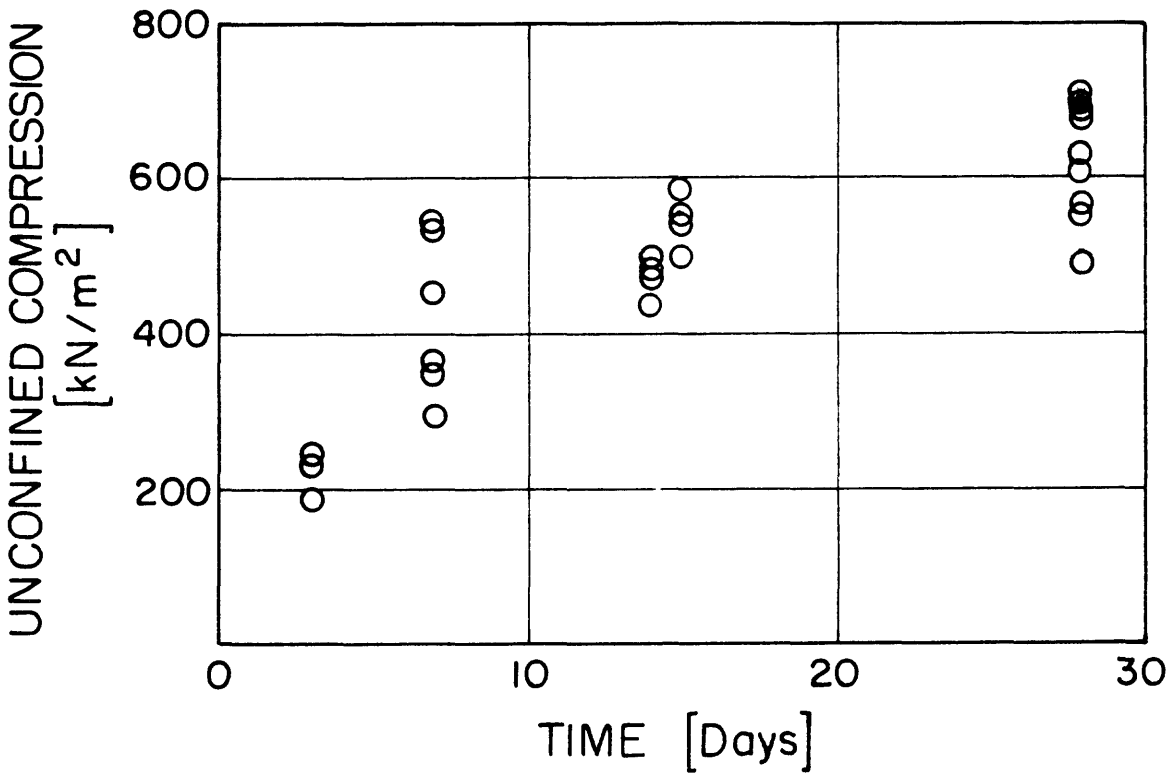

Figure 4-2 UNCONFINED COMPRESSIVE STRENGTH AS A FUNCTION OF CURING TIME FOR 4 PERCENT CEMENT MIX.

Table 4-1

FINAL CEMENT-SAND MIX PROPERTIES

	Mix Number	
	1	2
Water Content,* percent	8.0	8.0
Cement,* percent	4.0	2.0
Dry unit weight, kN/m^3	15.8	15.5
14 day UC strength, kN/m^2	504.0	147.0
Relative density, percent	74.0	74.0

*By dry weight of sand.

4.3 Choice of Laboratory Tests

The objectives of the laboratory testing were to: (1) define the strength and the stress-strain behavior of the artificial soil so that a meaningful comparison with naturally occurring soils could be made; and (2) subject the soil to loading conditions expected to occur in slopes under static and dynamic loading. Static unconfined compression, triaxial compression, and Brazilian tension tests were used to achieve the first objective and dynamic triaxial, Brazilian tension, and static and dynamic unconfined simple shear tests were used to achieve the second objective. Of these tests, the unconfined and triaxial compression tests are the most commonly used in geotechnical engineering. The Brazilian tension and the unconfined simple shear deserve further comment.

In the Brazilian tension test a cylindrical sample is compressed at two diametrically opposite points (Jaeger and Cook, 1976). On a Mohr Diagram the test is represented by a circle starting as a point at the origin of axes and expanding concentrically until failure occurs. At failure the minor principal stress is tensile and the major principal stress is compressive. The minor principal stress acts perpendicular to the failure plane and the failure is in pure tension. The advantages of the Brazilian tension test lie in its simplicity and the fact that the failure can be forced to occur perpendicular to possible bedding planes or other planes of weakness in the samples. This test is particularly useful in view of the existence of tensile stresses in steep cemented soil slopes (see Fig. 2.4).

The unconfined simple shear test is the most complex of all the tests used in this study in terms of the loading conditions and the laboratory procedures. Normally in a simple shear test, a cylindrical

sample of soil is trimmed to fit tightly into a wire reinforced membrane. During the test an initial normal, axial, load is applied to the ends of the sample. The tendency of the sample to deform laterally under the axial load is opposed by the wire reinforced membrane producing a restraining stress, which is usually referred to as the k_o stress. Thus, initially, the axial stress is the major principal stress and the k_o stress is the minor principal stress as illustrated in Figure 4-3. Next, a shear stress is applied on the plane on which the major principal stress acts. Finite element analyses indicate that although the stress distribution within the sample is nonuniform, simple shear loading condition is created in its interior. Details on this phenomenon are given in Appendix C. As a result of this type of loading the principal stress plane rotates, the minor principal stress decreases, and the major principal stress increases until failure. Normally, both major and minor principal stresses are in compression.

In this investigation it was desired to achieve a condition where the major principal stress is compressive and the minor principal stress tensile. This models the conditions in many portions of a steep cemented soil slope. The unconfined simple shear test is suited to simulate the combined tension-compression state.

In the unconfined simple shear tests the ends of the samples were bonded to the loading plattens, partially preventing radial strains under axial loading (for details of the test procedure see Section 4.5). Finite element analyses of this condition, discussed in detail in Appendix C, show that under the application of the initial vertical stress, the lateral stress or σ_3 value increases to a level somewhat less than that dictated by the normal k_o condition. However, the initial σ_3

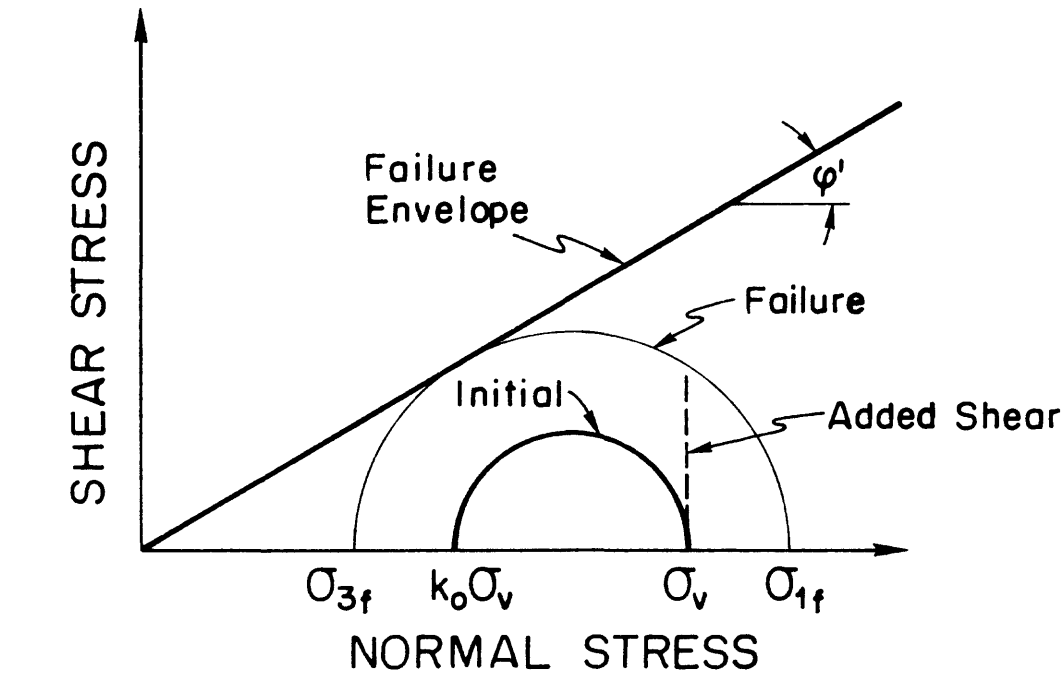

(a) Stress conditions in center of Specimen-
Confined Simple Shear, Uncemented Sand

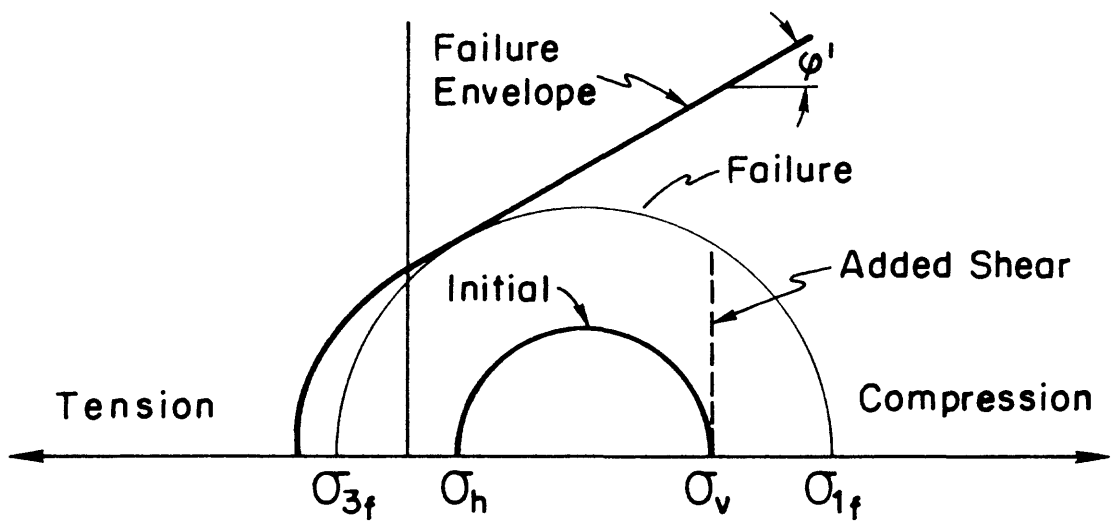

(b) Stress conditions in center of Specimen-
Unconfined Simple Shear, Cemented Sand

Figure 4-3 STRESS CONDITIONS IN THE CENTER OF A SIMPLE SHEAR SPECIMEN UNDER CONFINED AND UNCONFINED CONDITIONS.

value is small enough for the vertical stress level used that upon shear loading it decreases into the tensile region. At failure, the minor principal stress in the unconfined simple shear test is tensile and the major principal stress is compressive. The normal stress on the failure plane can be tensile or compressive depending upon the relative magnitudes of the principal stresses (Figure 4-3). This type of loading is representative of that which occurs along the lower fringes of the tension zones in the slopes under static loading.

The dynamic tests differed from static tests only in the rate and cyclic nature of the loading. In the dynamic, cyclic triaxial compression a load increment ($\Delta\sigma$) was added and then removed from the major principal stress (σ_1) at a rate of 1 Hz. The cyclic load increment increases the shear stress in the specimen. The loading was repeated until failure occurred or a steady state condition was reached. Similar procedure was used for the Brazilian tension tests. In the simple shear test a shear stress increment ($\Delta\tau$) was applied in alternating directions at a rate of 1 Hz.

The purpose of all the cyclic tests was to simulate earthquake loading. In general, for horizontal soil deposits, cyclic simple shear test is thought to most closely approximate the actual earthquake loading. However, near a slope face other types of loading may occur. Therefore, performance of cyclic triaxial and Brazilian tension tests was felt to be appropriate.

4.4 Sample Preparation

Different size samples were required for the triaxial and simple shear tests. The samples for triaxial tests were cylindrical, 70 ± 2 mm in diameter, and 138.4 mm high. The samples for simple shear tests had

the same diameter but their height was only 27.7 mm. Cylindrical plexiglass molds with a narrow longitudinal split on one side were used for sample compaction and curing. The split in the molds was kept closed during the compaction and the curing using clamps. After curing, the clamps were released; the elasticity of the plexiglass then caused the mold to open slightly along the split and the samples slid freely from the molds. An aluminum cap closed one end of the mold and it also served as a compaction base. Because the internal diameter of the plexiglass was somewhat variable, each individual mold was measured in order to determine the amount of material to be compacted.

The procedure for compacting the specimens is given in Appendix A. Because of the many factors affecting the ultimate strength of the mix, the procedure for preparation of the specimens was adhered to strictly.

4.5 Testing Procedures and Equipment

4.5.1 Static Tests

Unconfined Compression Tests The samples used in the unconfined compression tests were capped with a capping compound (Hydrostone) after extrusion from molds. The caps helped to provide a good contact between the loading plattens and the sample. The samples were then tested without membranes in a standard triaxial cell at a strain rate of .06 percent per minute.

Consolidated Drained Triaxial Tests The samples were enclosed in .01 inches thick latex membrane and placed in a triaxial cell. Plexiglass endplattens were carefully seated on the ends of the samples. No water was added and no back pressure was used during the tests since the samples were moist but not saturated. Volume change was measured during some of the tests using an open ended adjustable U-tube. The strain rate

of 0.06 percent per minute was used in all the static triaxial tests unless otherwise specified.

Unconfined Simple Shear Tests A simple shear loading device developed at the Norwegian Geotechnical Institute (NGI) was used for the tests. A special method of securing the sample in the loading device was developed in order to prevent slippage between the endplattens and the sample. The bottom platten of the simple shear device was machined with a 3 mm lip around the circumference. This lip formed a shallow depression which was filled with Hydrostone; the top of the sample was pressed into it and the Hydrostone was allowed to set for 45 minutes. The top platten of the simple shear device was converted into a circular clamp. This clamp then served to grip the aluminum compaction base of the sample. With the top and bottom plattens secure the sample was firmly in place and the bond between the sample and plattens was firm. At the top a bond was developed between the aluminum cap and the sample during curing. At the bottom the Hydrostone served as the connecting agent between the soil and the platten. Failure of all samples occurred in the soil, and no slippage between the soil and the plattens was observed. Normal load was applied immediately prior to a test and the shear load was applied at a strain rate of .12 percent per minute.

Brazilian Tension Tests The samples were placed lengthwise on a 12 mm thick steel plate. The load was applied through a 12 mm diameter steel rod placed lengthwise on the top of a sample. Care was taken that the loading rod was in contact with the sample along its full length and at the same time diametrically opposite the line of contact between the sample and the steel plate. A sketch of the setup is shown in Figure 4-4. The tests were performed rapidly and only the load at failure was recorded.

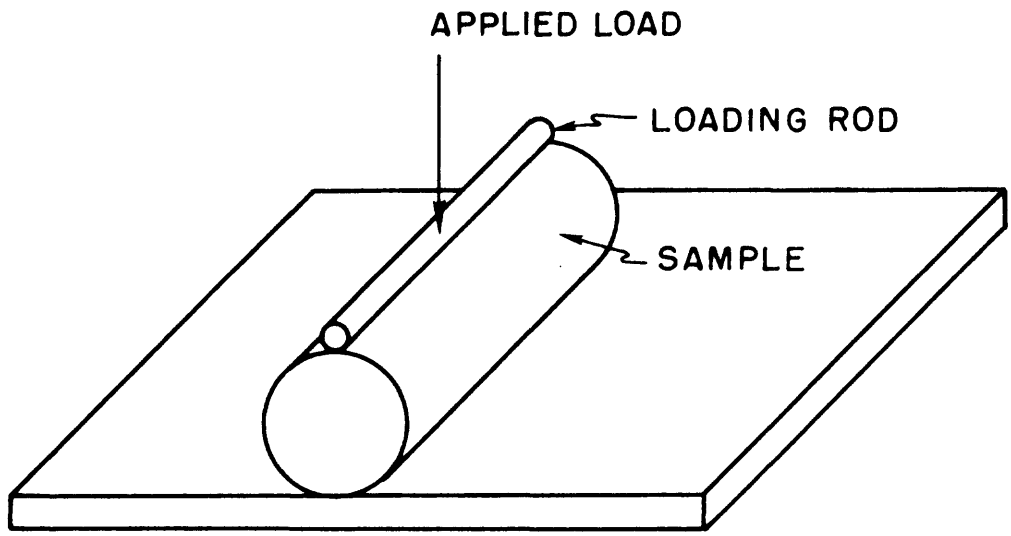

Figure 4-4 SKETCH OF THE BRAZILIAN TENSION TEST

4.5.2 Dynamic Tests

The procedures used to prepare the samples for the dynamic tests were identical to those used for static tests. Cyclic loads were generated by a pneumatic sinusoidal load generator designed at the University of California at Berkeley (Chan and Mulilis, 1976). The rate of load application for all tests was 1 Hz.

4.6 Data Acquisition

The load-displacement measurements in all the above tests were obtained through electronic load cells and linear variable differential transformers (LVDT), respectively. The progress of the static tests was monitored on an X-Y plotter and a multichannel datalogger recorded the data.

In the cyclic tests, the output from the load cells and LVDTs was monitored on a continuous strip chart recorder, an X-Y plotter, and recorded on a four channel instrumentation tape recorder. The data recorded on tape were later processed by a minicomputer in the John A. Blume Earthquake Engineering Center (JABEEC), at Stanford University.

4.7 Summary

The testing of artificially cemented sand was undertaken because uniform specimens of cemented soil with predetermined characteristics could be manufactured. This eliminated concern about scatter in the test data produced by inherent variability of naturally cemented soils and effects of sample disturbance.

Portland Cement was chosen as the cementing agent because it produces a brittle response of the cemented sand and it can generate strengths which cover the entire range of interest, 0 to 690 kN/m^2

unconfined compressive strength. Standardized sample preparation procedures were developed to assure uniformity of samples.

The laboratory test program consisted of static and dynamic triaxial tests, static and dynamic simple shear tests, and static and dynamic Brazilian tension tests. These tests produce stress conditions thought to be representative of major portions of a cemented soil slope subjected to seismic loading. Standardized test procedures were developed for all of the tests.

CHAPTER V

Artificially Cemented Sand
Static and Dynamic Test Results

5.1. Introduction

A laboratory testing program consisting of over 170 static and dynamic laboratory tests was carried out. Sand cemented with 4 percent Portland cement was used in over 120 tests. The remaining tests were performed on uncemented sand and sand cemented with 2 percent Portland cement. A classification of 146 of the tests according to test and material type is presented in Table 5-1. Excluded from the table are preliminary tests which were done to establish the initial material properties and laboratory procedures.

The main objectives of the testing program were: (1) to define the basic strength and deformation characteristics of an undisturbed weakly cemented soil subjected to static and dynamic loading; and (2) to determine the influence of the amount of cementation and the dry density on the static response of the weakly cemented soil. The tests on the sand with a relative density of 74 percent cemented with 4 percent cement were used to meet the first objective. The influence of the different amounts of cementation on the static soil response was determined from tests on uncemented sand and sand cemented with 2 percent cement at a relative density of 74 percent. Finally, tests on sand cemented with 4 percent and relative densities of 60 and 90 percent were used to observe the influence of the dry density on the static soil response (Table 5-1).

Table 5-1

LABORATORY TESTING PROGRAM

Cement Content (%)	Relative Density (%)	Test Type	Number of Tests	
			Static	Dynamic
0	74	Triaxial	5	-
4*	60	Triaxial	6	-
	74	Unconfined	28	1
		Triaxial	28	27
		Brazilian Tension	4	2
		Simple Shear	4	24
	90	Triaxial	5	-
2*	74	Unconfined	2	-
		Triaxial	5	-
		Brazilian Tension	2	-
		Simple Shear	3	-
		Total	92	54

*By dry weight

5.2 Static Test Results

5.2.1 Drained Triaxial Compression and Brazilian Tension

Confining pressures (minor principal stress) from 0 to 414 kN/m^2 were employed in the drained triaxial tests. The confining pressures were chosen to cover the range of minor principal stress levels expected to occur near vertical slopes in cemented slopes. For example, using the results of the finite element analysis in Figure 2-4 and most unit weight of the artificially cemented sand of 17.1 kN/m^3, the confining pressure of 414 kN/m^2 would correspond to minor principal stress occurring at the base of a vertical slope roughly 81 m high.

Stress-strain, volumetric change, and strength data were obtained from the tests. In the following discussion, the stress-strain response will be covered first, strength behavior second, and initial tangent modulus for the stress-strain curves third.

Stress-Strain Response Data consisting of confining pressure, principal stress difference, axial strain, volume change, and initial tangent modulus for individual tests on the 4 percent cement, 2 percent cement, and uncemented sand at 74 percent relative density are presented in Tables 5-2, 5-3, and 5-4. Representative stress-strain and volumetric change curves from these tests are shown in Figures 5-1, 5-2, and 5-3. The shape of the curves closely reflects different phases of the soil response during loading.

For example, the stress-strain curve for a test on cemented sand at confining pressure of 207 kN/m^2 in Figure 5-1 can be divided into four segments separated by points A, B, and C. The initial part of the stress-strain curve is almost linear until just prior to peak (point A),

Table 5-2

RESULTS OF STATIC TRIAXIAL TESTS ON SAND CEMENTED WITH 4 PERCENT CEMENT (D_r = 74%)

Sample No.	σ_3 kN/m^2	Peak Strength			Residual Strength			Initial Tangent Modulus E_i kN/m^2
		$(\sigma_1 - \sigma_3)$ kN/m^2	Axial Strain %	Volume Change %	$(\sigma_1 - \sigma_3)$ kN/m^2	Axial Strain %	Volume Change %	
23	0	435	0.46	---	---	---	---	122,810
24	0	469	0.42	---	---	---	---	146,238
25	0	494	0.61	---	---	---	---	97,487
29	0	490	0.58	---	---	---	---	117,000
35	0	483	0.50	---	---	---	---	137,400
26	35	575	0.58	---	162	4.05	---	155,077
31	35	644	0.60	---	150	4.36	---	141,333
35	35	703	0.63	---	161	4.42	---	148,353
39	35	680	0.52	---	131	3.97	---	175,813
40	35	737	0.55	---	153	4.78	---	182,829
42	35	714	0.51	0.0	198	2.79	2.31	176,943
45	35	657	0.44	0.02	144	4.83	3.18	202,414
44	103	845	0.87	0.0	342	7.58	1.17	172,967
46	103	813	0.71	-0.35	394	8.87	0.98	161,075
47	103	876	0.67	---	417	7.63	---	201,657
48	103	886	0.68	-0.28	346	6.86	1.08	188,225
52	138	1034	0.75	---	447	6.43	---	211,139
49	207	1125	0.84	---	612	7.76	---	205,417
50	207	1096	0.80	-0.29	613	7.59	-0.02	243,000
51	207	1146	0.92	-0.17	709	11.35	1.72	208,375
53	310	1364	1.61	-0.51	914	9.53	-0.45	273,382
54	310	1391	1.16	---	891	8.44	---	259,116
55	310	1412	1.25	-0.43	943	7.56	0.13	269,737
56	414	1711	2.57	-0.15	1205	11.46	0.17	287,200
57	414	1608	2.81	-0.51	1251	9.49	-0.36	253,786
58	414	1597	3.11	-0.66	1091	8.84	-0.66	243,000
59	414	1516	2.91	---	982	12.31	---	250,423

Table 5-3

RESULTS OF STATIC TRIAXIAL TESTS ON SAND CEMENTED WITH 2 PERCENT CEMENT (D_r = 74%)

Sample No.	σ_3 kN/m^2	Peak Strength			Residual Strength			Initial Tangent Modulus E_i kN/m^2
		$(\sigma_1 - \sigma_3)$ kN/m^2	Axial Strain %	Volume Change %	$(\sigma_1 - \sigma_3)$ kN/m^2	Axial Strain %	Volume Change %	
104	0	164	0.37	---	---	---	---	58,600
107	0	129	0.33	---	---	---	---	58,125
105	103	438	2.09	---	315	12.31	---	74,242
111	103	458	1.75	1.04	326	11.72	4.69	114,568
106	207	757	3.64	0.47	519	13.59	2.33	94,714
108	414	1216	4.97	---	959	19.59	---	151,000
110	414	1204	5.07	0.44	997	16.51	1.27	170,897

Table 5-4

RESULTS OF STATIC TRIAXIAL TESTS ON UNCEMENTED SAND (Dr = 74%)

Sample No.	σ_3 kN/m^2	Peak Strength			Residual Strength			Initial Tangent Modulus E_i kN/m^2	R_f
		$(\sigma_1-\sigma_3)$ kN/m^2	Axial Strain %	Volume Change %	$(\sigma_1-\sigma_3)$ kN/m^2	Axial Strain %	Volume Change %		
1-0	35	103	5.9	1.39	93	19.9	2.87	47,754	0.93
2-0	103	288	5.00	0.56	239	16.5	1.83	65,116	0.87
3-0	207	549	8.5	---	423	21.7	---	95,742	0.9
1-0	310	834	7.5	0.25	635	18.8	1.69	107,393	0.87
5-0	414	1068	6.9	-0.25	887	15.3	0.35	141,317	0.87

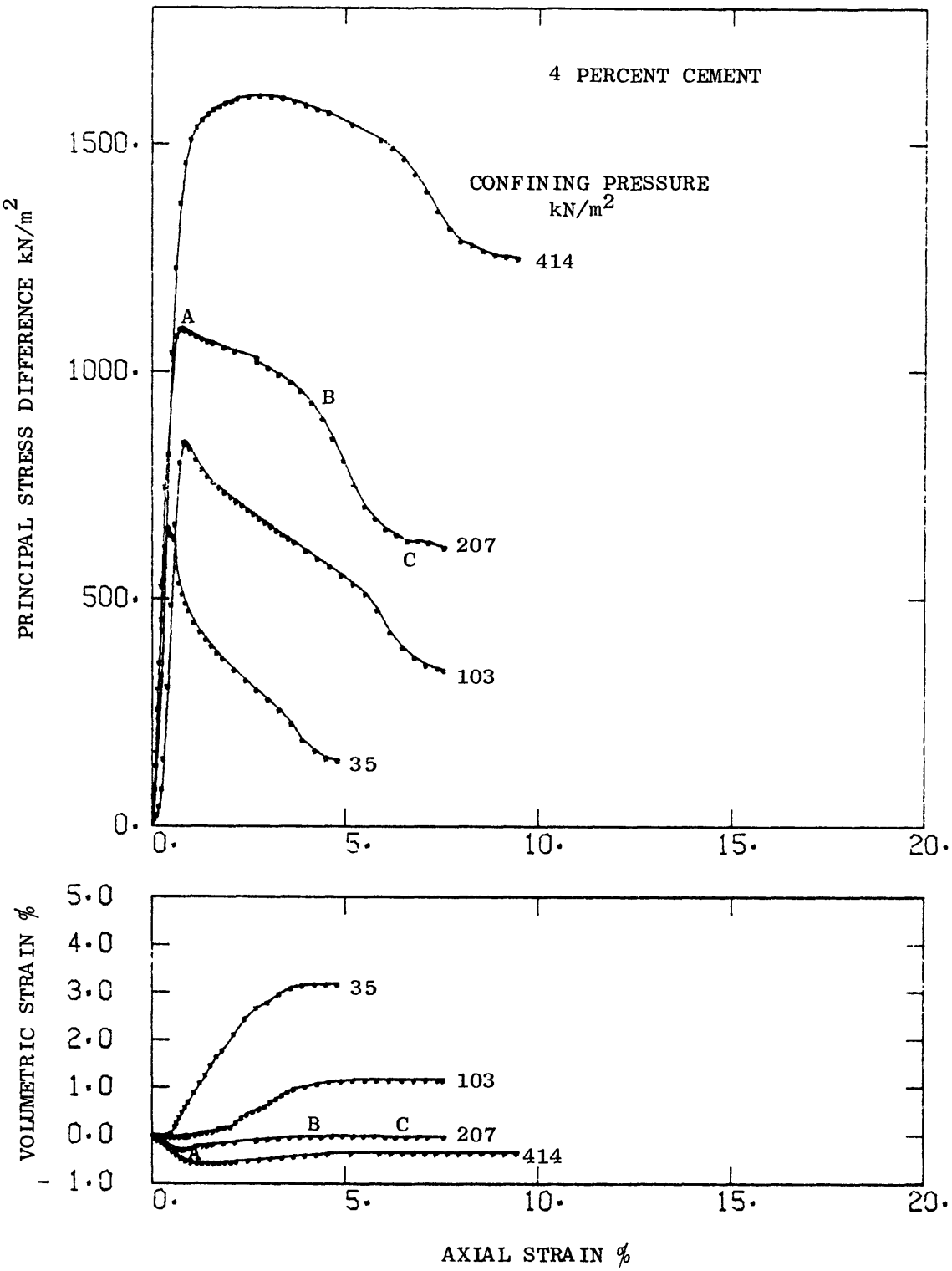

Figure 5-1 REPRESENTATIVE TRIAXIAL STRESS-STRAIN CURVES FOR SAND CEMENTED WITH 4 PERCENT CEMENT (D_r = 74%)

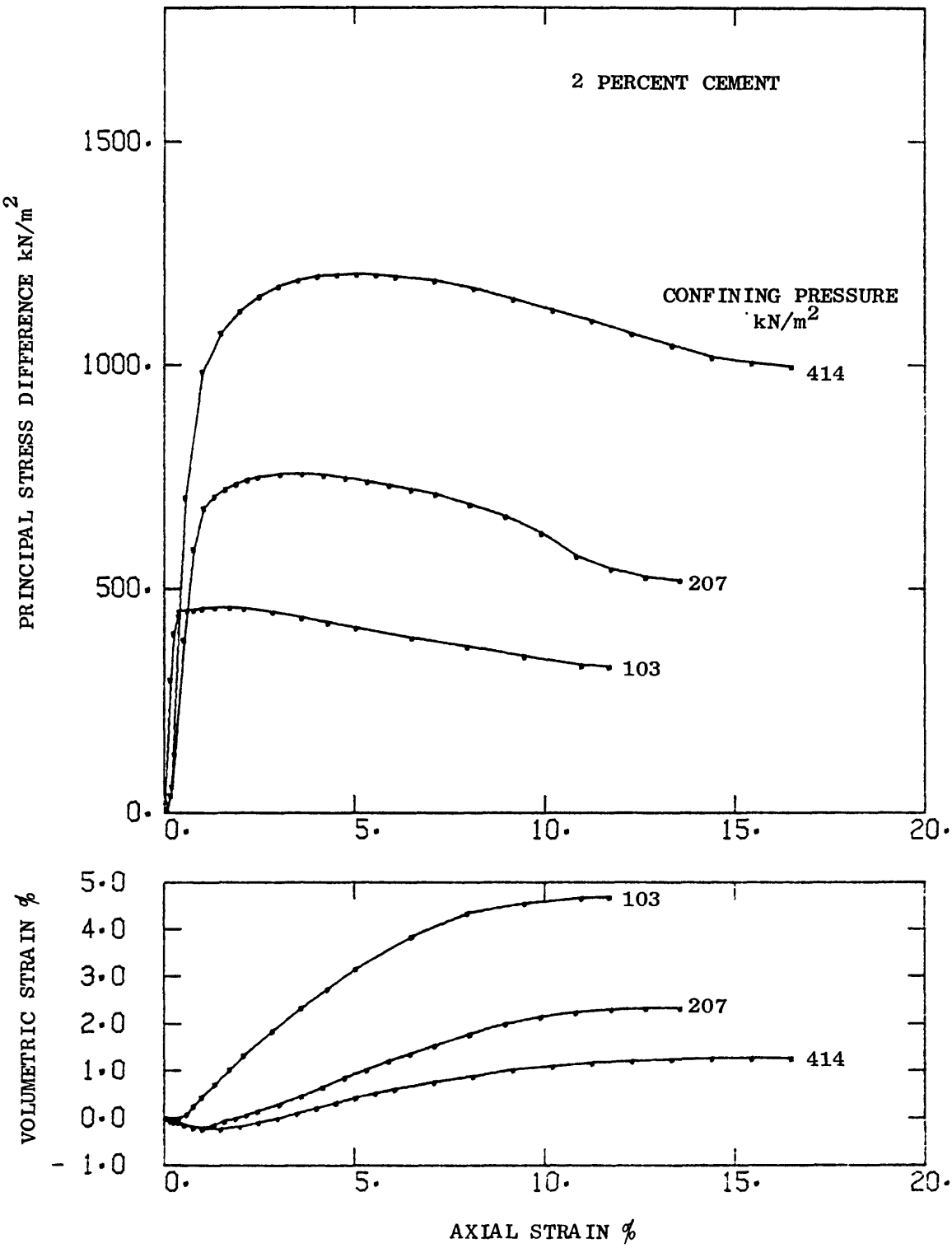

Figure 5-2 REPRESENTATIVE TRIAXIAL STRESS-STRAIN CURVES FOR SAND CEMENTED WITH 2 PERCENT CEMENT (D_r = 74%).

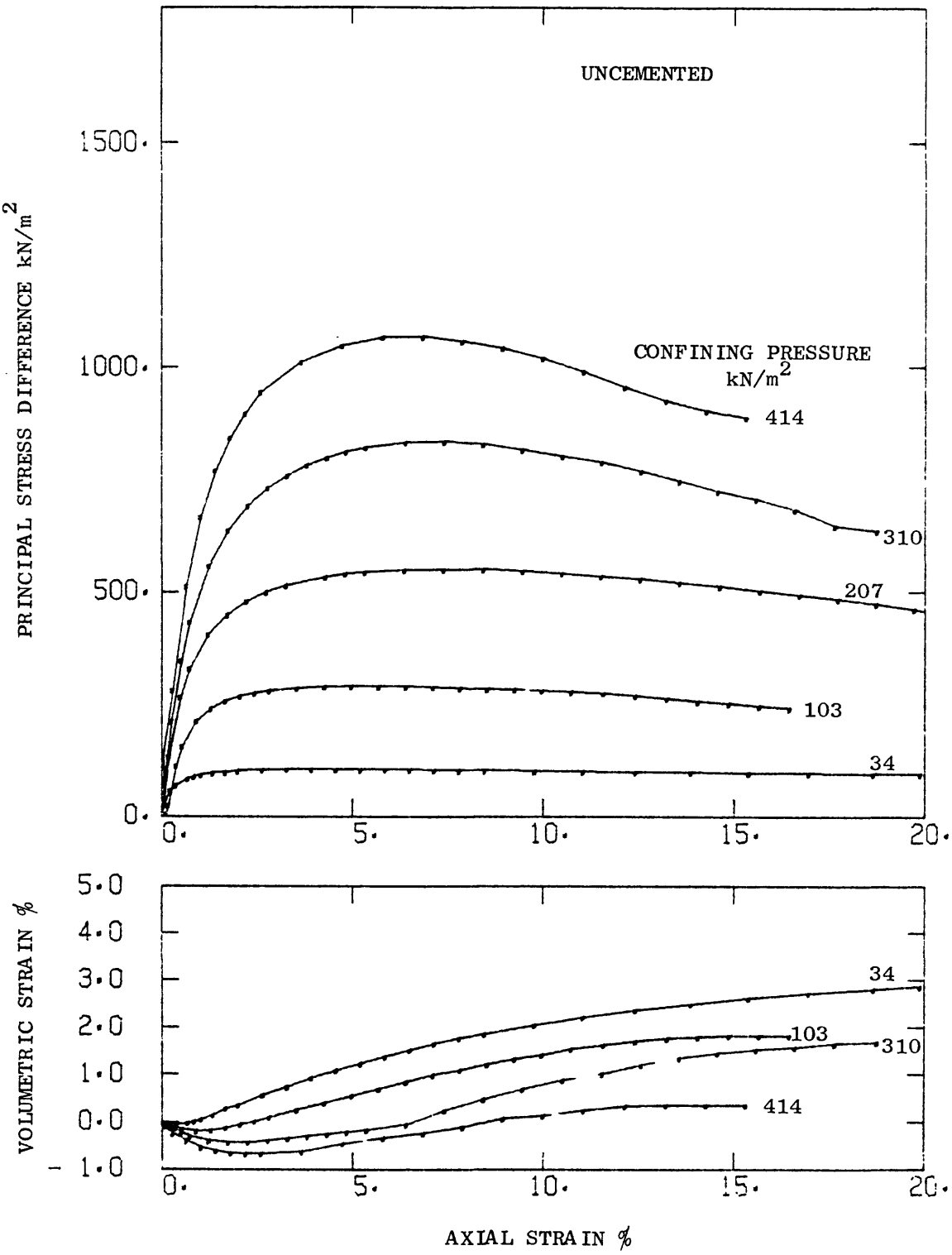

Figure 5-3 TRIAXIAL STRESS-STRAIN CURVES FOR UNCEMENTED SAND (D_r = 74%).

and the soil tends to decrease in volume. The linear soil response is apparently caused by the presence of cementation which prevents intergranular movement during this stage of loading.

Near the peak, the stress-strain response of the soil becomes nonlinear and the post-peak response is characterized by strain softening (points A to C). The nonlinear soil response is initiated by yielding of the cement bonds along the failure plane. Once the cement bonds have yielded (point A), the shear resistance along the failure plane is provided by the intergranular friction of the sand. At low confining pressures, the distance between the opposing surfaces along the failure plane increases in order to allow the sand grains to slip by each other with a relatively small amount of reorientation. This process occurs in the loading interval between points A and B on the stress-strain curve. It is accompanied by a rapid loss of strength and a volumetric expansion. In general, a soil exhibiting these stress-strain characteristics is considered to be brittle.

At higher confining pressures, the forces acting to separate the soil along the failure plane are opposed by the confining pressure and the sand grains are forced to reorient themselves before slippage can occur. Therefore, the amount of volumetric expansion during a triaxial test decreases with increasing confining pressure (see Figures 5-1, 5-2, and 5-3). The work done in rearranging the sand grains along the failure plane is reflected in a more ductile soil response and broader peaks on the stress-strain curves (points A to B)

At point B, the failure plane becomes fully developed, volumetric change stops, and uniform translational movement along the failure plane starts. The shear strength of the soil drops rapidly to its residual level at point C. From point C on, the shear strength of the soil is constant and it is provided largely by the frictional resistance of the sand along the failure plane.

Additional stress-strain and volumetric change curves are presented in Appendix B, Figures B-1 through B-6. These show that the shape of the stress-strain curves is consistent for tests at identical confining pressures and the strengths are generally within ±10 percent of mean. The observed stress-strain behavior of the artificially cemented sands is quite similar to that of the naturally cemented soils described in Chapter III. The soil response is brittle at low confining pressures and becomes more ductile with increasing confining pressures. The range of brittle response of cemented soils varies with the strength of cementation and dry density. For example, the stress-strain curves for sand at 74 percent relative density cemented with 2 percent cement show ductile failure at confining pressures as low as 103 kN/m^2 (Figure 5-2) whereas the sand cemented with 4 percent is still relatively brittle at 414 kN/m^2 (Figure 5-1). Similarly, the stress-strain curves for sand cemented with 4 percent cement but relative densities of 60, 74, and 90 percent presented in Figures 5-1, 5-4, and 5-5 show that the cemented soil response is increasingly more brittle with increasing dry density at all confining pressures. The brittle nature of cemented soils, especially under low confining pressures, is significant in considering the slope response, because levels of the minor principal stress near

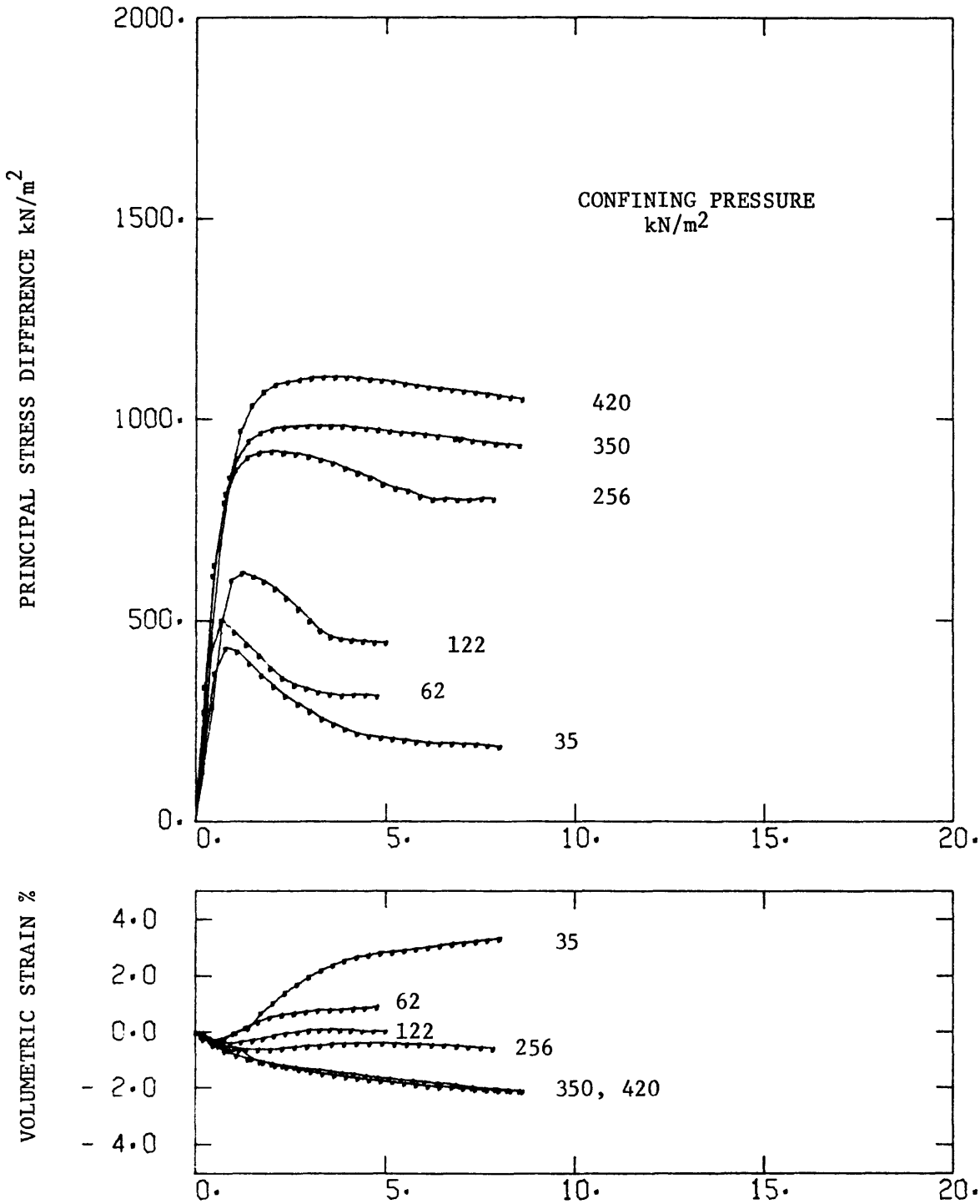

Figure 5-4 REPRESENTATIVE TRIAXIAL STRESS-STRAIN CURVES FOR SAND CEMENTED WITH 4 PERCENT CEMENT (D_r = 60%).

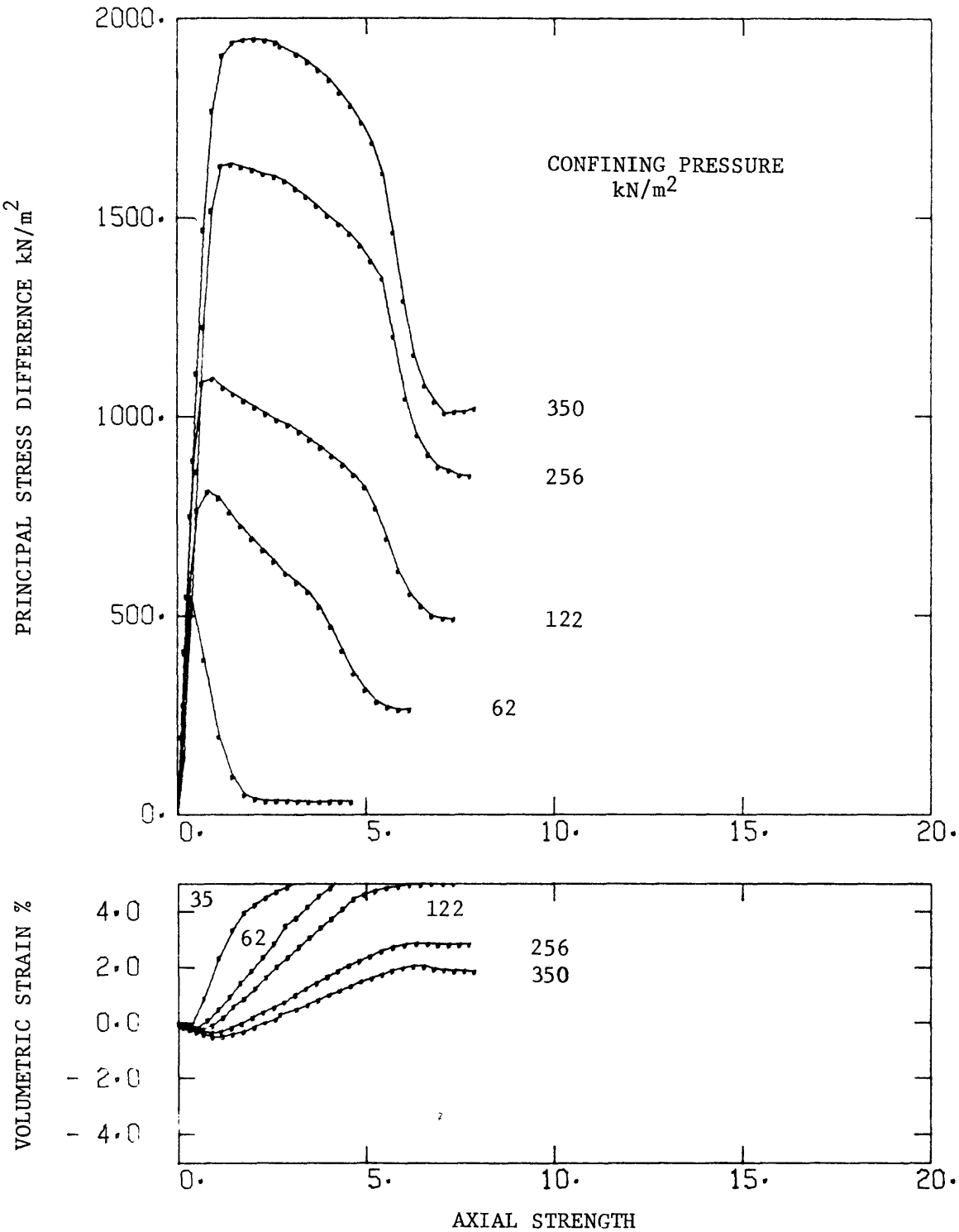

Figure 5-5 REPRESENTATIVE TRIAXIAL STRESS-STRAIN CURVES FOR SAND CEMENTED WITH 4 PERCENT CEMENT (D_r = 90%)

a free slope face are generally very low and the landslides observed in the field are shallow.

An additional distinguishing characteristic of the cemented soil behavior is the initially linear stress-strain response. In contrast, the stress-strain behavior of the uncemented sand is entirely nonlinear at all confining pressures (Figure 5-3). The frictional resistance of the uncemented sand is mobilized gradually and, at low confining pressures, there is very little difference between the peak and residual strengths. At higher confining pressures, the sand exhibits more distinct peak and residual strengths. The difference between the peak and residual strengths represents the work done in rearranging the sand grains along the failure plane.

Strength Characteristics The stress-strain data presented in the previous section show that the peak strength of cemented sand increases with confining pressure, cement content, and dry density. A convenient way of expressing the strength characteristics of the soil as a function of confining pressure and cement content is to plot Mohr failure envelopes. Mohr failure envelopes for the peak strengths of the 4 percent cement, 2 percent cement, and uncemented sand at 74 percent relative density are plotted in Figure 5-6. The parameters which describe the failure envelopes, friction angle, ϕ, cohesion intercept, c, and tensile strength, are given in Table 5-5.

The Mohr envelopes for the cemented soil are essentially straight in compression regime and curved in the tension regime. The shape of the Mohr envelopes can be satisfactorily described using modified

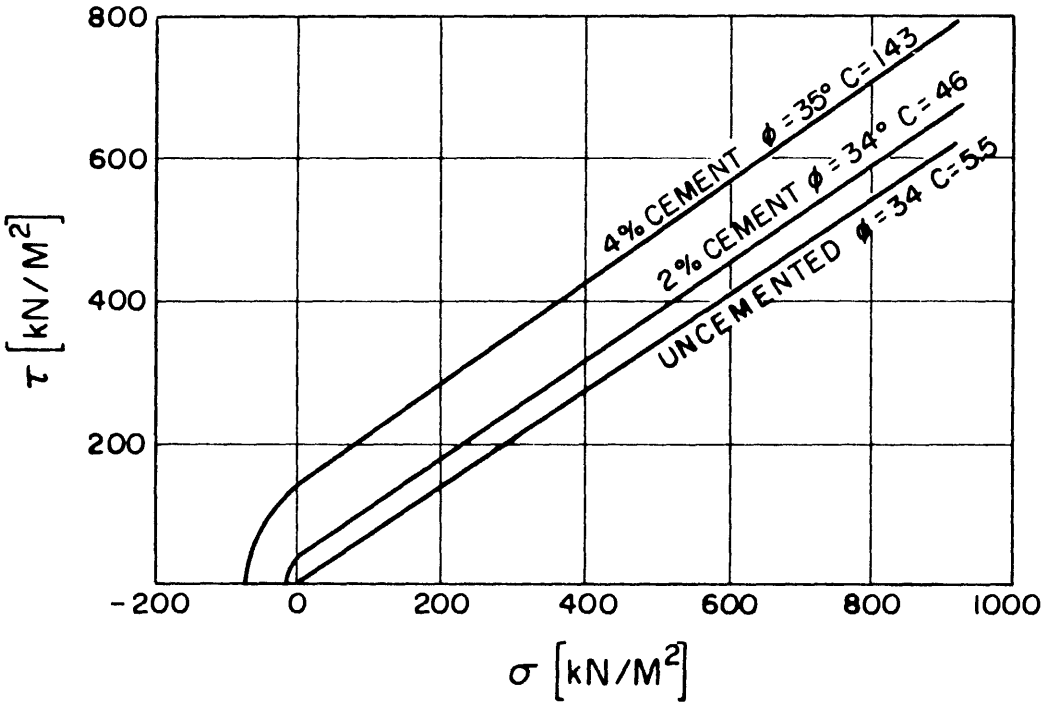

Figure 5-6 MOHR DIAGRAM FOR PEAK STRENGTH FROM TRIAXIAL AND BRAZILIAN TENSION TESTS (D_r = 74%)

Table 5-5

STRENGTH CHARACTERISTICS OF UNCEMENTED
AND ARTIFICALLY CEMENTED SAND

Cement Content %	Dr %	Strength kN/m^2	Average Tensile Strength kN/m^2	Cohesion kN/m^2	Peak ϕ Degrees	Residual ϕ Degrees
0	74	-	-	5.5	34	30.5
2	74	146	20	46	34	31
4	60	-	-	123	28	33
	74			143	35	34.5
	90			152	40.5	36

Griffith theory of failure (Jaeger and Cook, 1976). This theory describes the curved portion of the strength envelope in the tensile stress region by a parabola of the form

$$\tau^2 + 4T\sigma - 4T^2 = 0 \quad \text{for} \quad \sigma < 0 \tag{2}$$

where τ is shear stress, T is tensile strenth, and σ is normal stress; and also requires that

$$\sigma_{uc} = -8T \tag{3}$$

where σ_{uc} is unconfined compressive strength. The tensile strength of the cemented soils as determined from Brazilian tension tests is one seventh of the unconfined compressive strength (see Table 5-5), and the cohesion intercept (τ at $\sigma = 0$) is about twice the tensile strength. Equations (1) and (2) are both fairly well satisfied. This finding agrees with Mitchell's (1976) observations of strength envelopes for cement stabilized soils. In the compressive stress region the modified Griffith and the Coulomb theories are identical and the linear shape of the strength envelope can be described in terms of the friction angle, ϕ, and cohesion intercept, c, by equation

$$\tau = c + \sigma \tan \phi \quad \text{for} \quad \sigma > 0 \quad . \tag{4}$$

The peak friction angle ranges from 28 to 41 degrees for the soils at 60 and 90 percent relative densities, respectively and the frictional resistance accounts for a substantial portion of the peak strength. The peak friction angle is found to increase with increasing dry density

as illustrated in Figure 5-7, however, it seems to be independent of the amount and strength of cementation. The cohesion intercept, on the other hand, increases both as a result of increasing amount of cementation and increasing dry density as shown in Table 5-5 and Figure 5-7.

The friction angles observed in the testing of the denser artificially cemented samples (D_r ~ 75-90°) are consistent with those observed from the tests on naturally occurring weakly cemented samples from both the SLAC and Pacifica sites. Friction angles observed for the strongly cemented sand from the SLAC site which ranged from 47 to 49 , are greater than those for the artificially cemented sands. This may be attributed to the very high density of the strongly cemented sands and the unique interlocking effect noted for the grain structure of the strongly cemented sand.

Initial Tangent Modulus A simple inspection of the stress-strain curves for cemented sands in Figures 5-1 and 5-2 shows that the initial portions of the stress-strain curves are almost linear. Consistent values of initial tangent modulus, E_i can be determined directly as slopes of the initial portion of the stress-strain curves. The E_i values for the sand cemented with 2 and 4 percent cement are included in Tables 5-2 and 5-3, respectively. The stress-strain curves for the uncemented sand, however, are nonlinear, and a direct determination of the initial tangent modulus by drawing a tangent to the initial portion of the stress-strain curve is highly subjective. Instead, a more consistent method suggested by Duncan and Chang (1970) based on the

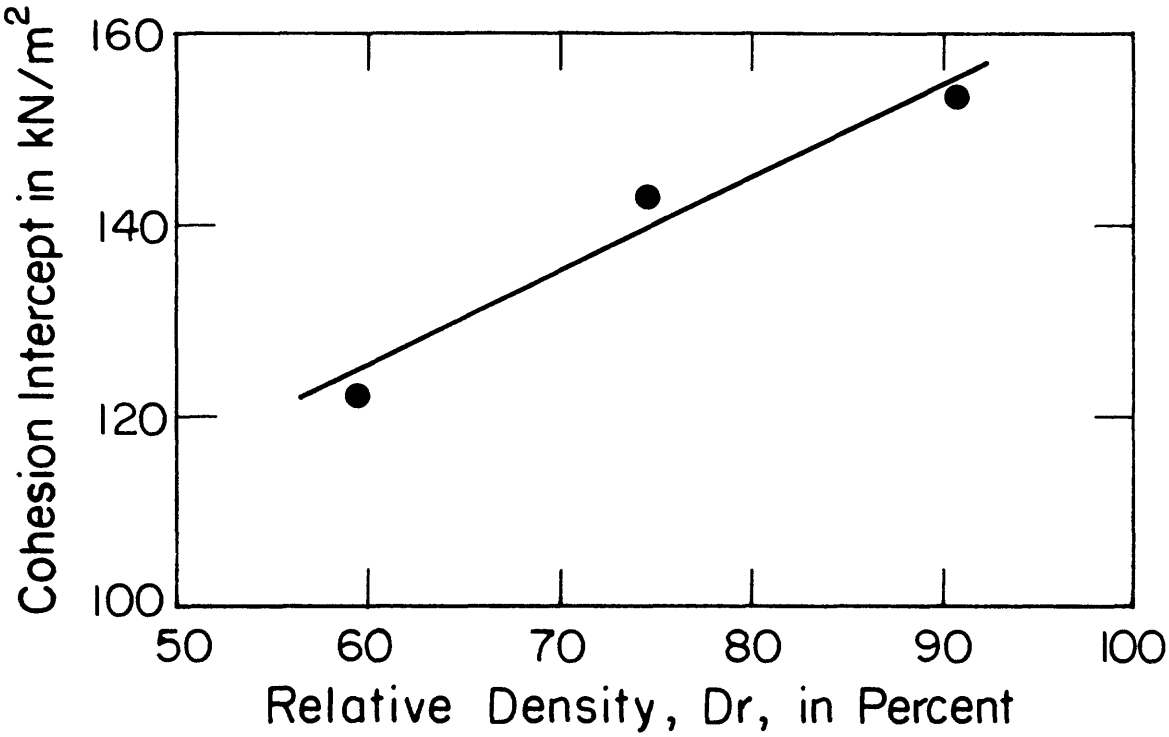

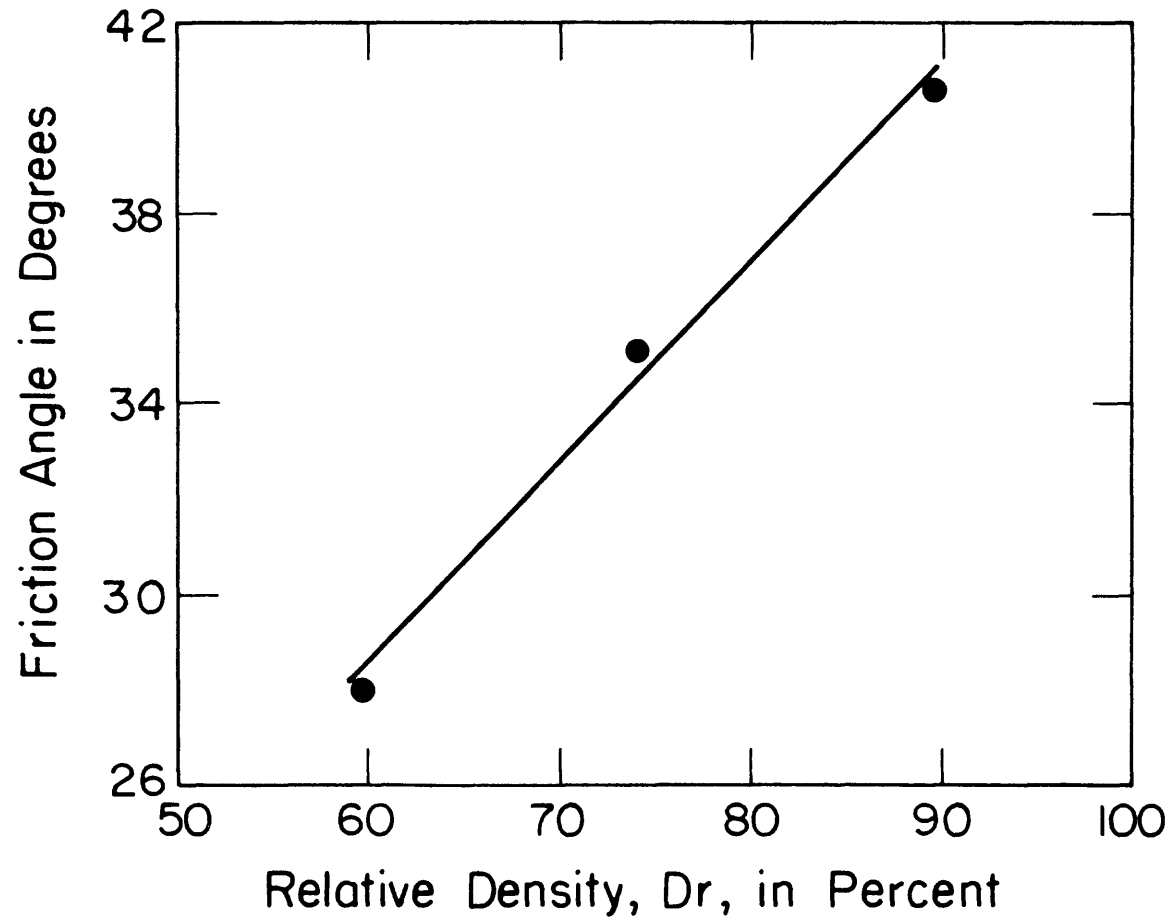

Figure 5-7 VARIATION OF FRICTION ANGLE AND COHESION INTERCEPT WITH RELATIVE DENSITY

assumption that the observed stress-strain curves can be approximated by hyperbolas is used. The extrapolated values of E_i determined by this method are given in Table 5-4.

Soils generally exhibit increasing initial tangent modulus with increasing confining pressure, and the materials tested for this study are no exception. The average E_i values at different confining pressures for the uncemented and cemented sands at relative density of 74 percent are presented in Table 5-6. In Figure 5-8 the E_i and σ_3 are normalized by atmospheric pressure and plotted using log scales for both axes. As was the case for the naturally cemented sands, the data follow a straight line on this plot showing E_i to increase with σ_3. The value of $K = 700$ (E_i value at $\sigma_3/Pa = 1$) for the uncemented sand is well within the range given by Wong and Duncan (1974). The K values of 860 and 1960 for the sand cemented with 2 and 4 percent cement, respectively, are at the lower end of the range for cemented treated soils reported by Mitchell (1976). The increase in K with increasing cement content is not surprising since the value of K is directly proportional to E_i. The values of n (slope of the straight line) decrease from 0.43 to 0.19, with cement content increasing from 0 to 4 percent. This indicates that, in the triaxial tests, the influence of confining pressure on the initial tangent modulus decreases with increasing cement content.

Summary The triaxial and Brazilian tension test results shows that the artificially cemented samples behave in a manner very similar to that of the naturally cemented soils described in Chapter III. However, general response trends are defined better for the artificial samples

Table 5-6

INFLUENCE OF CONFINING PRESSURE ON INITIAL TANGENT MODULUS, E_i (D_r = 74%).

Confining Pressure (kN/m^2)	Average Initial Tangent Modulus, E_i (kN/m^2)		
	Uncemented	2% Cement	4% Cement
0	---	58,400	124,200
35	47,800	---	169,000
103	65,100	94,400	181,000
207	95,700	94,700	218,900
310	107,400	---	267,400
414	141,300	160,900	258,600

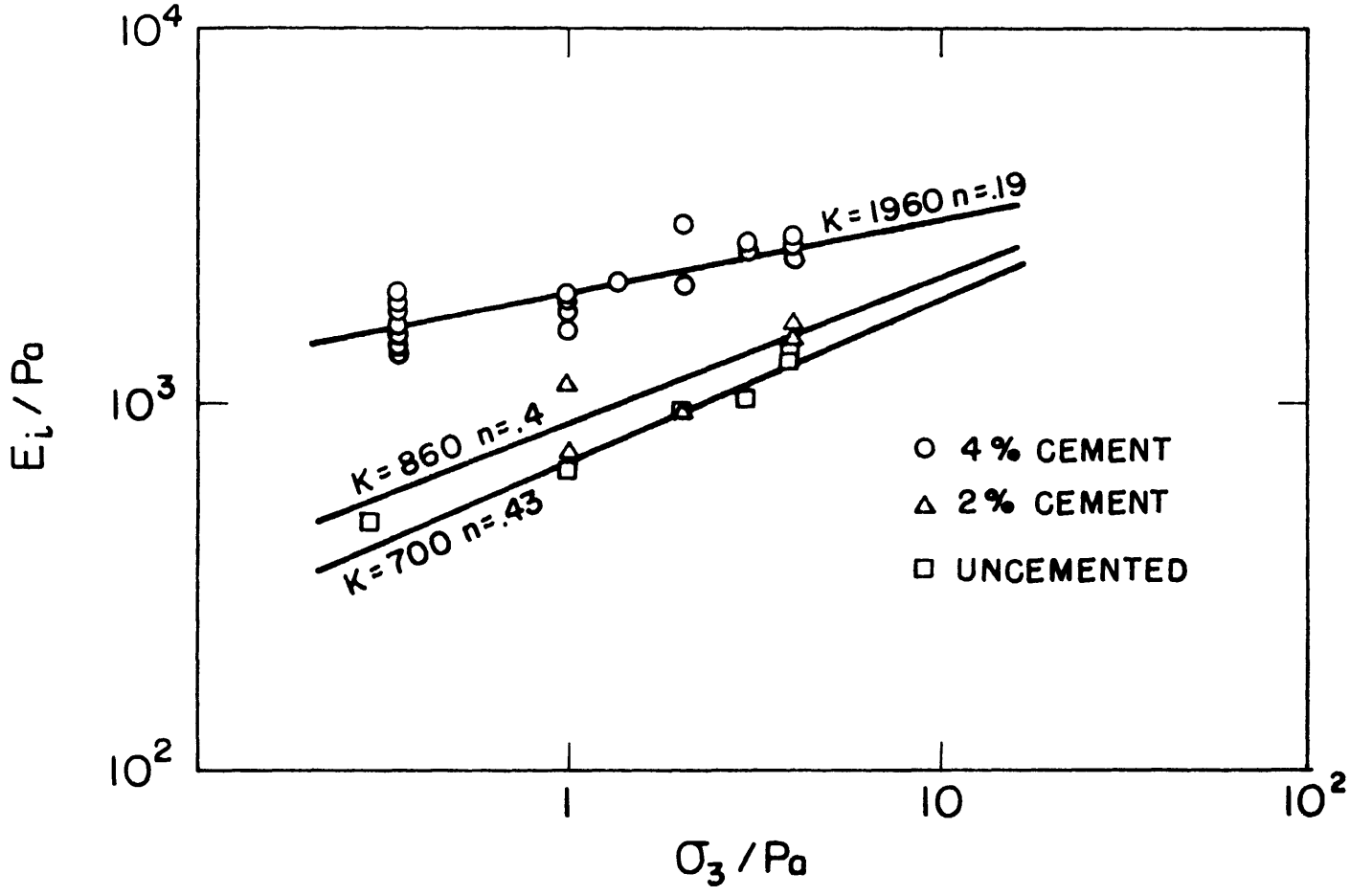

Figure 5-8 VARIATION OF INITIAL TANGENT MODULUS WITH CONFINING PRESSURE

because their properties are more uniform. It is apparent from the results that the pre-failure behavior of a cemented sand is strongly influenced by the cementation agent, while the post-failure behavior is most affected by the sand after the cementation bonds are broken. This is reflected by the fact that the initial tangent modulus values of the cemented sands are very much greater than those of the uncemented sand, but the friction angles, reflecting failure conditions, are essentially the same. The failure envelopes of the cemented sands are most different from those of the uncemented sand by the presence of a cementation intercept and a tensile strength.

Small increases of cementation agent are found to significantly increase the cementation intercept and tensile strength but not to affect the friction angle. Increases in density lead to increases in both friction angle and cementation.

5.2.2 Unconfined Simple Shear

Unconfined static simple shear tests were performed on samples cemented with 2 and 4 percent cement at 74 percent relative density. Normal stresses ranging from 35 to 310 kN/m^2 were used, and stress-strain curves and strengths were obtained. The test results consisting of shearing stress at failure, shear strain at failure, computed principal stresses at failure, and initial shear moduli are given in Table 5-7.

A set of representative stress-strain curves plotted in Figure 5-9 shows that the peak strength and the ductility of the soil increase with increasing normal stress and the soil becomes more brittle with increasing cement content. The initial shear modulus also appears to

Table 5-7

RESULTS OF STATIC SIMPLE SHEAR TESTS ON ARTIFICIALLY CEMENTED SAND WITH 74 PERCENT RELATIVE DENSITY

Test No.	Cement %	σ_n kN/m^2	τ_f kN/m^2	γ_f %	σ_{3f}^* kN/m^2	σ_{1f}^* kN/m^2	G_i kN/m^2
1	4	103	152	-	-77	231	-
2	4	103	157	-	-82	236	-
3	4	207	189	-	-41	351	-
4	4	207	191	-	-43	353	-
5	4	310	237	-	-17	482	-
6	4	310	238	-	-18	483	-
7	4	414	249	-	41	580	-
8	4	414	267	-	24	597	-
9	4	103	154	.43	-79	233	100 000
10	4	103	151	.46	-76	230	87 000
11	4	207	228	.50	-79	389	111 100
12	4	310	279	.69	-57	522	94 800
13	2	207	109	1.85	35	276	71 400
14	2	103	66	.61	6	148	62 500
15	2	35	43	.36	-17	70	48 800

*Computed assuming $k_o = .5$

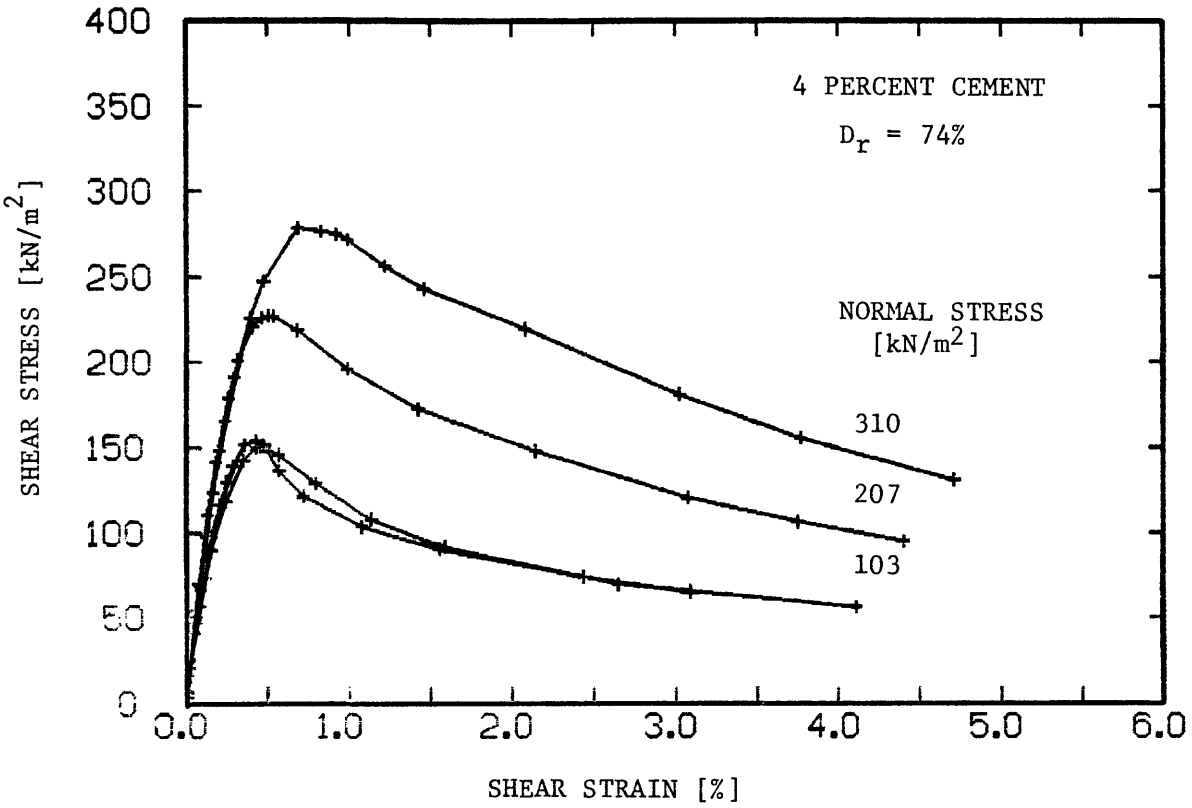

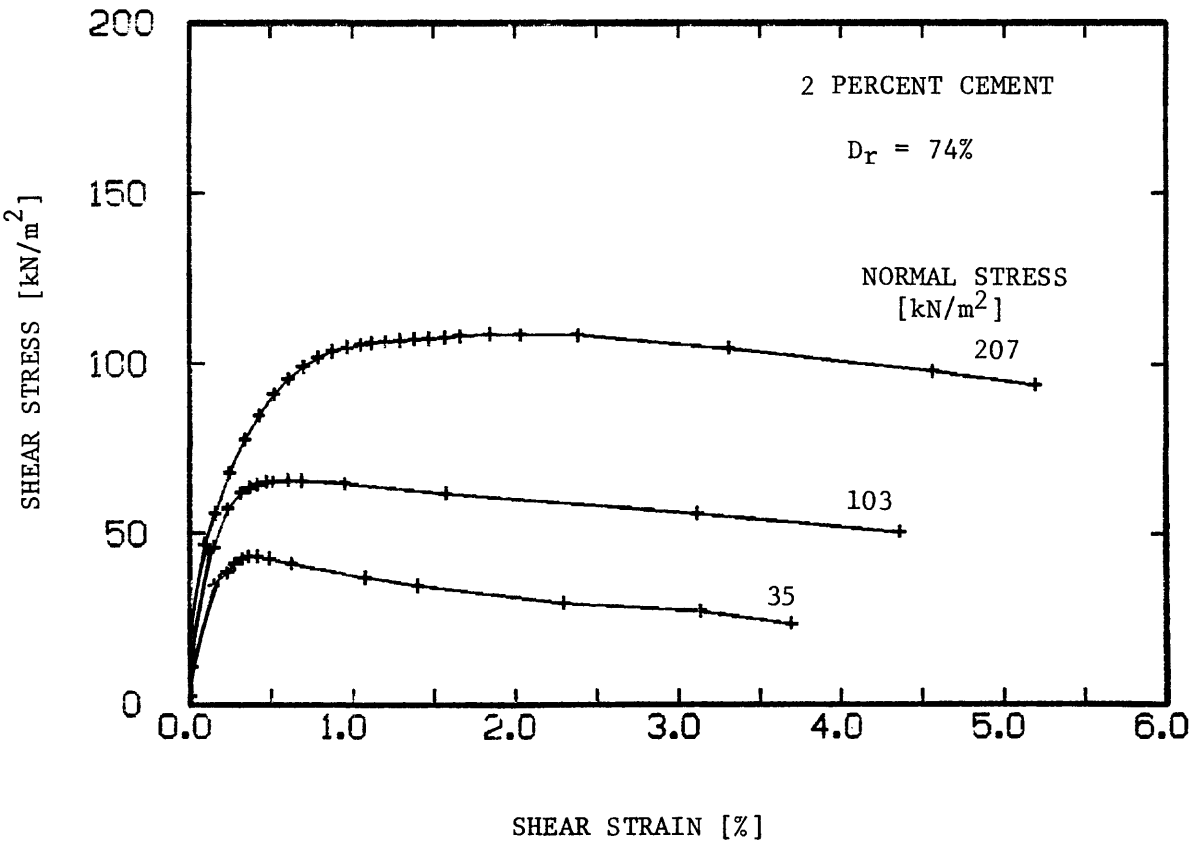

Figure 5-9 REPRESENTATIVE UNCONFINED SIMPLE SHEAR STRESS-STRAIN CURVES FOR ARTIFICIALLY CEMENTED SAND

increase with increasing normal stress although the data is fairly scattered and limited (Table 5-7). In general, the stress-strain response of the artificially cemented sand in the unconfined simple shear tests is qualitatively similar to that observed in the triaxial tests.

The strength data obtained from the tests were interpreted assuming that the application of the normal load on a specimen results in a lateral k_o stress. The mechanism by which the k_o stress is generated in these tests is discussed in Section 4.3 and Appendix C. A value of $k_o = .5$ was chosen as the most appropriate and the resulting Mohr circles representing the stresses at failure in the individual tests are drawn in Figure 5-10. Although there is some scatter in the results, a comparison with the failure envelopes obtained from the triaxial and Brazilian tension tests shows a reasonable correlation. Thus, the results indicate that the simple shear test does provide the capability to define a continuous failure envelope in both the compressive and tensile stress region. However, it is desirable in future work to obtain a better control of the k_o stress during the tests by redesigning the equipment.

5.3 Dynamic Test Results

The range of confining pressures in the cyclic triaxial compression tests and the range of the normal stresses in the cyclic unconfined simple shear tests were the same as used in the static tests. Data consisting of cyclic stress levels, cyclic stress-strain curves, and number of loading cycles were collected during both types of tests.

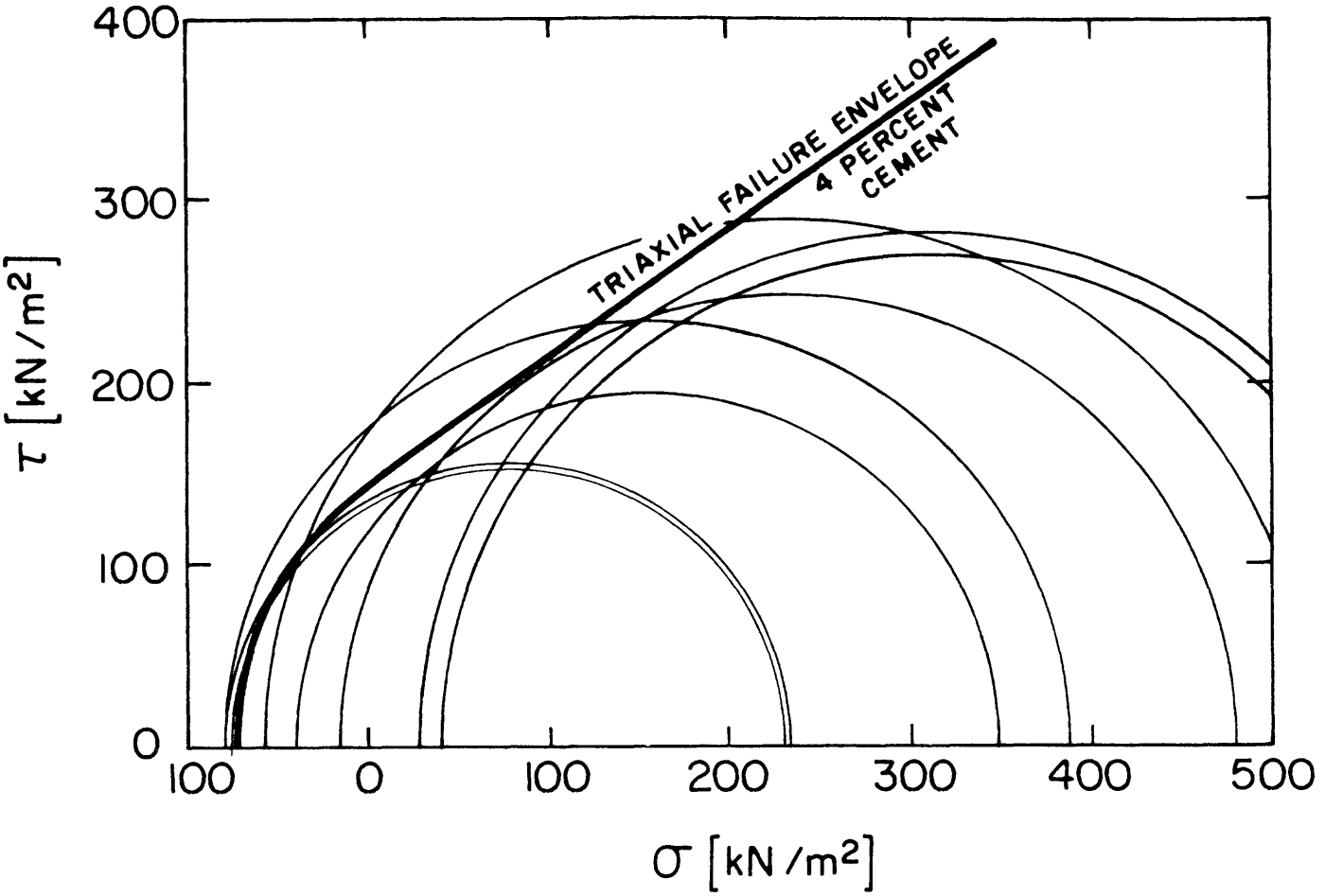

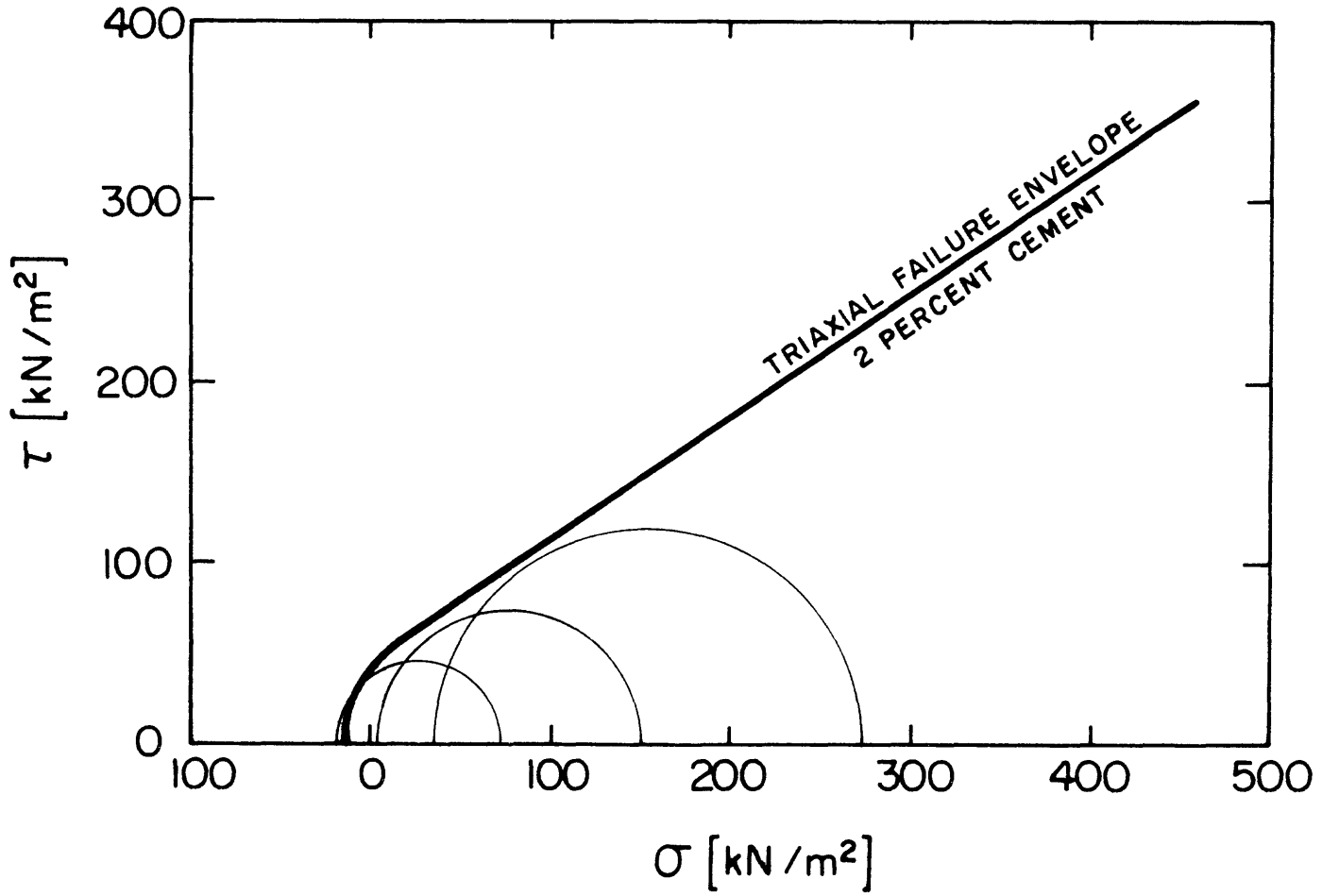

Figure 5-10 MOHR CIRCLES AT PEAK STRENGTH FROM UNCONFINED SIMPLE SHEAR TESTS ON ARTIFICIALLY CEMENTED SAND AT 74 PERCENT RELATIVE DENSITY.

5.3.1 Cyclic Triaxial Compression

The samples tested in the cyclic triaxial compression tests were subjected to an initial static shear stress ranging from 5 to 90 percent of the static shear stress at failure. The dynamic load was then applied. The reason for this procedure was that, in slopes, soil is subjected to varying levels of shear stress due to the anisotropic static principal stress distribution and, during earthquakes, the dynamic stresses are superimposed on the existing static stresses. Thus, the influence, if any, of the initial static shear stress on the dynamic strength of the cemented soil had to be investigated.

The values of the initial static shear stress $(\sigma_1 - \sigma_3)$ and the values of the dynamic $(\sigma_1 - \sigma_3)$ at failure can be normalized by dividing by the static $(\sigma_1 - \sigma_3)$ at failure. The normalized values of the initial static shear stress, the dynamic stress at failure, and the number of cycles to failure for individual tests are presented in Table 5-8. Figure 5-11 shows the relationship between the dynamic triaxial strength and the initial shear stress applied to the sample. Two trends emerge upon examination of Figure 5-11: (1) In all cases, regardless of confining pressure or level of initial static shear stress, the dynamic compressive shear strength is slightly larger than the corresponding value of the static shear strength; and (2) the dynamic compressive shear strength is apparently independent of the initial static shear stress.

In Figure 5-12, the dynamic to static shear strength ratio is plotted versus the number of cycles to failure. The results suggest that the dynamic shear strength is not strongly affected by the number of loading cycles. Again, it is apparent that the dynamic shear

Table 5-8

RESULTS OF CYCLIC TRIAXIAL TESTS ON SAND CEMENTED WITH 4 PERCENT CEMENT

Sample No.	σ_3 kN/m^2	$\frac{(\sigma_1-\sigma_3)\ \text{Initial}}{(\sigma_1-\sigma_3)_f\ \text{Static}}$	$\frac{(\sigma_1-\sigma_3)_f\ \text{Dynamic}}{(\sigma_1-\sigma_3)_f\ \text{Static}}$	Number of Cycles to Failure
61	0	0.90	1.2	49
68	34.5	0.06	1.10	174
69	34.5	0.06	1.16	27
70	34.5	0.05	1.30	1
71	34.5	0.81	1.14	166
72	34.5	0.80	1.23	2.5
73	34.5	0.80	1.23	2.5
74	34.5	0.83	1.22	41.5
75	34.5	0.83	1.23	151.5
76	34.5	0.80	1.19	20.5
77	34.5	0.81	1.20	264
78	207	0.20	1.03	>153
79	207	0.33	1.12	36.5
80	207	0.42	1.24	1.5
81	207	0.30	1.07	35.5
82	207	0.78	1.18	0.5
83	207	0.79	1.14	0.5
90	414	0.24	0.97	>272
91	414	0.32	1.05	17
92	414	0.36	1.02	>185
93	207	0.31	1.09	68
94	414	0.24	1.02	0.5
95	414	0.78	1.09	26
97	414	0.80	1.07	0.5
98	207	0.37	1.11	0.5
99	207	0.38	1.04	3
102	414	0.85	1.12	>179
103	414	0.82	1.11	6

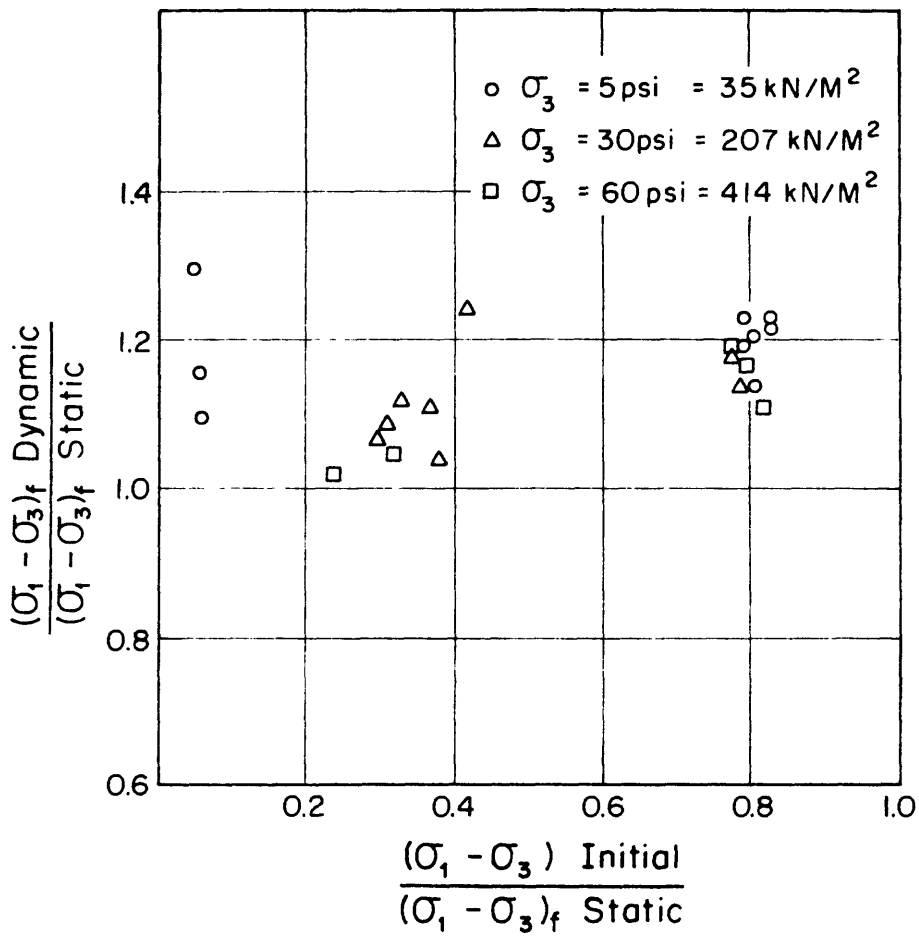

Figure 5-11 RELATIONSHIP BETWEEN DYNAMIC AND STATIC COMPRESSIVE STRENGTH AS A FUNCTION OF THE AMOUNT OF INITIAL SHEAR STRESS APPLIED TO SAMPLE.

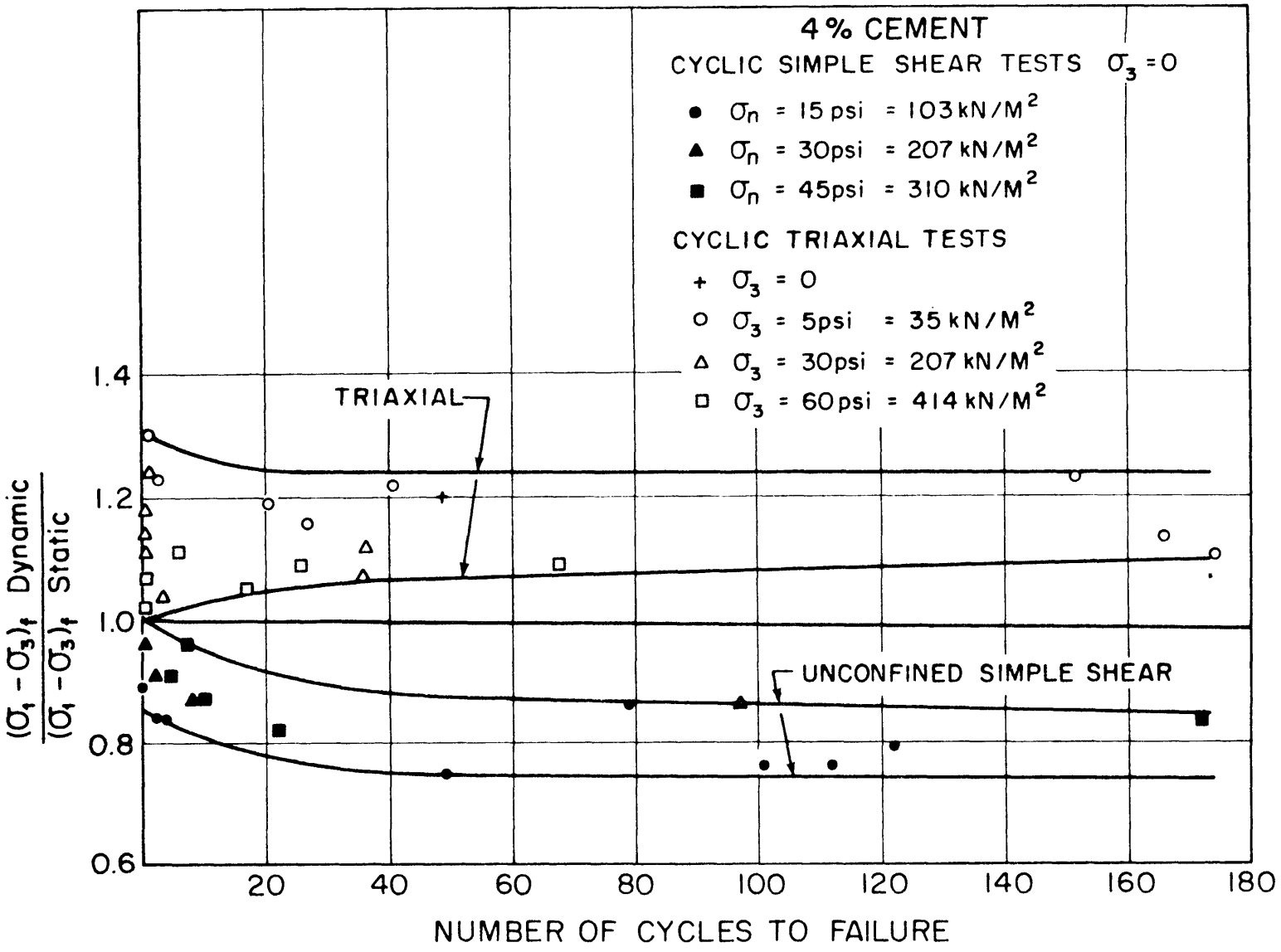

Figure 5-12 RELATIONSHIP BETWEEN DYNAMIC AND STATIC COMPRESSIVE STRENGTH AS A FUNCTION OF NUMBER OF LOADING CYCLES.

strength of the cemented soil subjected to cyclic triaxial tests is greater than the corresponding static shear strength.

The stress-strain response of the cemented soil in the cyclic triaxial tests is illustrated in Figure 5-13. In this case, a confining pressure of 207 kN/m^2 was used and initial static shear stress corresponding to about 38 percent of the static shear stress at failure was applied. The sample was then subjected to dynamic axial loading at a rate of 1 Hz. The failure occurred suddenly and the only indication of its approach was provided by the relatively large amount of essentially plastic yielding at the top of the previous loading cycle. At lower confining pressures or at lower cyclic stress levels, the yielding is more uniformly distributed between load cycles and the failure tends to be explosive, without any prior warning.

Interestingly, the dynamic unload-reload modulus does not deteriorate significantly with the number of load cycles or prior to failure (see Figure 5-13). However, the dynamic unload-reload modulus does decrease with increasing amplitude of the cyclic axial strain. The values of dynamic unload-reload modulus, corresponding cyclic axial strain amplitude, and ratios of dynamic modulus to static initial tangent modulus are presented in Table 5-9. The relationship between the ratio of the dynamic modulus to the static initial tangent modulus and the amplitude of cyclic axial strain is illustrated in Figure 5-14, it is evident that, although the dynamic unload-reload modulus decreases with the increasing amplitude of the cyclic axial strain, it is more than ten

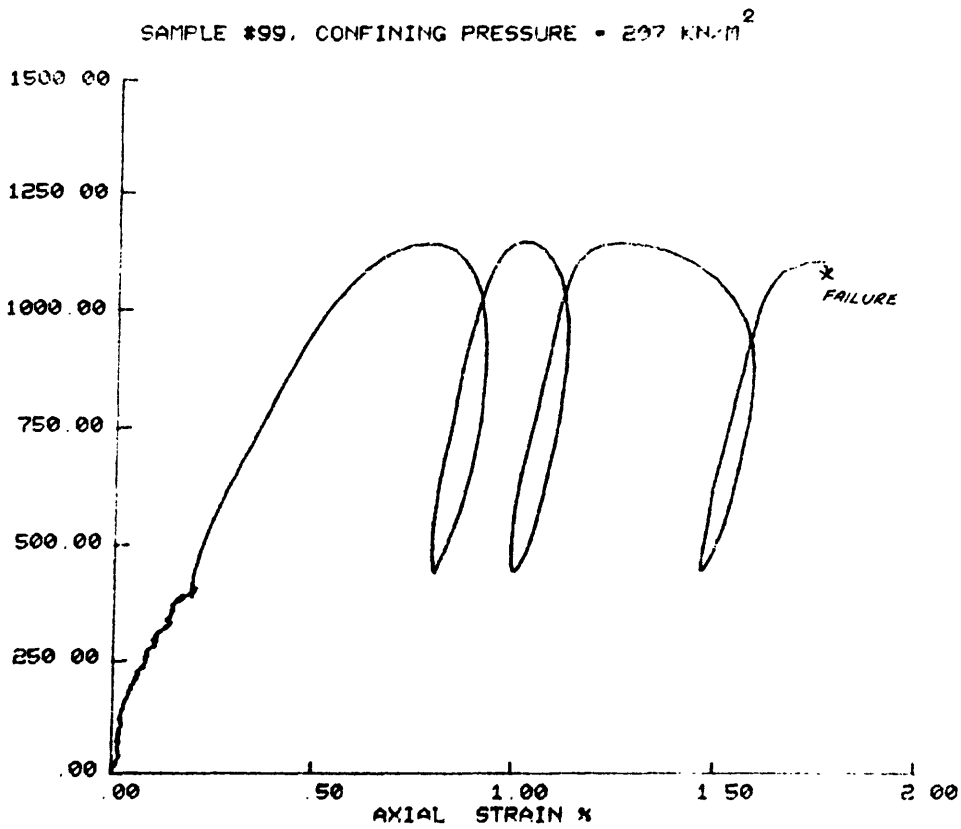

Figure 5-13 TYPICAL STRESS-STRAIN CURVE FROM A CYCLIC TRIAXIAL COMPRESSION TEST.

Table 5-9

DYNAMIC MODULUS AND CYCLIC AXIAL STRAIN VALUES OBTAINED FROM CYCLIC TRIAXIAL TESTS ON SAND CEMENTED WITH 4 PERCENT CEMENT

Sample No.	σ_3 kN/m^2	Cyclic Axial Strain [%]	Dynamic Modulus kN/m^2	Dynamic Modulus / Static Initial Tangent Modulus	Cycle No.
70	35	0.39	210,497	1.3	1
73	35	0.02	1,683,333	10.0	2
78	207	0.12	763,636	3.5	5
79-1	207	0.06	1,587,500	7.3	5
79-2	207	0.08	1,133,929	5.2	35
80	207	0.07	1,260,000	5.8	2
81	207	0.02	3,150,000	14.4	29
82	207	0.27	325,862	1.5	1
90-1	414	0.16	724,956	2.8	2
90-2	414	0.18	688,814	2.7	31
91	414	0.15	738,909	2.9	10
93	414	0.29	325,244	1.3	50
95	414	0.01	4,445,000	17.2	2
99	414	0.14	488,461	1.9	2
102	414	0.03	1,760,221	6.8	40

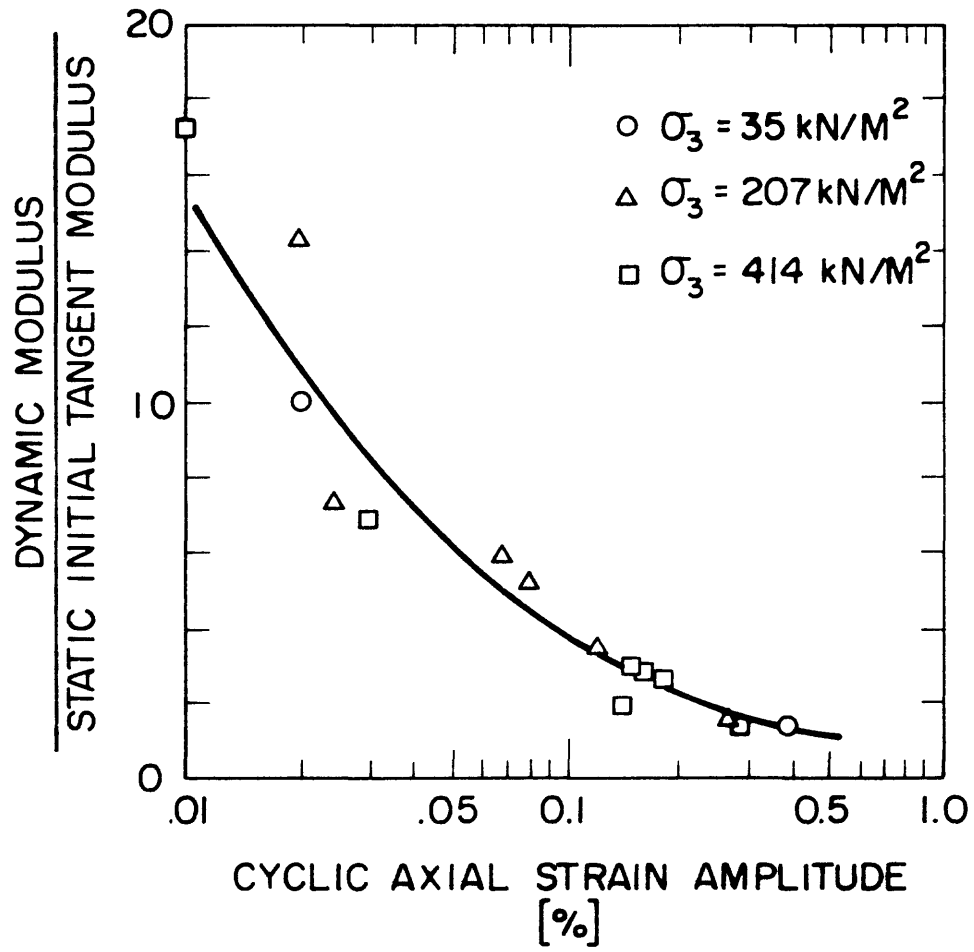

Figure 5-14 DYNAMIC TANGENT MODULUS AS A FUNCTION OF CYCLIC AXIAL STRAIN IN CYCLIC TRIAXIAL TESTS.

times higher than the static initial tangent modulus at strain levels of less than 0.02 percent and over four times higher at strains of less than 0.1 percent.

5.3.2 Cyclic Unconfined Simple Shear

The results of the cyclic unconfined simple shear tests are markedly different from the results of the cyclic triaxial tests. The dynamic shear strength is consistently lower than the shear strength from equivalent static tests (see Figure 5-12). Also, the dynamic-to-static shear strength ratio from the simple shear tests decreases with increasing number of load cycles. The reason for this difference apparently lies in the fact that the unconfined simple shear loading produces a partial state of tension in the soil, and repeated tension loadings have a more destructive effect than repeated compression loadings. This finding is supported by the results of two cyclic Brazilian tension tests which show that the dynamic tensile strength is lower than the static tensile strength (see Table 5-10).

Table 5-10

CYCLIC BRAZILIAN TENSION TEST RESULTS

Sample No.	$\frac{\sigma_T \text{ Cyclic}}{\sigma_T \text{ Static}}$	Number of Cycles to Failure
100	0.86	2.5
101	0.61	11.5

A typical stress-strain curve from a cyclic unconfined simple shear test is given in Figure 5-15. For each cycle of loading and unloading, a hysteresis loop is formed. The slope of a straight line connecting the extreme ends of a hysteresis loop (AB in Figure 5-15) is the equivalent linear shear modulus. The equivalent viscous damping ratio can be determined using the following expression (Jacobsen, 1930):

$$\text{DAMPING RATIO} = \frac{\text{Area of Hysteresis Loop AB}}{2\pi \times (\text{Area OBC} + \text{Area OAD})} \qquad (5)$$

The values of shear moduli, damping ratios, and corresponding cyclic shear strain levels together with all other information about the tests are presented in Table 5-11.

In general, the test results show that the shear modulus of the cemented soil decreases with increasing number of loading cycles and with increasing levels of shear strain. Figure 5-16 illustrates the degradation of the shear modulus with increasing cyclic shear strain. The shear modulus values are different for each given normal stress level; however, the rate of degradation appears to be similar. In Figure 5-17, the damping ratio is plotted versus the cyclic shear strain. In this case, the damping ratio increases from about 13 percent at 0.1 percent strain to 28 percent at about 0.55 percent strain. The influence of the initial normal stress on the damping ratio appears to be negligible.

A comparison of the dynamic simple shear data for cemented sand with the results obtained by Seed and Idriss (1969) for uncemented sand at the same relative density shows: (1) the dynamic shear modulus of the cemented sand is much higher than the dynamic shear modulus of uncemented sand (see Figure 5-15) and (2) the damping ratio for the cemented sand

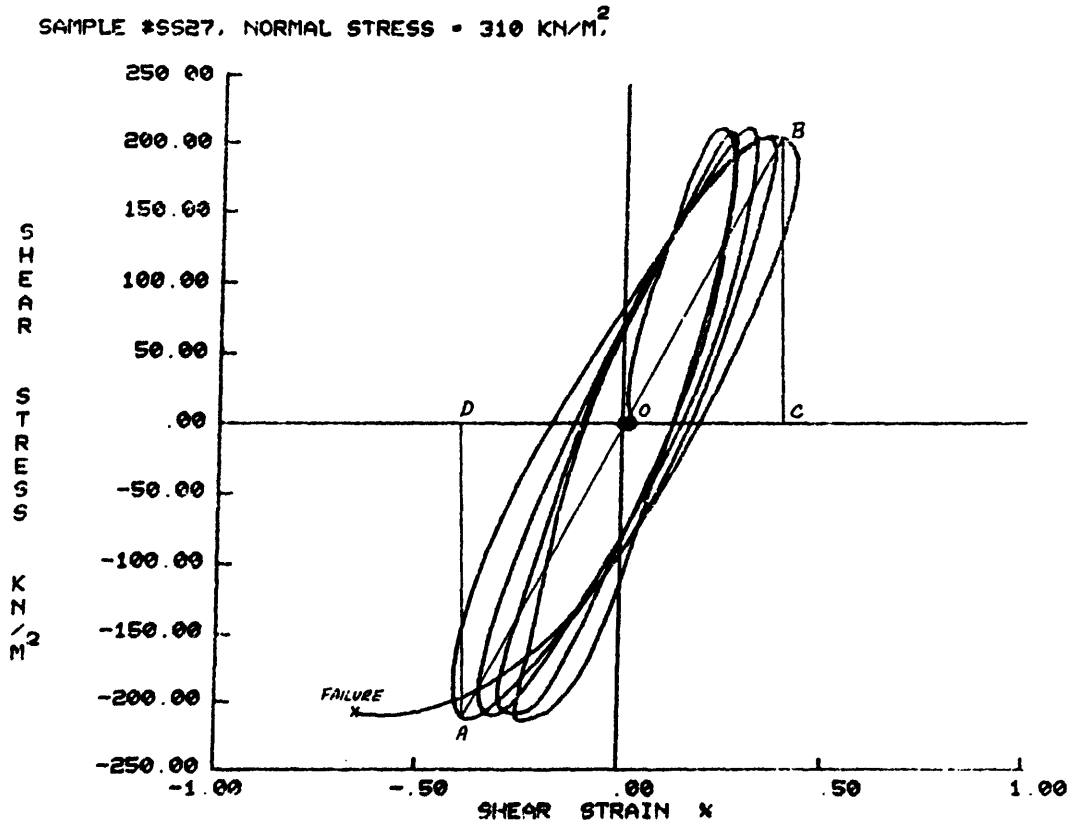

Figure 5-15 TYPICAL STRESS-STRAIN CURVE FROM A CYCLIC UNCONFINED SIMPLE SHEAR TEST.

Table 5-11

RESULTS OF CYCLIC UNCONFINED SIMPLE SHEAR TESTS ON SAND CEMENTED WITH 4 PERCENT CEMENT

Sample Number	σ_n (kN/m^2)	Cyclic Shear Strain (%)	Shear Modulus (kN/m^2)	Damping Ratio (%)	Cycle Number	$\frac{(\sigma_1-\sigma_3)_f \text{ Dynamic}}{(\sigma_1-\sigma_3)_f \text{ Static}}$	Number of Cycles to Failure
11	103	*	*	*	*	0.55	14
12	103	*	*	*	*	0.84	3.5
13	103	*	*	*	*	0.61	>200
15	103	*	*	*	*	0.76	101
16	103	*	*	*	*	0.79	122
17	103	*	*	*	*	0.76	112
18	103	*	*	*	*	0.84	2.5
19	310	*	*	*	*	0.83	172
20	310	*	*	*	*	0.96	7.5
22	103	0.23	59,500	*	0.5	0.89	0.5
23	103	0.133	84,300	16.0	1-4	0.74	49.5
25-1	103	0.117 0.141 0.143 0.148 0.158 0.164	99,000 84,400 80,800 79,000 73,799 69,700	14.7 13.7 14.4 15.4 14.7 15.1	1 6 22 31 46 85	0.80	>142

Table 5-11

CONTINUED

Sample Number	σ_n (kN/m^2)	Cyclic Shear Strain (%)	Shear Modulus (kN/m^2)	Damping Ratio (%)	Cycle Number	$\frac{(\sigma_1-\sigma_3)_f \text{ Dynamic}}{(\sigma_1-\sigma_3)_f \text{ Static}}$	Number of Cycles to Failure
25-2	103	0.197	64,500	14.1	3	0.86	79
		0.209	61,200	14.4	9		
		0.208	61,200	14.9	16		
		0.230	55,300	15.5	31		
		0.281	44,100	16.6	58		
		0.318	39,400	17.3	69		
		0.395	31,800	18.1	75		
		0.447	27,800	20.8	77		
26-1	310	0.158	105,600	14.1	5	0.76	>144
		0.168	98,800	14.6	11		
		0.170	97,600	14.8	18		
		0.182	92,600	13.1	52		
		0.191	86,085	12.6	100		
26-2	310	0.256	75,800	12.9	5	0.82	205
		0.271	68,000	14.7	30		
		0.293	62,800	14.7	55		
		0.329	55,300	17.0	108		
		0.378	48,800	18.7	146		
		0.419	43,500	21.0	173		
		0.523	36,300	23.1	192		
		0.822	21,900		204		

Table 5-11

CONTINUED

Sample Number	σ_n (kN/m^2)	Cyclic Shear Strain (%)	Shear Modulus (kN/m^2)	Damping Ratio (%)	Cycle Number	$\frac{(\sigma_1-\sigma_3)_f \text{ Dynamic}}{(\sigma_1-\sigma_3)_f \text{ Static}}$	Number of Cycles to Failure
27	310	0.25	83,600	18.1	1	0.91	4.5
		0.29	70,800	18.1	2		
		0.33	63,100	18.7	3		
		0.38	54,116	20.2	4		
28	310	0.233	87,900	18.3	1	0.87	10
		0.267	74,800	16.7	3		
		0.316	63,000	18.5	5		
		0.426	46,300		9		
		0.564	34,500	26.7	10		
29	310	0.207	91,400	20.2	1	0.82	22.5
		0.248	73,700	14.9	6		
		0.291	63,600	15.9	10		
		0.318	58,400	17.6	14		
		0.407	44,200	20.7	19		
		0.465	38,700	24.7	21		
		0.527	34,300	27.9	22		
31-1	207	0.131	98,800	15.0	1	0.70	>151
		0.147	87,000	15.2	85		
31-2	207	0.174	82,000	12.8	1	0.77	>149
		0.178	80,700		13		
		0.196	73,200		52		
		0.198	72,100	15.0	104		

Table 5-11

CONTINUED

Sample Number	σ_n (kN/m^2)	Cyclic Shear Strain (%)	Shear Modulus (kN/m^2)	Damping Ratio (%)	Cycle Number	$\frac{(\sigma_1-\sigma_3)_f \text{ Dynamic}}{(\sigma_1-\sigma_3)_f \text{ Static}}$	Number of Cycles to Failure
31-3	207	0.229	70,300	13.9	1	0.86	97
		0.242	65,900	15.5	12		
		0.295	54,200	16.9	51		
		0.362	44,200	17.8	77		
		0.533	29,800	23.4	94		
32	207	0.217	79,900	18.6	0.5	0.96	0.5
34	207	0.197	84,457	17.1	1	0.87	8
		0.256	63,631	18.3	5		
		0.322	48,526	19.4	8		
35	207	0.202	84,900	21.4	1	0.91	2
		0.227	73,300	20.6	2		

*Data not available.

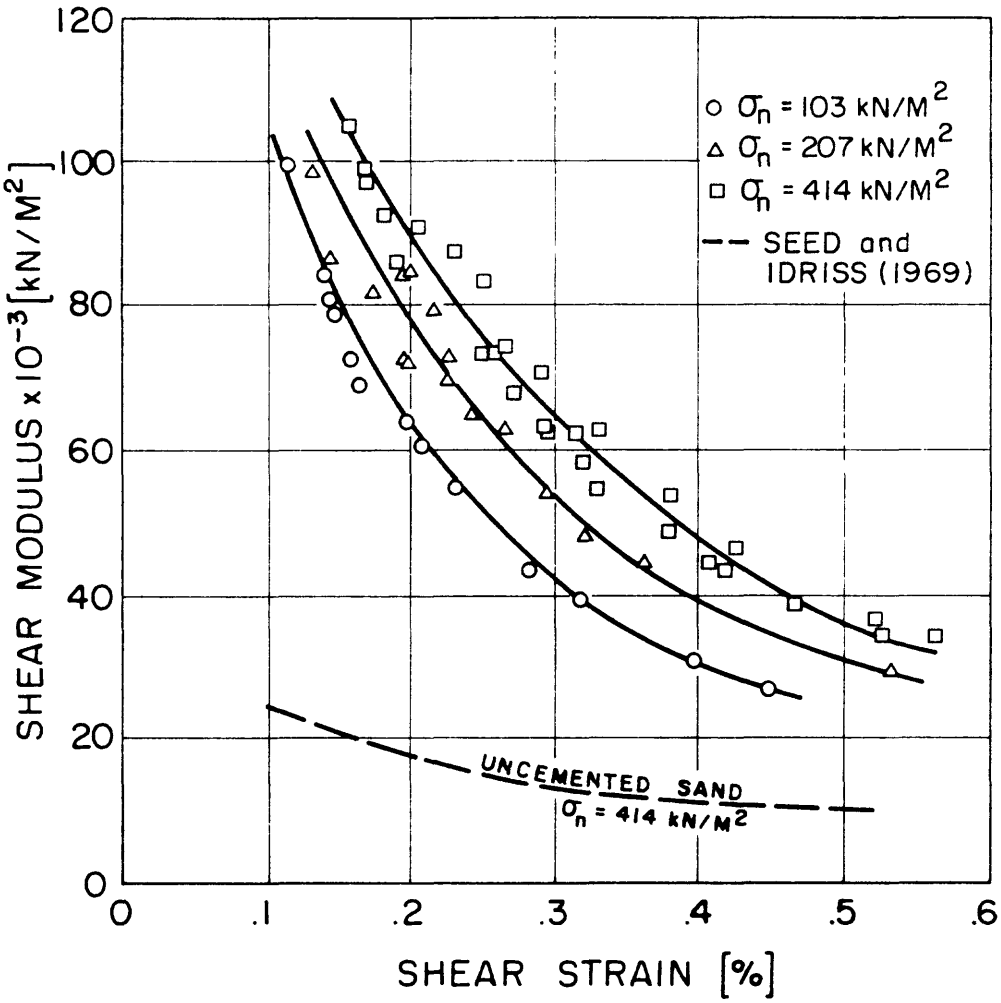

Figure 5-16 SHEAR MODULUS AS A FUNCTION OF CYCLIC SHEAR STRAIN.

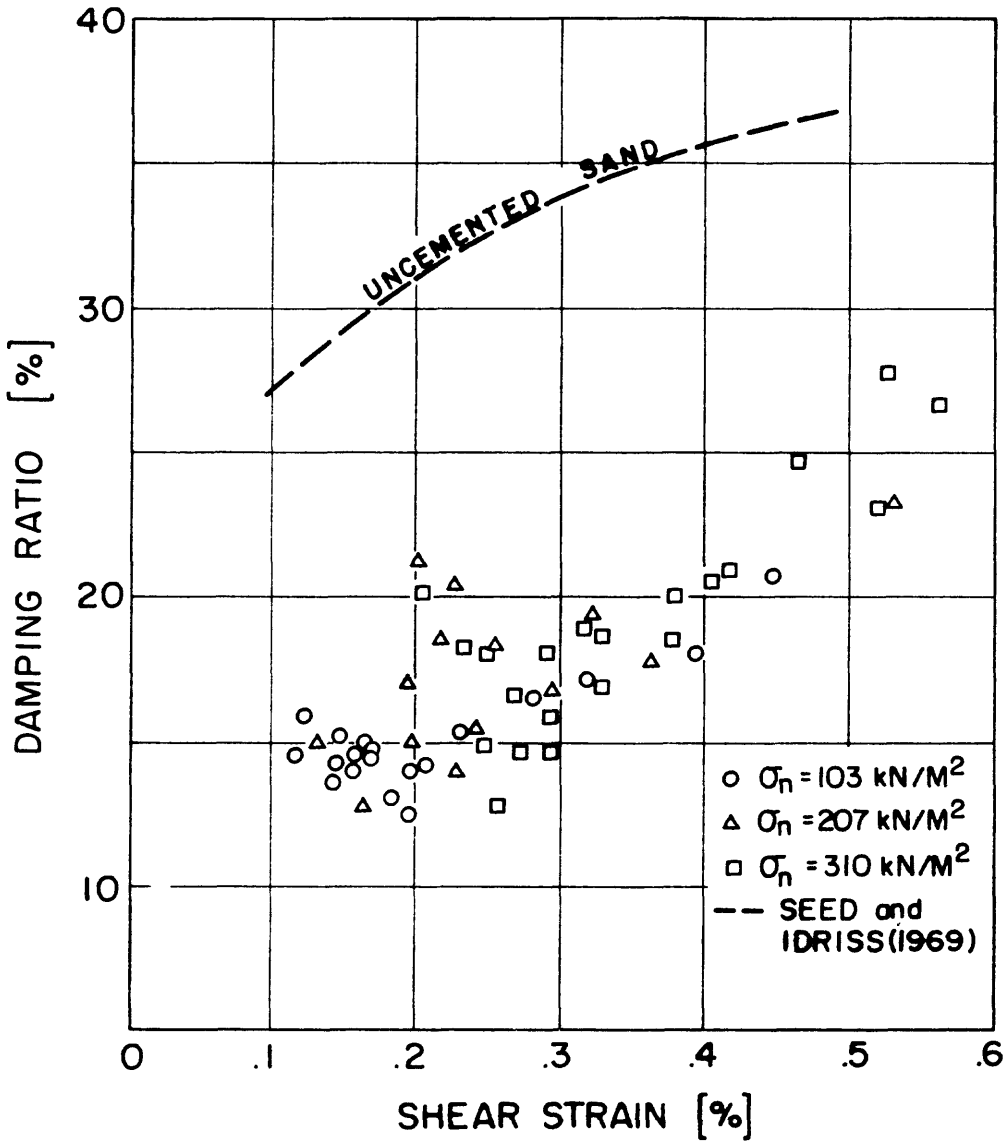

Figure 5-17 DAMPING RATIO AS A FUNCTION OF CYCLIC SHEAR STRAIN.

is on the order of one half of the damping ratio observed in uncemented sand (see Figure 5-16). Therefore, cemented sands subjected to dynamic loading can be expected to be much more brittle and to provide a greater amplification of ground motion than uncemented sands of equivalent density.

5.4 Summary

Over 170 static and dynamic laboratory tests were carried out on artificially cemented sands. The results of the static tests show that the cemented sands are brittle at low confining pressures and become increasingly more ductile with increasing confining pressure. The strength of the cemented sands increases considerably with confining pressure, reflecting the presence of a significant frictional component of strength. The tensile strength is about 14 percent of the unconfined compressive strength. Mohr envelopes for the cemented sands are essentially straight in the compression regime and curved in the tension regime. By varying the amount of cementation and the densities of the artificially cemented samples, it is demonstrated that both of these factors are important to the response of cemented soils. Increasing cementing agent increases the tensile strength and cementation strength, but doesn't change friction angle. Increasing density increases friction angle and degree of cementation.

Under dynamic loading, the response of the cemented sand subjected to compressive loading in the cyclic triaxial tests is significantly different from the one observed under tensile loading in the cyclic unconfined simple shear test. The dynamic triaxial tests consistently yield

values of shear strength at failure higher than the corresponding static strength. In the dynamic simple shear tests, the dynamic shear strength at failure is always lower than the static strength. The unload-reload moduli observed in the dynamic triaxial tests do not appear to deteriorate with the number of loading cycles, and the failure tends to be sudden and explosive. On the other hand, the equivalent linear shear modulus obtained from the dynamic simple shear tests decreases monotonically with the increasing number of cycles and increasing cyclic shear strain, and failure develops gradually.

Thus, apparently, the repeated tension loadings produced by the unconfined simple shear test have a more destructive effect than repeated compression loadings. This behavior has important implication in analyses of slope response in cemented soils, since the steep natural slopes often found in cemented soils are theoretically partially in tension. During earthquakes, these tensile loads can be increased and cycled.

Also, the dynamic shear modulus tends to be much greater for cemented sand than for uncemented sand, while the damping ratio for cemented sand is about one half of the one reported for uncemented sand by Seed and Idriss (1969).

CHAPTER VI

Selection of Approach to Evaluation of Dynamic Slope Response in Cemented Soils

6.1 Introduction

The problem of determining dynamic slope response and slope stability during earthquakes has received considerable attention in the last 15 years. The main focus has been on analyzing the stability of earth-fill dams, however, the methods which were developed are applicable to slopes in general.

In this chapter, the methods for static and dynamic slope stability analyses are reviewed, and their applicability to evaluating the dynamic slope stability in weakly cemented soils is discussed.

6.2 Static Slope Stability Analyses

The methods used in static slope stability analyses usually employ either the limiting equilibrium or the finite element approach. Following is a brief description of the basic principles and of the advantages and disadvantages of each approach.

6.2.1 Limiting Equilibrium Procedures

In the limiting equilibrium procedures, the slide mass is treated as a discrete, rigid body sliding along a thin failure plane. The results of the analyses are expressed as factors of safety against sliding. The factors of safety are determined by comparing the shear stress required to keep the slide mass from moving to the shear resistance of the soil on the failure plane. There are many different variations of the basic procedures, and their use is governed by the importance and complexity of a specific problem. An in-depth discussion of the individual

methods is provided by Wright (1969), and general descriptions of the methods can be found in most geotechnical textbooks.

The limiting equilibrium methods are best suited for analysis of cases where the slide mass is separated from the rest of the slope by a distinct, narrow failure surface. Failure planes with arbitrary geometry can be considered and the calculations may be done either by hand or by a small computer. However, the stress-strain characteristics of the soil are not accounted for, and the deformations of the soil mass cannot be determined.

6.2.2 Finite Element Procedures

The finite element method has been extensively described in literature (for example, Zienkiewicz, 1971) and only a brief outline is presented here. The method is based on the concept that a continuous body can be represented by a set of finite (discrete) elements which are connected along their common boundaries at nodal points. The variations of displacements, strains, and stresses within the elements can be approximated in terms of the forces and displacements at the nodal points. The static equilibrium equation for an element can be written in the form (Zienkiewicz, 1971):

$$[F] = [k]\{u\}$$

where $[F]$ are the element nodal forces, $\{u\}$ are the nodal displacements, and $[k]$ is the element stiffness matrix which incorporates the stress-strain characteristics of the material. The equations for the individual elements are added together to form a set of algebraic equations which are then solved subject to a given set of boundary conditions.

In most geotechnical problems, the external forces acting on the system are known, and the objective is to compute the displacements and stresses.

In slope stability analyses, the finite element method can be used to determine the distribution and orientation of stresses in the slope, and a potential failure plane can be identified. A comparison of the maximum shear stress with the shear strength of the soil can be interpreted to yield a factor of safety in a manner analogous to the limit equilibrium techniques. For homogeneous materials, the results of the finite element analyses are comparable to those obtained by the limiting equilibrium methods (Wright, Kulhawy, and Duncan, 1973).

The advantages of the finite element methods are that the general deformations of the soil mass prior and during the failure can be determined, and nonlinear stress-strain response of the soil can be modeled. However, due to the coarse nature of the finite element mesh, the method cannot model the development of a thin failure plane at some initially unknown location within the slope or the large displacements that may occur during failure.

6.3 Dynamic Slope Stability Analyses

The usual approach to evaluating slope stability under dynamic loading is to incorporate the effects of dynamic forces and dynamic soil response models into the procedures used for static analyses. Based on the manner in which the dynamic forces and dynamic soil strength are incorporated in the dynamic analyses and the way the resulting deformations and safety factors are computed, the methods for dynamic slope stability analyses may be divided into three categories:

(1) Pseudo-static limiting equilibrium methods,

(2) Cumulative deformation methods, and

(3) Direct analytical (finite element) methods.

The basic assumption used in the slope stability analyses belonging to the first two categories is that the dynamic forces acting on the earth structure, slope or embankment, can be replaced by equivalent static forces. Thus, the analyses basically consist of two parts: 1) the determination of the dynamic forces and their corresponding equivalent static values; and, 2) a static stability evaluation in which the equivalent static forces are used to load the slopes. Therefore, these methods are referred to as pseudo-static slope stability analyses.

In the following discussion, the methods for determination of dynamic forces for the pseudo-static procedures are discussed, and the basic procedures used in the three categories of dynamic slope stability analyses are presented.

6.3.1 Determination of Dynamic Forces for Psuedo-Static Analysis

The simplest approach to obtaining the dynamic forces in an earth structure subjected to an earthquake is to assume that it behaves as a rigid body. In that case, the accelerations throughout the structure are the same, and they are equal to the input accelerations at any instant in time. The dynamic or inertia forces within the structure can then be computed directly from the input accelerations using Newton's second law. This procedure was used for many years to determine dynamic forces in slopes.

Of course, earth structures are flexible and different portions of slopes accelerate in different modes. Therefore, the simple rigid body

concept is not correct. In an attempt to address this problem, Ambraseys (1960) used theory of elasticity to analytically compute the distribution of accelerations at different levels within an embankment and suggested a new method of determining the equivalent static forces. Similarly, Seed and Martin (1966) obtained analytical solution for accelerations assuming that the earth embankment could be modeled as a visco-elastic shear beam. These methods were useful for simple problems, but they still could not model the heterogeneity of earth structures or the non-linear stress-strain characteristics of the soil.

With the advent of the finite element method, it has become possible to model the complex geometries and the heterogeneity within earth structures and to compute the dynamic stresses and accelerations virtually anywhere within the modeled regions. Clough and Chopra (1966) were first to use a linear elastic finite element analysis to model the dynamic response of a dam embankment. Idriss and Seed (1967) showed that the results of linear elastic dynamic finite element analyses could be readily used to determine the equivalent static forces. Since then, the finite element procedures have been improved to more accurately reflect the non-linear soil response. Seed and Idriss (1969) introduced strain dependent equivalent linear modulus into the finite element analyses of soil response, and Kovacs, Seed, and Idriss (1971) showed that the finite element method gave results which satisfactorily compared with experimentally measured dynamic response of small scale models of clay banks. Finally, Idriss, Seed, and Serff (1974) included strain dependent variable damping into an equivalent linear finite element model. Using this approach, it is possible to obtain a fair representation of the time histories of

stresses and accelerations and the corresponding equivalent static forces at required locations within earth structures subjected to dynamic loading (Makdisi and Seed, 1978).

Presently, substantial effort is focussed on developing methods capable of modeling the nonlinear stress-strain soil response including hysteretic damping (Finn, Martin, and Lee, 1978; Hardin, 1978; Idriss, Dobry, and Singh, 1978). Theoretically, these methods should be capable of accurately modeling the dynamic response of earth structures, but this has not been confirmed as yet.

6.3.2 Pseudo-Static Limiting Equilibrium Methods

As noted earlier, in the pseudo-static limiting equilibrium slope stability analyses, dynamic forces are replaced by equivalent static forces, and in this manner the dynamic problem is transformed into a pseudo-static one. The factor of safety against sliding is determined using one of the limiting equilibrium methods. The basic assumption in this approach is that a slope failure will occur if the value of the factor of safety drops below one when the pseudo-static dynamic forces are applied. However, this assumption is not necessarily accurate.

In nature, when a statically stable slope or embankment is subjected to dynamic loading, the factor of safety may drop below one only during certain time intervals. Permanent deformations will occur primarily during these time intervals and, unless the material is extremely brittle or strain softening, the deformations will stop once the dynamic forces decrease or reverse. Since the dynamic forces are transient in nature and they are applied and removed fairly rapidly, the magnitude of the deformations may not be large enough to actually constitute a failure.

In such cases, the factor of safety determined by the pseudo-static stability analysis is not a sufficient indication of the dynamic slope stability. In order to cope with this problem, methods of dynamic slope stability analysis based on the evaluation of cumulative deformations have been developed.

6.3.3 Cumulative Deformation Methods

Newmark (1965) first suggested that the dynamic stability of earth dams should be evaluated in terms of potential deformations rather than factors of safety. He proposed a method based on the concept of yield acceleration, which is defined as the acceleration required to reduce the factor of safety for a potential sliding mass to one. Accelerations in excess of the yield acceleration are assumed to cause displacements which can be computed using the equation of motion and the time history of accelerations.

Goodman and Seed (1966) successfully used Newmark's method to predict displacements in a cohesionless soil with strain softening stress-strain behavior. Finn (1966) developed a formulation for infinite slopes in cohesive soils, and Ambraseys and Sarma (1967) analyzed triangular wedge failures in dam embankments. The most elaborate method for evaluation of dynamic slope stability using the cumulative deformation approach has been recently presented by Makdisi and Seed (1978). This technique uses a dynamic finite element analysis to determine the time history of accelerations acting on a potential sliding mass. The yield acceleration is determined using a pseudo-static limiting equilibrium analysis, and the displacements along the potential failure plane are computed from the equation of motion.

The cumulative deformation methods discussed so far assume that: 1) the slide mass translates as a rigid body; 2) the failure occurs in shear along narrow plane; 3) the soil behavior is elastic-plastic (this is a usual, not a necessary assumption); and 4) all deformations occur parallel to the failure plane. Thus, these methods do not consider the overall deformations of the earth structure or brittle failure modes.

A variation on the cumulative deformation type of approach was proposed by Seed (1966) to determine potential shear strain levels in slopes. Instead of using the equation of motion for computing the displacements, Seed suggested comparing the expected stress levels on the potential failure plane to laboratory stress-strain data. The potential field strains could then be determined from the strains developed in laboratory samples which were subjected to the same stresses as were expected to occur in the earth embankment. Seed's method was later expanded by Arango and Seed (1974), who utilized the results of dynamic finite element analyses, laboratory shaking table experiments, and the strength characteristics of the soil to develop a method for evaluating slope behavior in cohesive soils. Although these methods are quite sophisticated, they contain the same assumptions and limitations as were already mentioned for the cumulative deformation methods. In addition, they assume that the stress conditions occuring in the field can be satisfactorily reproduced in the laboratory and that the strains observed in the laboratory tests are close to those that would occur in the field.

A characteristic common to all the methods discussed in this section is that the analyses are composed of two parts: 1) the determination of dynamic stress distribution; and 2) the determination of deformations of

a particular portion of the slope using equivalent static forces and laboratory test results. In general, the overall deformations of the earth structures are not computed and brittle behavior of soil cannot be modeled.

6.3.4 Direct Analytical Methods

The alternative to the two stage process of dynamic slope stability analysis described in the previous section is to use numerical methods, such as finite elements, to compute both the dynamic stresses and the resulting deformations. This approach requires a mathematical model of the soil behavior that accounts for the stress-strain response and damping.

The early finite element methods employed equivalent linear methods of representing the soil response (Idriss, Seed, and Serff, 1974), and progressive changes in modulus with time were often not modeled. Present efforts are oriented towards developing nonlinear constitutive models for dynamic soil response (Finn, Martin, and Lee, 1978; Hardin, 1978; Idriss, Dobry, and Singh, 1978). These new constitutive models allow the modeling of progressive changes in the soil characteristics with time. For example, Finn and Miller (1974) have demonstrated that nonlinear dynamic finite element analyses of dam embankments can be performed.

Unfortunately, the dynamic finite element analyses suffer from the same shortcomings mentioned in the discussion of the static finite element methods, namely: the development of a thin failure plane at some initially unknown location within the slope or the post failure displacements that may occur along the failure plane or within the failed mass cannot be modeled.

The discussion of the methods of slope stability analysis and their advantages and disadvantages serves to illustrate that there is not a single method that is applicable to all situations. Thus, each particular case has to be judged on its own merit in order to choose an appropriate slope stability analysis. In the next section the characteristics of the slopes in cemented soils are considered and the method of analysis felt most applicable is presented.

6.4 Analysis of Slopes in Cemented Sands

6.4.1 Background

In order to justify the approach to slope stability analysis adopted in this study, it is appropriate to first reconsider the characteristics of real slopes in the weakly cemented sands.

The slopes in the weakly cemented sands in Pacifica, California, are typical of the problem being discussed. They are up to 50 m high, and the inclination of the slope face varies from about 60 degrees to vertical. The sands are generally massively bedded with individual beds containing various amounts of cementation. The near surface portions of the slopes are apparently weathered, however, the depth of weathering and its effect on the strength of the cementation have not been investigated yet. Static finite element analyses of such steep slopes indicate a zone of tension in the upper portion of the slope (see Fig. 2-4). It seems likely that the natural slopes in cemented soil are to some extent jointed.

A failure in one of the steep slopes of cemented sand is usually initiated by splitting along a near surface subvertical plane, most likely a joint plane, in the upper part of the slope (see Chapter II,

Fig. 2.3). Because the weakly cemented soil exhibits a brittle response at low confining pressures, the failure mass tends to disintegrate after the initial displacements. Prior to failure, the initial stress-strain response of intact weakly cemented soils can be considered essentially linear relative to other soils, and the strains required to reach failure are low, usually less than 2%. The tensile strength of the cemented soil deteriorates rapidly under cyclic loading.

Thus, in order to accurately analyze the dynamic response of slopes in the weakly cemented sands, such as those near Pacifica, it would be desirable to employ a method capable of modeling the following characteristics:

(1) Geometry of the slope;

(2) Heterogeneity of the soil and presence of jointing;

(3) Slope response and failure under complex, seismically induced motions; and

(4) Brittle and sudden failure due to overloading by either tension or compression.

Although it may be argued that the previously discussed methods of slope stability analysis could be adapted to consider some of the complexities of the cemented soil slope problem, the actual slope failure cannot be satisfactorily modeled. The brittle nature of the failure and the possibility of initial jointing complicate the situation. In fact, post failure deformations of the slide mass are irrelevant since it collapses and disintegrates. Therefore, it is most important to predict those circumstances which lead to the failures.

6.4.2 Method of Analysis

The finite element method was felt to be best suited for the task of defining initial failure conditions in a cemented soil slope, since it can be used to predict stress distribution within a slope of essentially arbitrary geometry. None of the other possible procedures have this capability. Therefore, finite element procedures were used to perform parametric studies of simple, idealized cases with vertical slopes composed of linear elastic material with 10% damping. The reasons for the use of the simple soil behavior model are as follows:

1. The stress-strain response of cemented soil is nearly linear up to peak strength. A damping ratio of 10% represents a lower limit to all values measured in the laboratory tests.

2. Available nonlinear continuum models of stress-strain and damping characteristics do not inherently improve the simulation of the actual behavior of jointed cemented soil slopes.

3. Results of linear elastic analyses are independent of modulus, and they can be nondimensionalized and extrapolated to other problems.

4. Accurate representation of initial jointing or effects of nonuniform weathering within the slopes is not possible at this time because of a lack of information as to the extent and nature of these phenomena.

5. The linear elastic dynamic analyses can be performed in frequency domain resulting in lower computer costs.

The analyses of the slope response were performed in two steps. First, the static stress distribution caused by gravity was computed; and second, the dynamic stresses due to earthquake loading were superimposed onto the static stresses. The static analyses were performed using SOILSTRUCT, a computer program developed by Hansen (1979) at Stanford University. The dynamic analyses were done using FLUSH, a computer

program developed by Lysmer and others (1975) at the University of California at Berkeley. Two dimensional plane strain finite elements were used for discretization in both types of analyses.

The basic principles of static finite element analysis have already been discussed. The dynamic finite element analyses are based on the same principles of discretization and the displacements at each node are computed from the equations of motion. In general, solutions can be obtained either by integration in time or by transforming the problem into frequency domain. The integration in time has the advantage that nonlinear material properties changing with time can be modeled. The solution in the frequency domain is much faster in terms of computer time, however, it requires that the material properties remain constant and linear during the modeled time intervals. In the program used for this work, the equations of motion are solved in the frequency domain using the complex response method (Lysmer and others, 1975). Therefore, the program is suitable for equivalent linear type of dynamic analysis as used herein.

The results of the individual analyses and their discussion are presented in the following chapter.

CHAPTER VII

Analytical Studies of Dynamic Slope Response in Cemented Soils

7.1 Introduction

The analytical studies described in this chapter are designed to develop an understanding of the dynamic response of steep slopes in cemented soils. Specifically, the magnitude of the ground accelerations and the nature of the dynamic stress distribution for different types of earthquake loading and different soil properties are investigated. Numerical solutions along with results of the laboratory test program are used to define potential slope failure modes. Where possible, the results of the analyses are addressed to the observations of behavior of the cemented sand slopes along the Pacific Coast near Pacifica, California. In this regard, many of the properties used in the analyses were selected to be reasonably similar to those expected to characterize the cemented sand at Pacifica. Particularly interesting trends of behavior are defined and potentially fruitful directions for future research are established.

7.2 Input Acceleration Records

The input acceleration records used in the analyses were the S 80°E component of motion recorded at Golden Gate Park during the magnitude 5.3 1957 San Francisco earthquake and a synthetic acceleration record for a magnitude 8.25 earthquake generated by Seed and Idriss (1969) to represent the 1906 San Francisco earthquake. The epicenter of the 1957 earthquake was located on the San Andreas Fault near Mussell Rock only about 2 km from the slopes of the Pacifica area. The particular

accelerogram used in this study (Fig. 7-1) was recorded on rock 11 km from the epicenter. The maximum ground acceleration on that record is 0.105 g, the dominant period of motion is 0.22 seconds, and the length of record used in the analyses is 16 seconds (Table 7-1).

The synthetic accelerogram for the magnitude 8.25 earthquake (Fig. 7-2) is designed to represent the rock motion at a site 16 km from a fault break. Its maximum ground acceleration is 0.42 g, the dominant period of motion is 0.36 seconds, and the duration of significant shaking is 75.2 seconds (Table 7-1).

The 1957 Golden Gate record was chosen for use in the analyses because it was recorded in a close proximity to the epicenter of the earthquake and the earthquake is probably typical of moderate earthquakes in the San Francisco Bay area. Also there is a good record of slope behavior during that earthquake (see Chapter II). The magnitude 8.25 synthetic earthquake accelerogram is intended to be typical of a large earthquake which could occur along the San Andreas Fault close to the Pacifica site.

In the actual finite element analyses, the accelerograms were used without any rescaling of the peak accelerations in order to account for distance between site and earthquake source. However, since linear elastic material behavior is assumed, the results of the finite element analyses can be scaled for any peak acceleration desired. This aspect of the results will be examined in detail later in this chapter.

7.3 The Finite Element Model

The finite element model used in the analyses consisted of a rectangular region 400 m long, 25 m high on the left and 50 m high on the

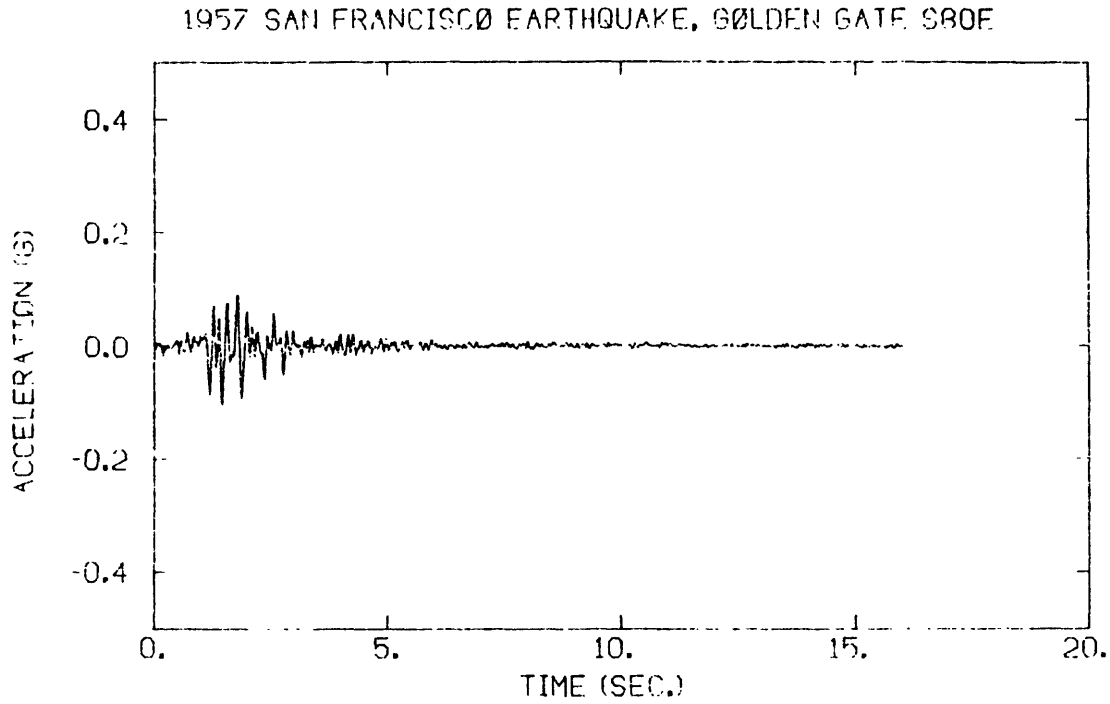

Figure 7-1 S 80° E COMPONENT OF MOTION RECORDED AT GOLDEN GATE PARK DURING THE 1957 SAN FRANCISCO EARTHQUAKE.

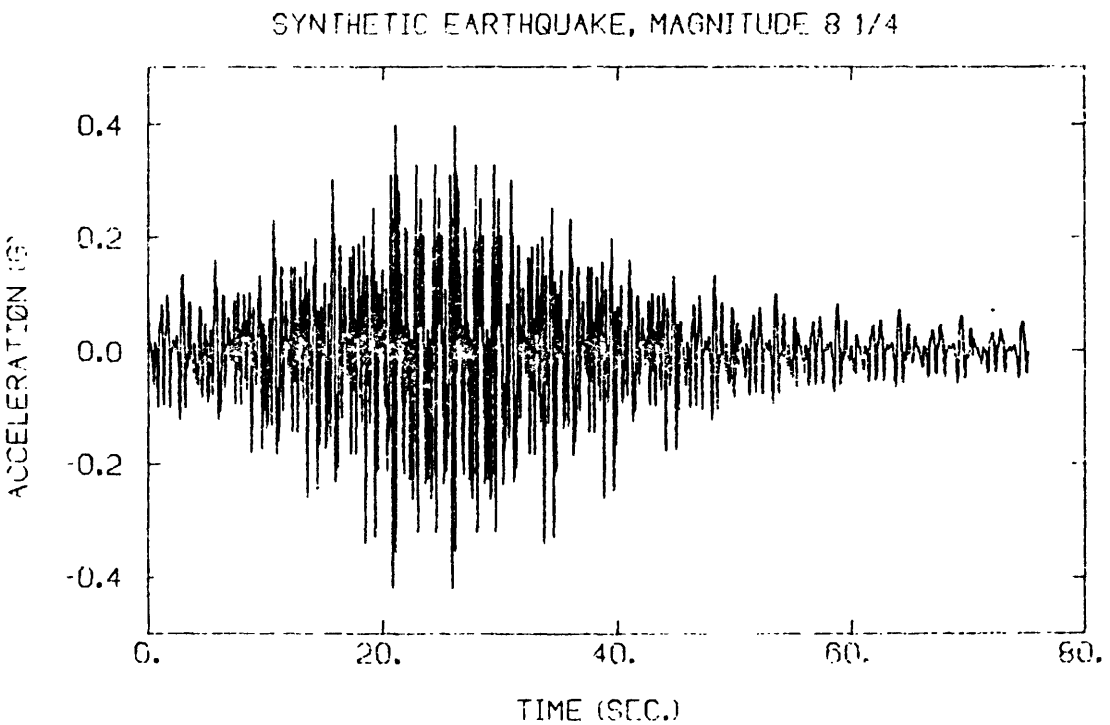

Figure 7-2 SYNTHETIC ACCELEROGRAM FOR A MAGNITUDE 8¼ EARTHQUAKE (Seed and Idriss, 1969).

Table 7-1

CHARACTERISTICS OF ACCELEROGRAMS USED IN THE ANALYSES

Earthquake	Record	Type of Site	Distance to Epicenter [km]	Magnitude	Maximum Acceleration [g]	Dominant Period [s]	Duration of Record [s]
1957 San Francisco	S 80°E Golden Gate	Rock	11	5.3	0.105	0.22	16
8¼ Synthetic	---	Rock	16	8.25	0.42	0.36	75.2

right, with a 25 m vertical slope in the middle (Fig. 7-3). The material was assumed to be linearly elastic with a Poisson's ratio $\nu = 0.3$. A damping ratio of 10 percent was used in the dynamic analyses. The vertical slope geometry and linear elastic material properties were chosen on the basis of laboratory results and field observations as explained in Chapter VI. The actual physical dimensions of the model and its subdivision into finite elements were governed by the considerations of solution accuracy and computer costs.

7.3.1 Determination of Proper Mesh Proportions

Static Analyses

In the static linear elastic finite element analyses, the nodal spacing and element size are generally independent of material properties. The main requirements are that the mesh should be sufficiently fine in the region of interest to provide results with acceptable accuracy and that the boundaries of the model be far enough from the region of interest so that they do not affect the accuracy of the solution.

Dynamic Analyses

In the dynamic finite element analyses the mesh spacing depends on factors described for the static case and, in addition, the shear modulus of the material. Idriss (1968) and Lysmer and others (1975) used parametric studies to arrive at the following information concerning the finite element mesh for dynamic analyses:

1. Recommended maximum height of layers in the mesh, h_{max}, should not exceed

$$h_{max} = \frac{1}{5} \frac{v_s}{f_{max}} \qquad (6)$$

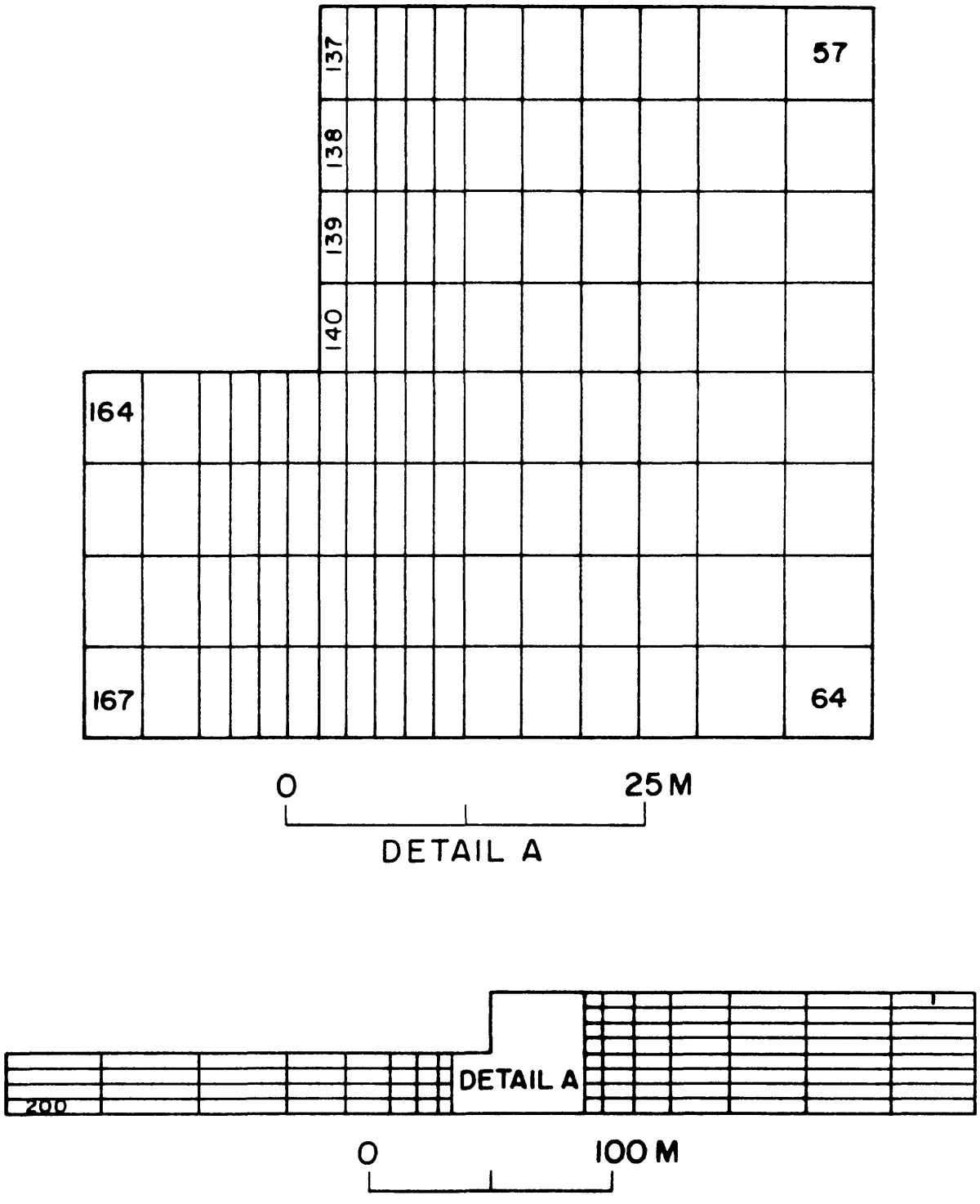

Figure 7-3 THE FINITE ELEMENT MESH USED IN THE STATIC AND DYNAMIC ANALYSES.

where v_s is the minimum shear wave velocity and f_{max} is the maximum frequency used in the analyses (Lysmer and others, 1975). A value of 8 Hz for f_{max} is considered appropriate in analyzing earth structures (Lysmer and others, 1975) and equation (6) reduces to

$$h_{max} = \frac{v_s}{40} \tag{7}$$

Note that since shear wave velocity is related to the shear modulus, G, as $G = v_s^2/\rho$ where ρ is density, equation (7) becomes

$$h_{max} = \frac{\sqrt{G/\rho}}{40} \tag{8}$$

2. The minimum number of layers in any region of interest should be at least four (Idriss, 1968).

3. The solution time increases approximately with the cube of the number of layers (Lysmer and others, 1975).

4. A slope influences the dynamic response of a horizontal soil deposit up to a distance of six times the height of the slope in each direction (Idriss, 1968).

Considering economic limitations and the criteria set forth in points 2, 3, and 4, the mesh for the model slope was divided into four layers on the left and eight layers on the right of the slope (Fig. 7-3). A transmitting boundary was placed on the right-hand side of the mesh and a symmetry boundary was used on the left. Both boundaries were at a distance of 8 times the height of the slope from the slope itself. The base of the mesh was assumed to be rigid.

The choice of the actual height of the individual layers, and, consequently, the physical size of the model was influenced by a desire to use the same mesh for a series of analyses with different material properties. Also, the dimensions were selected to model actual possible situations for cemented soils. In this regard, it was decided to use

50 m as the thickness of the soil deposit to the right of the slope (see Fig. 7-3) and 25 m for the soil to the left of the slope. It should be noted that the 50 m dimension and the requirement stated by equation (6) limits the minimum shear wave velocity which can be used in the analyses to 250 m/s.

7.3.2 Choice of Material Characteristics

In the dynamic analyses, the choice of a shear modulus not only affects the required nodal spacing but also determines the natural period of the soil deposit. This in turn controls the degree of response of the soil deposit to the input motion. The natural period, T_s, of a homogeneous soil deposit with constant shear wave velocity is a function of the shear modulus, G, the density, ρ, and the thickness of the soil deposit, H, (Dobry, Oweis and Urzua, 1976) as follows:

$$T_s = \frac{4H}{\sqrt{G/\rho}} \tag{9}$$

Or, in terms of the shear wave velocity, v_s,

$$T_s = \frac{4H}{v_s} \tag{10}$$

The relationship shown in equations (9) and (10) is graphically illustrated in Fig. 7-4 by plotting H versus T for different values of G and v_s. The dominant periods of the 1957 San Francisco and the synthetic earthquakes are identified by the vertical dashed lines. The horizontal dashed line marks a 50 m thick deposit which is equivalent to the height of the slopes in Pacifica. It is seen that, as the shear wave velocity increases, the ratio of the natural period of the soil deposit, T_s, to the dominant period of the earthquake, T_E, decreases

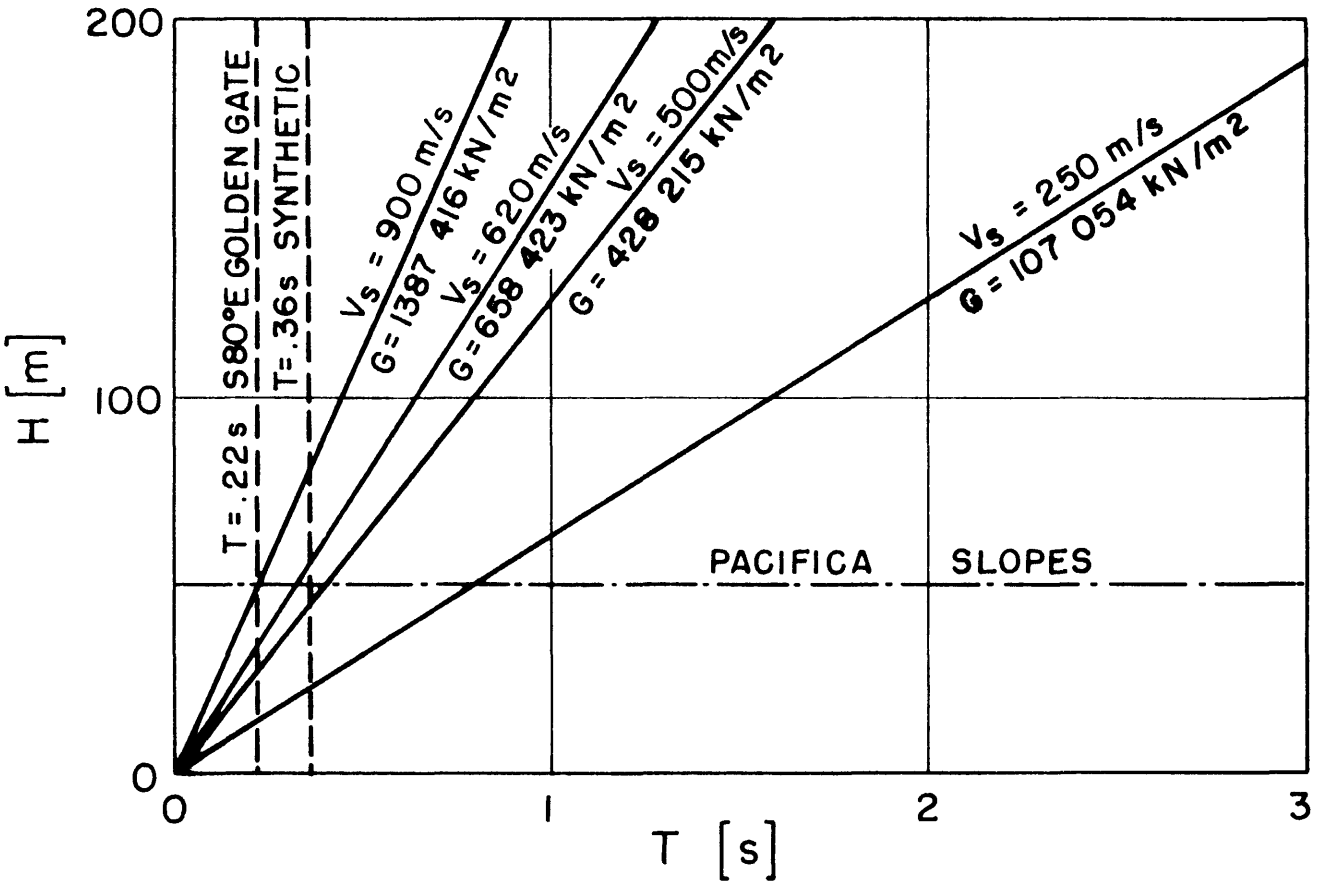

Figure 7-4 NATURAL PERIOD, T, VERSUS THE THICKNESS, H, FOR A SOIL LAYER WITH A CONSTANT SHEAR MODULUS.

(hereafter T_s/T_E will be referred to as the period ratio). For example, if the shear wave velocity of a 50 m thick deposit subjected to the 1957 earthquake increases from 250 to 900 m/s, the period ratio changes from 3.6:1 to 1:1. Similarly, the diagram is useful in estimating the effect of changing the height of the soil deposit or the dominant period of the earthquake on the period ratio and ultimately the slope response.

A range of shear wave velocities from 250 to 900 m/s was chosen for use in the dynamic analyses (Fig. 7-4) to cover as wide a range of period ratios as possible. This range corresponds to that normally reported for sands (Arango, Moriwaki, and Brown, 1978; Wilson, Warrick, and Bennett, 1978) and also to the range of modulus values obtained in the cyclic laboratory tests (see Chapter IV). The specific shear wave velocities and the corresponding period ratios used in the analyses are presented in Table 7-2.

Table 7-2

SHEAR WAVE VELOCITIES AND PERIOD RATIOS USED IN THE PARAMETRIC STUDIES

Analysis Number	Earthquake	Dominant Earthquake Period [s]	Shear Wave Velocity [m/s]	Period Ratio T_S^*/T_E
1	1957 San Francisco	0.22	250	3.6
2	1957 San Francisco	0.22	500	1.8
3	1957 San Francisco	0.22	900	1.0
4	Synthetic	0.36	250	2.2
5	Synthetic	0.36	620	0.9

* H = 50 m.

7.4 Results of Analyses

The analytical results consist of accelerations at the ground surface and dynamic stresses generated within the slopes. The ground accelerations are interpreted to provide information about the amplification of the input earthquake motion due to the presence of the slope and due to the natural period of the soil deposit. The dynamic stresses are used to predict the slope response and the slope stability during earthquakes.

7.4.1 Ground Accelerations

Predicted horizontal and vertical accelerations at the top of the soil deposit for the 1957 earthquake are shown in Fig. 7-5 and for the synthetic earthquake in Fig. 7-6. The following trends can be identified by inspecting the two figures:

1. Near the slope face the horizontal accelerations are amplified somewhat relative to those in the free field.
2. Significant vertical accelerations may occur near the slope face.
3. The amplification of the input acceleration is strongly dependent on the period ratio.

The strong influence of the period ratio on the amount of amplification of the input motion is further illustrated in Fig. 7-7. Here, the amplification factor, defined as the ratio of the maximum acceleration in the free field to the maximum acceleration on the input record, is plotted against the period ratio. Not unexpectedly, the amplification is the greatest at resonance, period ratio of one, and the amount of amplification decreases as the period ratio moves away from resonance.

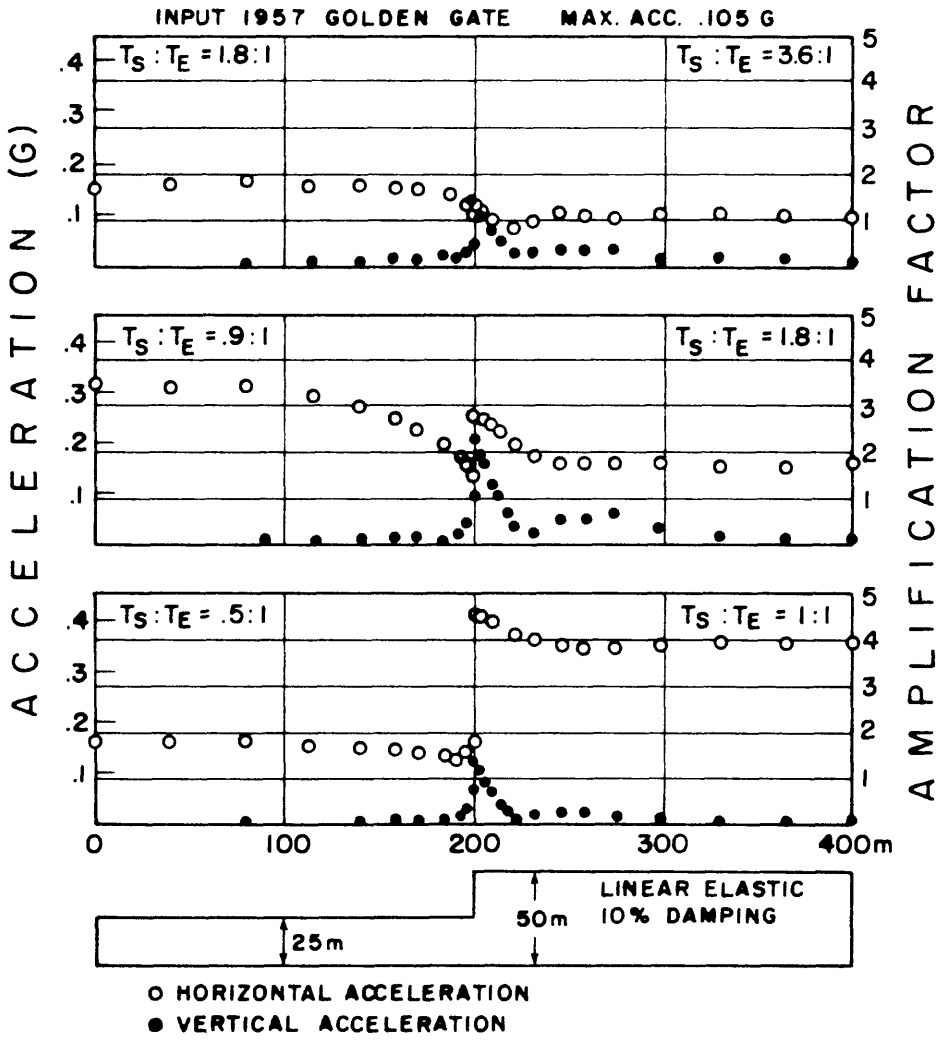

Figure 7-5 GROUND SURFACE ACCELERATIONS FOR DIFFERENT PERIOD RATIOS, 1957 SAN FRANCISCO EARTHQUAKE.

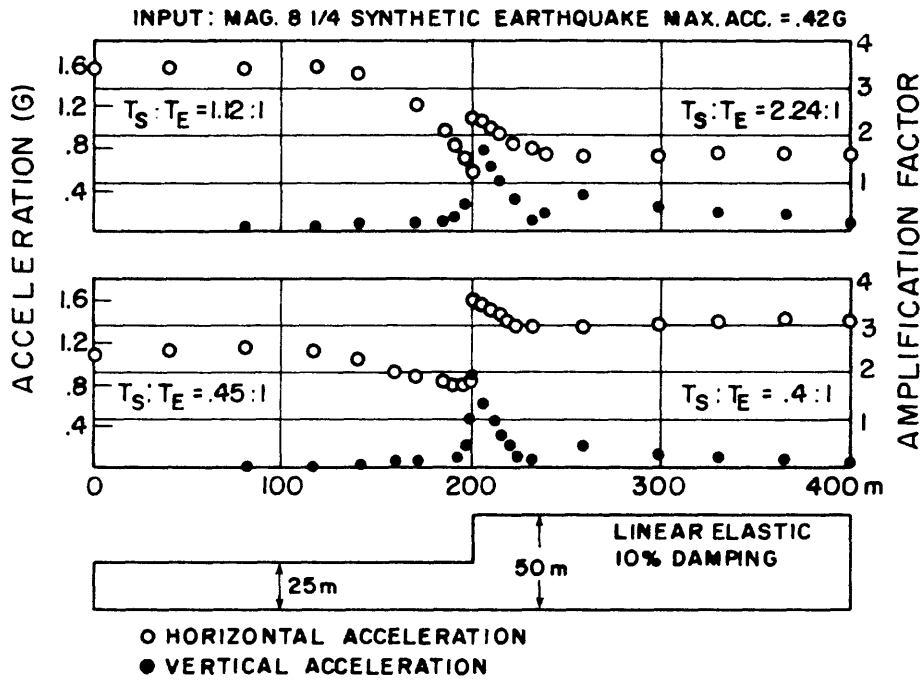

Figure 7-6 GROUND SURFACE ACCELERATIONS FOR DIFFERENT PERIOD RATIOS, MAGNITUDE 8-1/4 SYNTHETIC EARTHQUAKE.

The maximum amplification factors are 3.8 and 2.4 for linear elastic material with 10 and 20 percent damping, respectively. The relationship between the amplification factor and period ratio seems the same regardless of the input earthquake. Of course, this is only correct as long as the material behavior is assumed to be linearly elastic.

The observation that the ground motions are amplified near the slope is not surprising since the effect of topography on observed ground accelerations has been recognized for some time (Boore, 1972; Idriss, 1968; Kovacs, Seed, and Idriss, 1971). However, it is important to note that this effect is small compared to the amount by which the input motion is amplified as it travels through the soil deposit. For instance, in the case of 1:1 period ratio in Fig. 7-6 the maximum free field

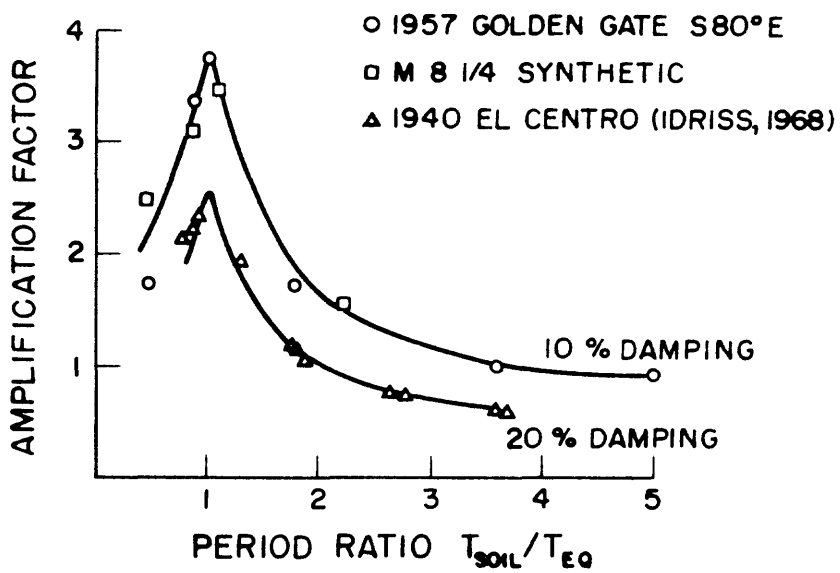

Figure 7-7 AMPLIFICATION OF THE INPUT ACCELERATION AS A FUNCTION OF THE PERIOD RATIO.

acceleration is already 3.8 times the base acceleration, and an increase of amplification factor to 4.4 near the slope represents only an additional 16 percent. Similar effects are exhibited in the other cases shown in Figs. 7-6 and 7-7. The zone of ground motion amplified above the free field acceleration extends to a distance of about twice the height of the slope from the vertical slope. Idriss (1968) shows that this distance increases to as much as 6 times the height of the slope for slopes from 14 to 45 degrees.

Although only horizontal input motion was used in the analyses, the results show that near the slope vertical accelerations may reach the same level as the horizontal. Thus, the results suggest that some of the increased earthquake damage that is often observed near slopes may in fact be caused by vertical motions rather than the horizontal accelerations amplified by the slopes. Near vertical slopes the vertical accelerations die out fairly rapidly and can be generally considered insignificant at distances beyond one height of the slope from the slope itself.

At this point, it should be noted that the observations thus far are specific to the case assumed for these studies in which the period of the soil deposit to the left of the slope is one half of the period of the soil deposit to the right of the slope. Different geometries of the soil deposit thickness may induce somewhat different predicted behavior. However, it is important that the present results are qualitatively similar to those obtained by Idriss (1968) and Kovacs, Seed, and Idriss (1971) for embankments on flexible and rigid foundations using

different modulus values and a range of slope angles from 14 to 45 degrees. Thus, it would appear that the general conclusions drawn from the present studies are applicable to a variety of slope conditions.

Another aspect of the analyses which should be taken into consideration is the effect of the assumption of a constant linear elastic response regardless of strain level or number of loading cycles. The shear modulus of soil decreases during cyclic loading, and the period of the slope system is likely to change during shaking, especially in a large seismic event. If the slope came into resonance early in the earthquake, the decrease in modulus during the cyclic loading would in effect increase the period ratio and lead to decreased amplification of the input motion (see Fig. 7-7) and the stresses in the slope. The change in modulus is not considered explicitely in the finite element analyses technique used herein, but its effect can be readily defined simply by comparing results of analyses using different modulus values.

7.4.2 Distribution of Static Stresses

The stress distribution for the static loading condition is presented in terms of nondimensionalized Cartesian stresses $\sigma_x/\gamma H$, $\sigma_y/\gamma H$, and $\tau_{xy}/\gamma H$ where γ is the unit weight of the soil and H is the height of the slope. In this form the results can be applied to other slopes with the same geometric shape and proportions but different size by applying direct scaling factors.

The orientations of the static principal stresses around a vertical slope are illustrated in Figure 7-8. The major principal stress direction is indicated by the longer bar and the minor principal stress direction by the shorter one. The crosses indicate locations at which the minor

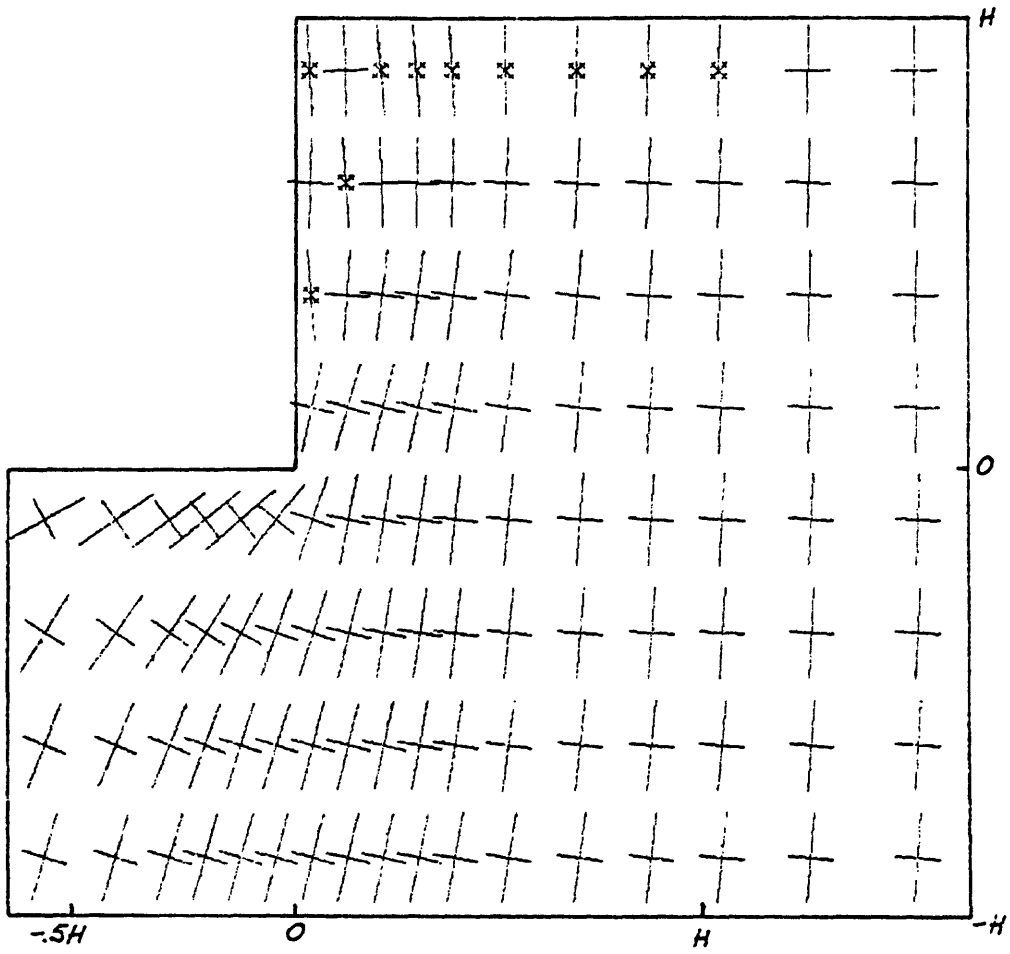

*Indicates Tensile Minor Principal Stress.

Figure 7-8 ORIENTATION OF STATIC PRINCIPAL STRESSES AROUND A VERTICAL SLOPE IN LINEAR ELASTIC MATERIAL, $\nu = 0.3$.

principal stress is tensile. As seen from the plot, there is a zone of tensile minor principal stress in the upper part of the slope (see also Figure 2-4). The zone of tension extends three quarters of the way along the slope face and about one slope height from the edge of the slope at the top. It is quite shallow, though, and at no point reaches beyond one quarter of the slope height into the slope. The nondimensionalized static stress distributions are presented in Figure 7-9. The zone of tension at the top of the slope is bounded by the zero contour on the σ_x/σ_y plot. It can be also seen that there is a region of shear stress concentration at the toe of the slope. The plots in Figure 7-9 can be used to compute static stresses in an arbitrary vertical slope through multiplying by the corresponding γH factor. It should be remembered, however, that a Poisson's ratio of 0.3 and 1:2 ratio of the slope height to the overall thickness of the deposit are implicit in the results shown in Figure 7-9.

7.4.3 Distribution of Dynamic Stresses

The objective of evaluating the dynamic stress distributions is to produce a set of diagrams similar to those shown for the static case which characterize the dynamic stress conditions that exist in a slope subjected to seismic loading. These can then be used in evaluating the stability of slopes subjected to different earthquakes.

In order to be able to develop the dynamic stress distributions, it is necessary to characterize the time history of stresses at any point within the slope by a single representative value. A time history plot of Cartesian dynamic stress increments $\Delta\sigma_x$, $\Delta\sigma_y$, and τ_{xy} for element 140 located right on the slope face at the toe is presented in Figure 7-10. The plot shows one large peak, five intermediate, and a number of small

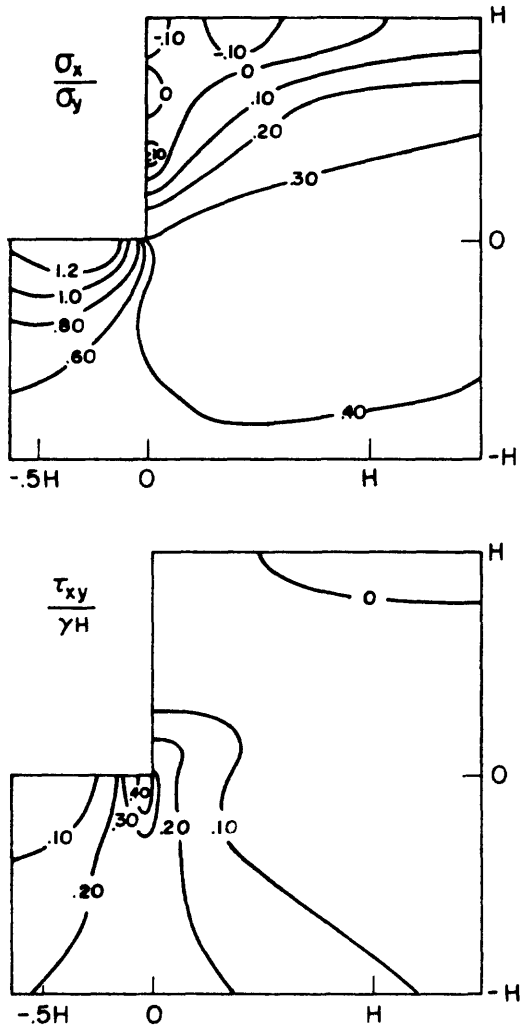

Figure 7-9 DISTRIBUTION OF STATIC STRESSES AROUND A VERTICAL SLOPE IN LINEAR ELASTIC MATERIAL, $\nu = 0.3$.

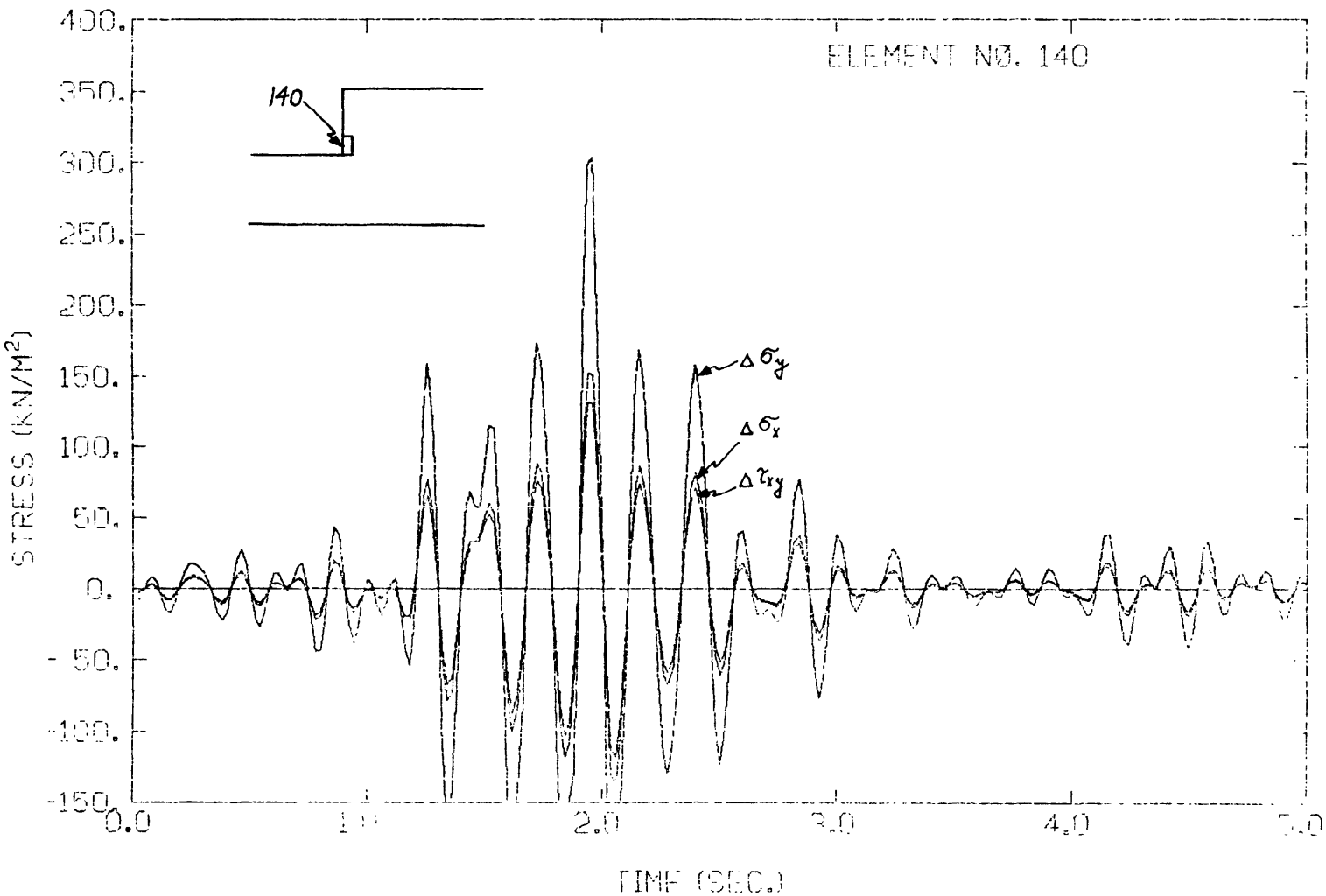

Figure 7-10 TIME HISTORY OF DYNAMIC STRESSES IN ELEMENT NO. 140 FOR 1:1 PERIOD RATIO, 1957 SAN FRANCISCO EARTHQUAKE.

peaks in the stresses generated during the 1957 San Francisco earhtquake. In this study, it was decided to characterize the time history by the maximum absolute value of the dynamic stress increment. The use of the maximum absolute value is common in earthquake engineering. It has the advantage that the results can subsequently be interpreted in terms of the effects of an equivalent number of cycles at some intermediate uniform stress level, usually 0.65 to 0.85 of maximum, as suggested by Lee and Chan (1972).

A disadvantage of using the maximum absolute values to represent the time history of stresses in an element is that the information about the direction of the stresses is lost. This does not cause a problem when the stresses are in phase as in element 140 (Figure 7-10). However, in parts of the slope the stresses are out of phase as, for example, in element 139 (Figure 7-11) which is located directly above element 140 at the slope face. In element 139, the dynamic stress increments $\Delta\sigma_x$ and $\Delta\tau_{xy}$ cycle out of phase with $\Delta\sigma_y$. In general, the dynamic stresses cycle out of phase in the same manner as in element 139 in the region of the slope above the zero contour line on the plot of σ_x/σ_y in Figure 7-9. Below this line they cycle in phase. The information about the out of phase and in phase dynamic stress response is important when the dynamic stresses are to be superimposed on the initial static stresses, as is shown later.

The distributions of the maximum absolute dynamic stress increments $\Delta\sigma_x$, $\Delta\sigma_y$, and $\Delta\tau_{xy}$ generated by the 1957 San Francisco earthquake in slopes with period ratios of 1:1, 1.8:1, and 3.6:1 (see Table 7-2) are presented in Figures 7-12, 7-13, and 7-14. Those generated by the

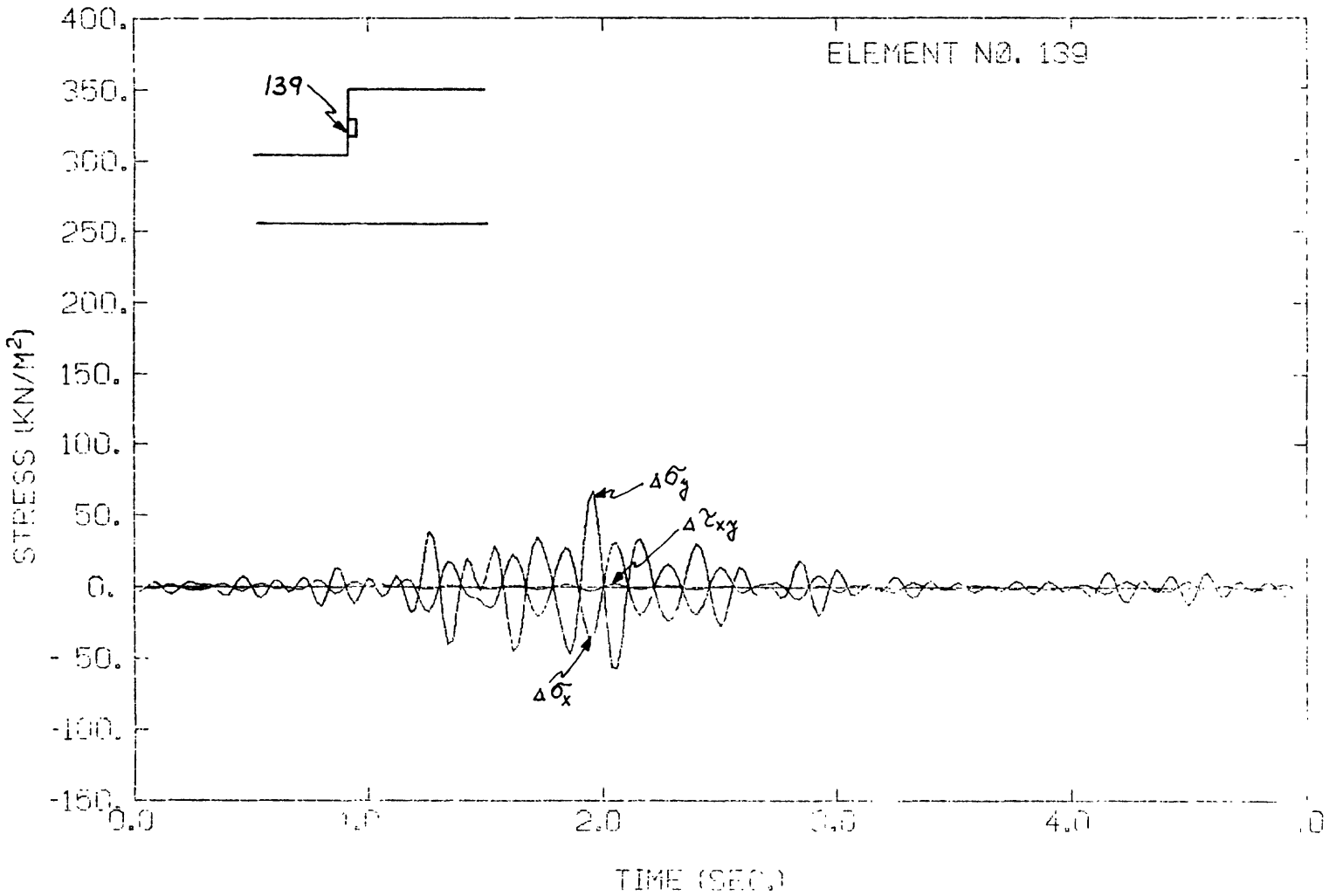

Figure 7-11 TIME HISTORY OF DYNAMIC STRESSES IN ELEMENT NO. 139 FOR 1:1 PERIOD RATIO, 1957 SAN FRANCISCO EARTHQUAKE.

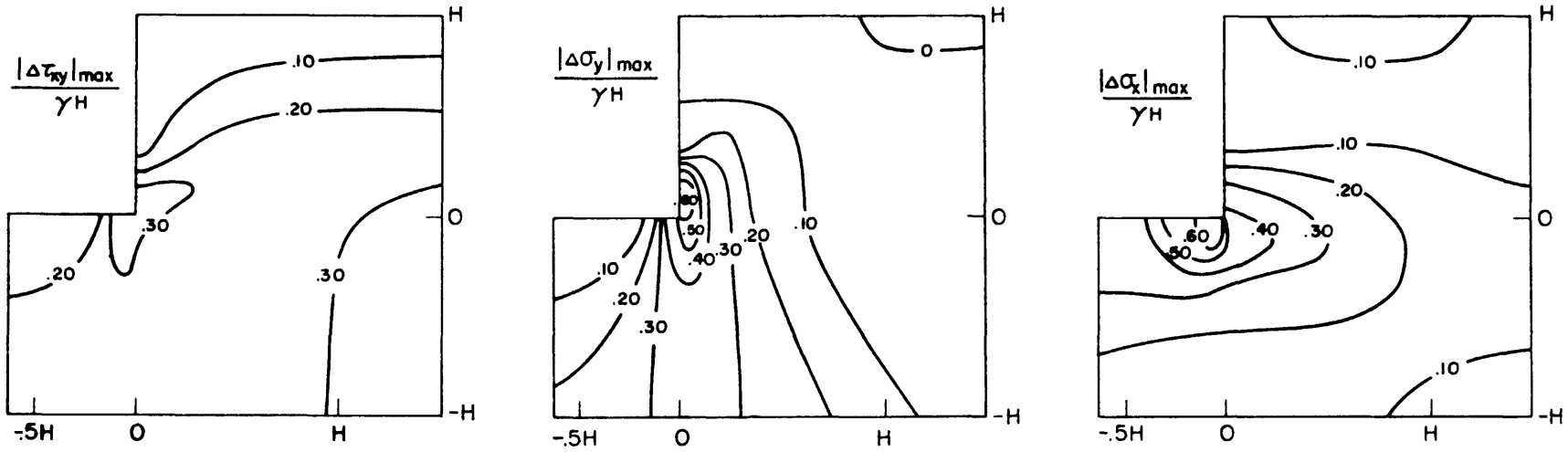

Figure 7-12 DISTRIBUTION OF MAXIMUM DYNAMIC STRESS INCREMENTS IN A VERTICAL SLOPE; 1:1 PERIOD RATIO, 1957 SAN FRANCISCO EARTHQUAKE, a_{max} = 0.105 g.

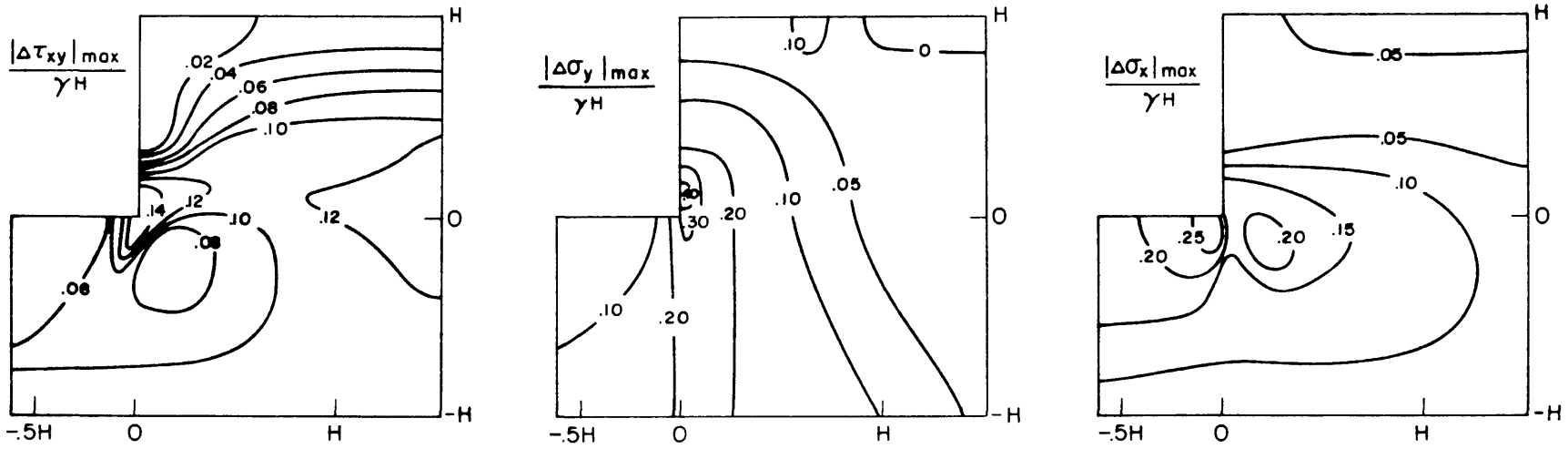

Figure 7-13 DISTRIBUTION OF MAXIMUM DYNAMIC STRESS INCREMENTS IN A VERTICAL SLOPE; 1.8:1 PERIOD RATIO, 1957 SAN FRANCISCO EARTHQUAKE, a_{max} = 0.105 g.

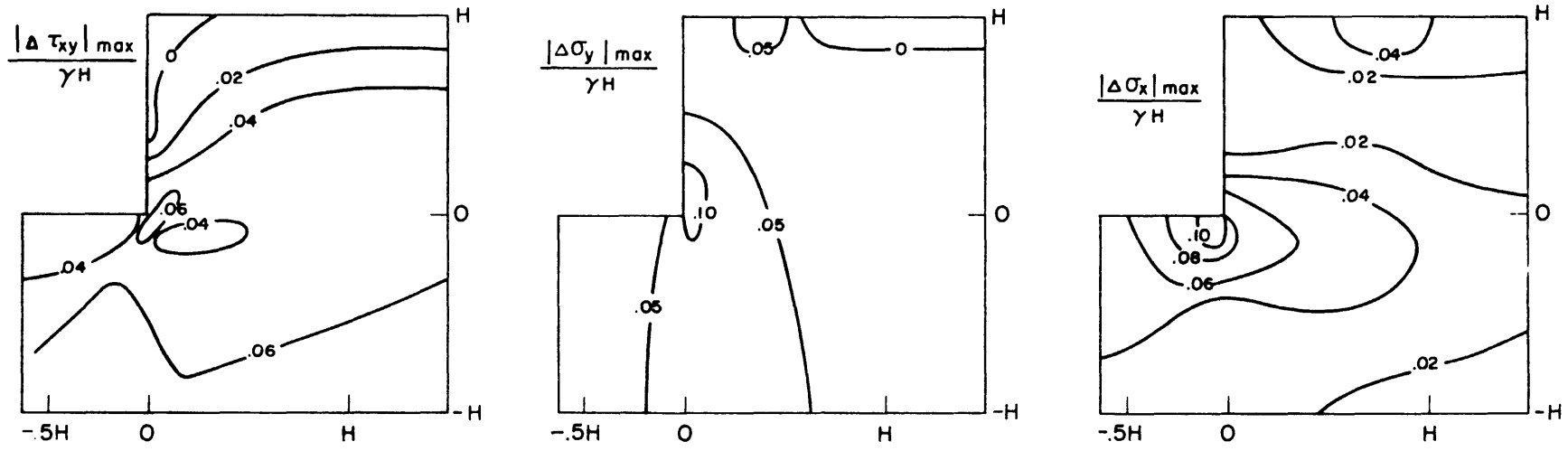

Figure 7-14 DISTRIBUTION OF MAXIMUM DYNAMIC STRESS INCREMENTS IN A VERTICAL SLOPE: 3.6:1 PERIOD RATIO, 1957 SAN FRANCISCO EARTHQUAKE, a_{max} = 0.105 g.

synthetic magnitude 8.25 earthquake in slopes with period ratios of 0.9:1 and 2.24:1 (see Table 7-2) are presented in Figures 7-15 and 7-16. For each plot, the values of the maximum absolute dynamic stress increments in 60 individual elements were determined, nondimensionalized in the same manner as the static stresses, and the ensuing stress distributions hand contoured. The reason for presenting the results in terms of the nondimensionalized Cartesian stresses is that in this form they can be applied to a wide range of problems as is explained in the following discussion.

Inspection of the dynamic stress distribution diagrams shows that the stresses in the slopes increase as the period ratio approaches resonance and also as a result of greater input acceleration. For example, the dynamic stresses for the 1:1 period ratio generated by the 1957 San Francisco earthquake input motion (Figure 7-12) are about 1.5 times greater than the dynamic stresses for the 1.8:1 period ratio (Figure 7-13) and about 5 times greater than the dynamic stresses for the 3.6:1 period ratio (Figure 7-14), but they are only about one third as large as those generated by the synthetic earthquake in a slope with 0.9:1 period ratio (Figure 7-15). In all the diagrams the stresses are distinctly concentrated around the toe of the slope. Also, it is very important that for a given stress component the patterns of the dynamic stress distribution obtained in the different analyses are the same.

A comparison of the magnitude of the nondimensionalized dynamic stress increments obtained using the two different earthquake records but essentially the same period ratio (for example, 1:1 in Figure 7-12 and 0.9:1 in Figure 7-15) shows that the stresses differ by a factor of

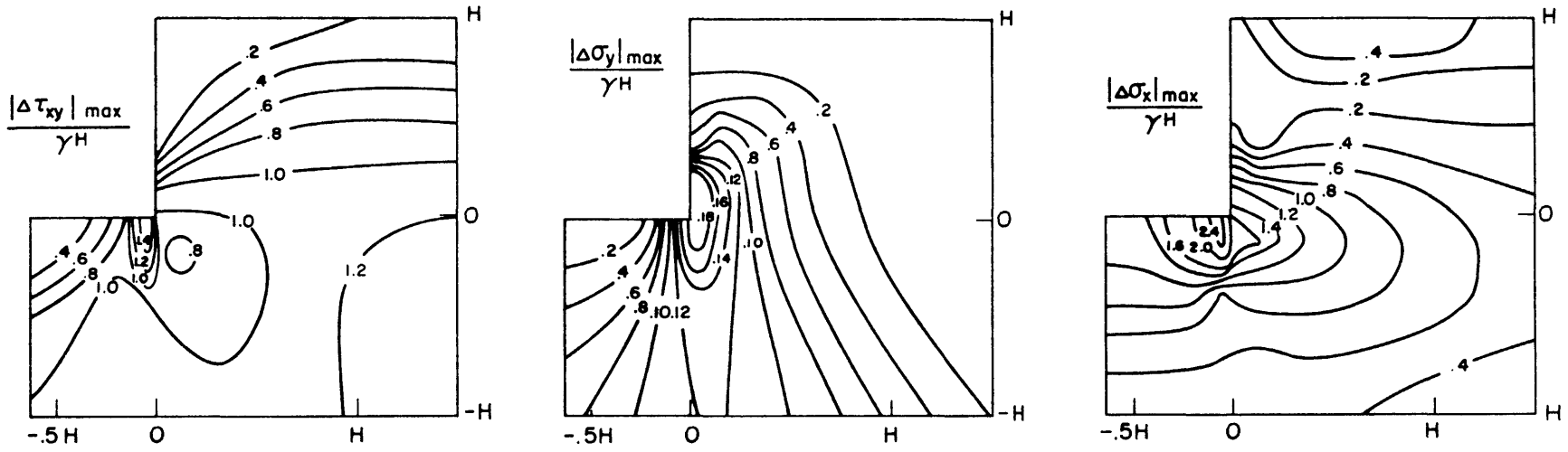

Figure 7-15 DISTRIBUTION OF MAXIMUM DYNAMIC STRESS INCREMENTS IN A VERTICAL SLOPE; 0.9:1 PERIOD RATIO, MAGNITUDE 8.25 SYNTHETIC EARTHQUAKE, a_{max} = 0.42 g.

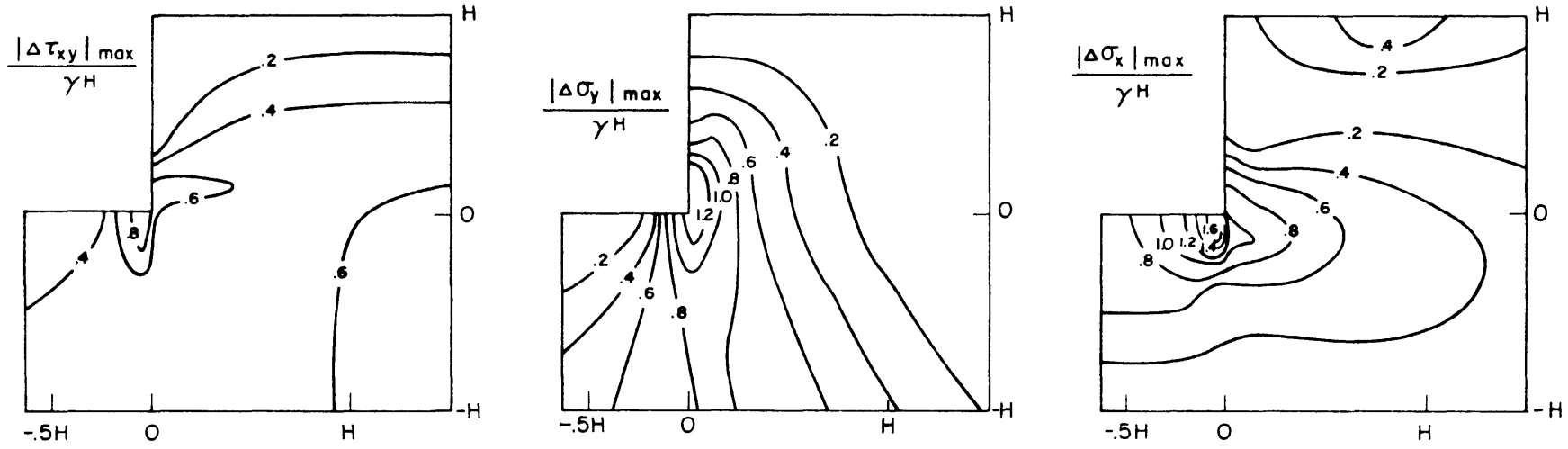

Figure 7-16 DISTRIBUTION OF MAXIMUM DYNAMIC STRESS INCREMENTS IN A VERTICAL SLOPE, 2.24:1 PERIOD RATIO, MAGNITUDE 8.25 SYNTHETIC EARTHQUAKE, a_{max} = 0.42 g.

four, which is the same as the ratio of the maximum accelerations in the two records. This observation is consistent with the fact that the soil is assumed to be a linear elastic material. It also fits with the observation that the relationship between the amplification factor and the period ratio (Figure 7-2) is independent of the input earthquake. Therefore, for a given period ratio, the results presented in Figures 7-12 through 7-16 can be used to determine the distribution of dynamic stresses in a vertical slope subjected to an earthquake of any magnitude by just multiplying by the ratio of the respective maximum earthquake accelerations.

This approach provides a way of estimating quickly and inexpensively the dynamic stresses that may develop in a slope during a seismic event. Similar solutions can be produced for other slope configurations, thus making these results more generally applicable.

With the dynamic stress increments in hand, it is necessary to superimpose them on the initial static stresses in order to determine the total stresses in the slope. For purposes of this discussion, the combined (static + dynamic) stresses are characterized by the values of the minor principal stress, σ_3, and the maximum shear stress, τ_{max}. The minor principal stress is important on two counts: (1) If it is negative, it indicates that tension exists in the slope, and its minimum value (the maximum tension) can be used to evaluate the possibility of tensile splitting; and (2) If the minor principal stress is positive, shear failure rather than tensile splitting is possible, and the value of the minor principal stress plays a role in evaluating the strength of a frictional material, such as the cemented sand. The maximum shear stress is important in considering the possibility of a shear failure.

Time histories for the combined (static + dynamic) minor principal and maximum shear stresses generated by the 1957 San Francisco earthquake in elements 139 and 140, which are the key elements in the lower part of the slope face (see Figure 7-3), are given in Figures 7-17 and 7-18, respectively. In both elements, the stresses cycle about the initial static value of each stress and duration of significant cycling is about the same. Three differences stand out in comparing the results for elements 139 and 140 however: (1) The cyclic stresses in element 140 are much higher than those in 139; (2) The minor principal stress cycles in element 140 are in phase with the maximum shear stress cycles, whereas, the stresses in element 139 are 90 degrees out of phase; and, (3) The minor principal stress in element 139 cycles entirely in the tensile stress region, while that in element 140 is tensile only for a small portion of one cycle. A particularly important finding with respect to evaluation of the potential for shear failure in a slope in cemented soil is the fact that the maximum shear stress may or may not be in phase with the minor principal stress. The shear strength is a function of the confining pressure which, for out of phase stress relationships, may be a minimum when the shear stress is maximum. In general, the minor principal and maximum shear stresses are found to be out of phase in the same region of the slope as the out of phase dynamic stress increments above the zero contour line for σ_x/σ_y as shown in Figure 7-9. Outside of this region they are in phase. Therefore, the in phase or out of phase relationship between the dynamic stress increments has to be taken into account when the dynamic stresses are superimposed onto the initial static stresses.

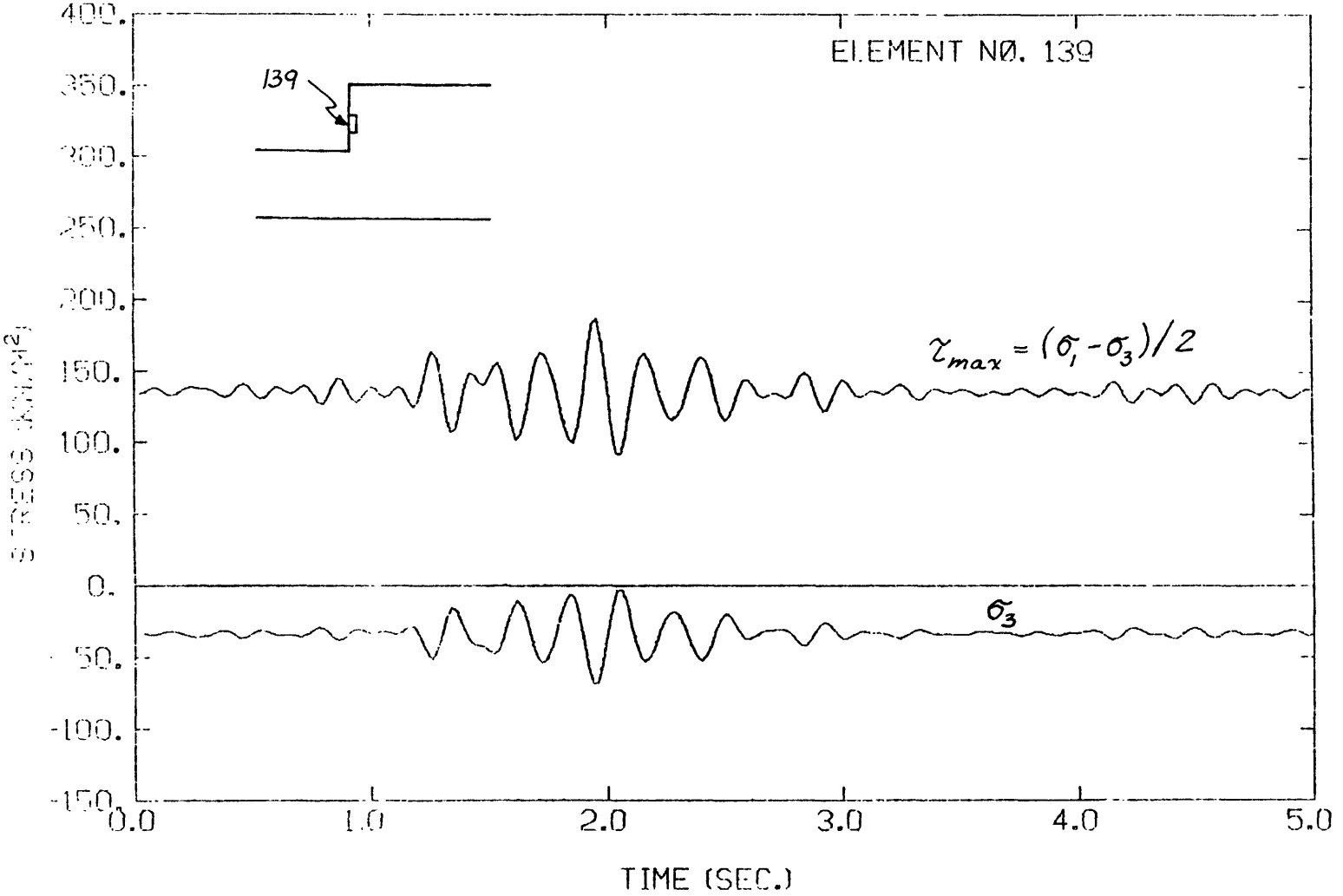

Figure 7-17 TIME HISTORIES OF τ_{max} AND σ_3 IN ELEMENT NO. 139 FOR 1:1 PERIOD RATIO, 1957 SAN FRANCISCO EARTHQUAKE.

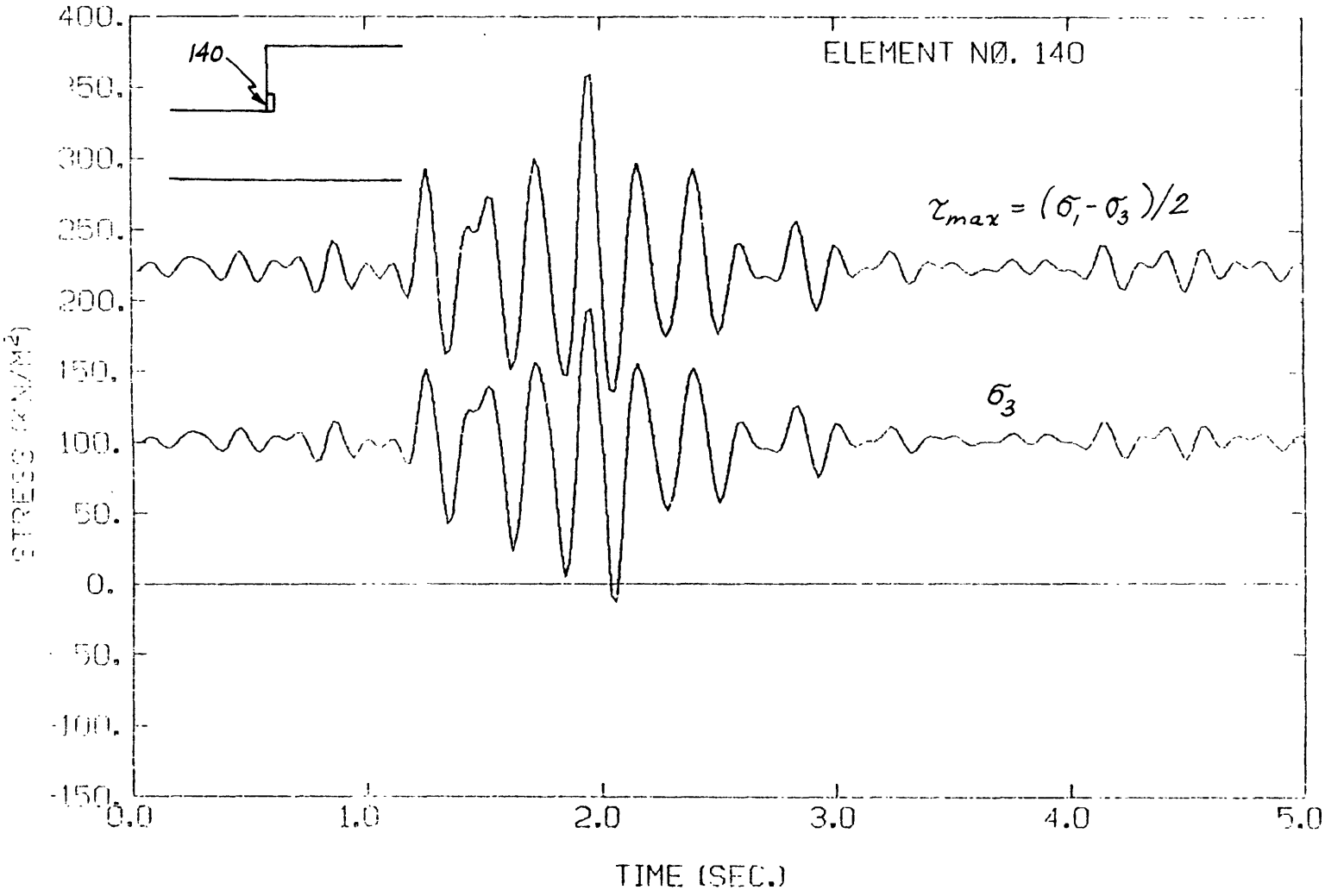

Figure 7-18 TIME HISTORIES OF τ_{max} AND σ_3 IN ELEMENT NO. 140 FOR 1:1 PERIOD RATIO, 1957 SAN FRANCISCO EARTHQUAKE.

For purposes of producing single-valued nondimensionalized stress charts representing the combined static and dynamic stresses, the dynamic stress peaks were superimposed onto the initial static stresses. Charts for the contours of the minimum values of the minor principal stress ($\sigma_3/\gamma H$), prepared in the same manner as those for the dynamic stress increments for all five earthquake conditions analyzed, are given in Figures 7-19 and 7-20. In all cases there are significant zones of tension, which are increased over those existing in the static condition. It should be remembered that the tension zones shown include elements in which the minimum minor principal stress becomes tensile for only a portion of one cycle (Figure 7-18), as well as those in which it stays in tension throughout the loading (Figure 7-17).

The contours in Figures 7-19 and 7-20 show that the magnitude and the extent of the tension zone in the slope are functions of both the period ratio and the size of the earthquake. For example, the tensile minimum σ_3 values generated by the 1957 San Francisco earthquake in a slope with a period ratio of 3.6:1 (Figure 7-19) occur in a zone only slightly larger than the one produced by static loading (Figure 7-9). However, in a slope with a 1:1 period ratio this zone encompasses the entire slope face, the top of the slope to a distance of at least 1.5 times the height of the slope, and the base of the slope to a distance of over 0.5 times the height (Figure 7-19). For the 8.25 synthetic earthquake similar period effects are found, and the zones of tensile minimum σ_3 are found to include much larger areas than those produced by the 1957 San Francisco earthquake. The results clearly show that a seismic event can induce significant levels of tension in a cemented soil slope. The importance of these findings with respect to the slope performance is considered in the next section of this chapter.

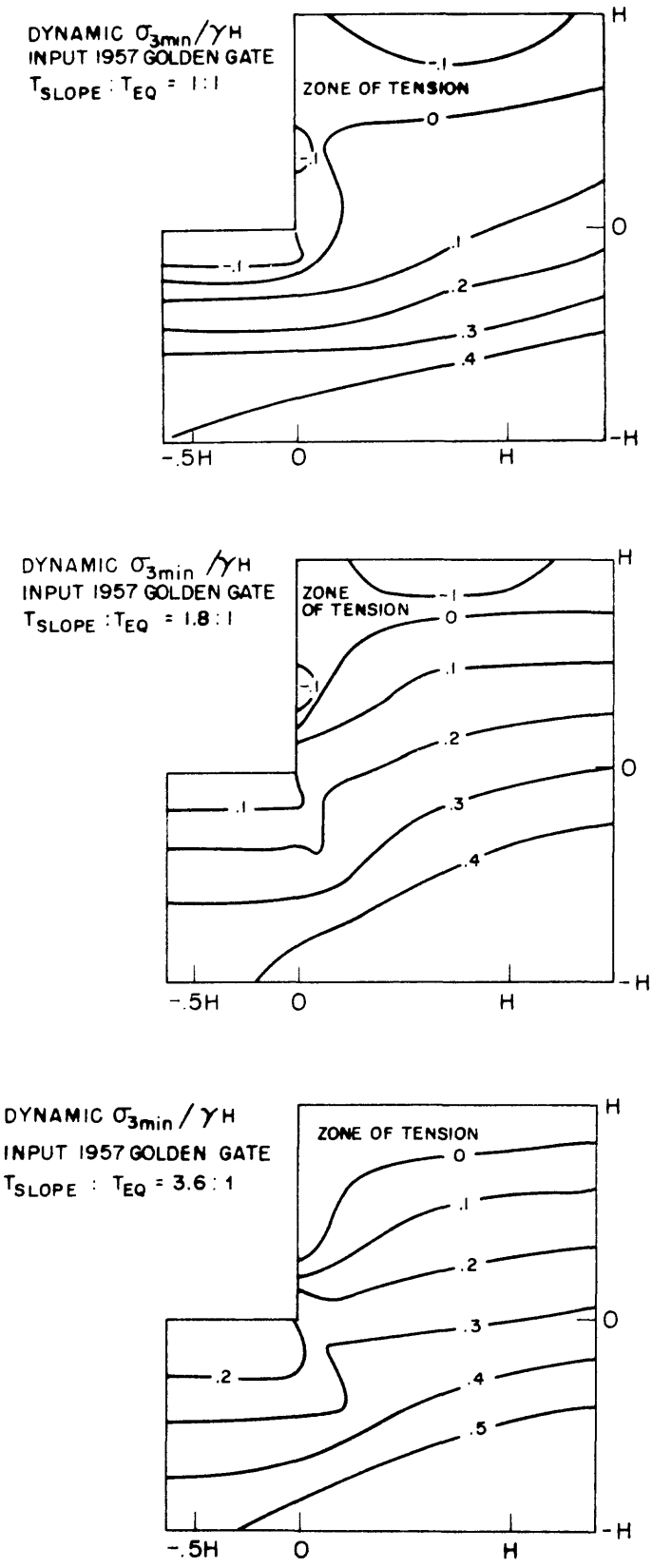

Figure 7-19 DISTRIBUTION OF MINIMUM $\sigma_3/\gamma H$ IN A VERTICAL SLOPE SUBJECTED TO THE 1957 SAN FRANCISCO EARTHQUAKE, H = 25 m, γ = 16.8 kN/m^3.

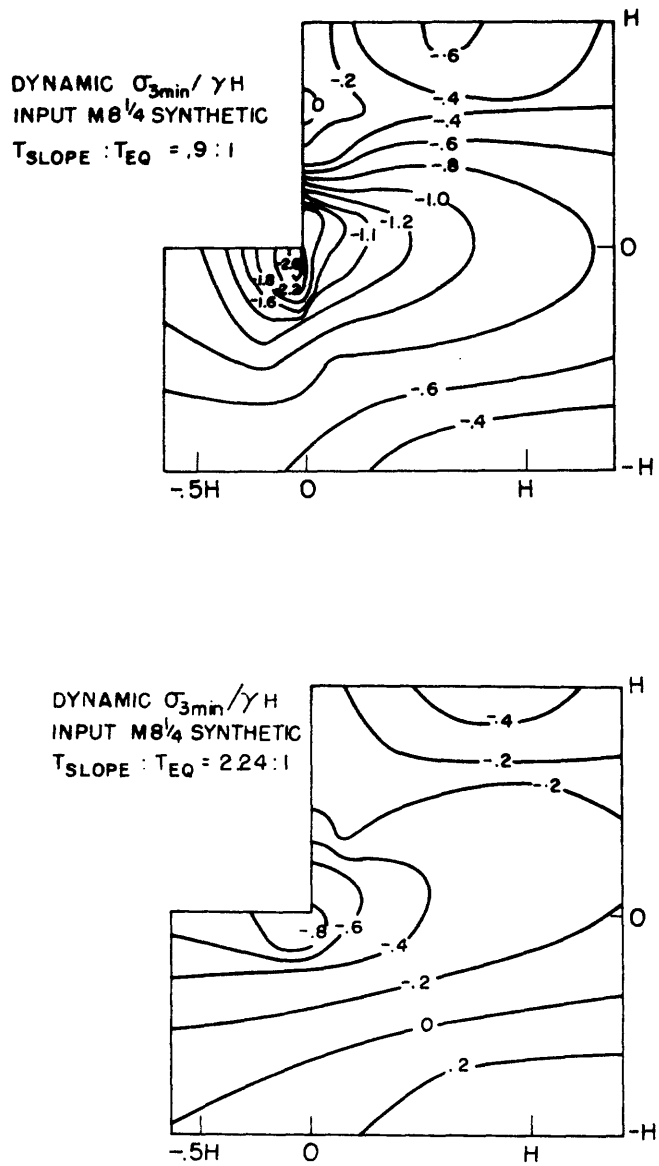

Figure 7-20 DISTRIBUTION OF MINIMUM $\sigma_3/\gamma H$ IN A VERTICAL SLOPE SUBJECTED TO A MAGNITUDE 8-1/4 SYNTHETIC EARTHQUAKE, H = 25 m, γ = 16.8 kN/m^3.

Values of combined static and dynamic maximum shear stress were contoured by the same procedures as for the minimum principal stress. The nondimensionalized contours of the maximum values of the maximum shear stress ($\sigma_{max}/\gamma H$) for all five earthquake analyses are given in Figures 7-21 and 7-22. It should be remembered that, in terms of time histories, the maximum shear stresses are in phase (occur at the same time) with the minimum minor principal stress values only in the upper portions of the slope. The maximum shear stresses can be seen to occur around the toe of the slope and to increase as the period ratio approaches one or when the earthquake magnitude is increased.

7.5 Stability of Steep Slopes in Cemented Soils - Implications of the Analytical Studies

Having determined the distribution of the static and dynamic stresses throughout the slope, it is now possible to address the question of slope stability in cemented soils. As already explained in Chapter VI, the approach adopted in this study is to compare the stress levels determined by the numerical analyses to the expected strength of the soil at different points within the slope. In this manner it is possible to identify the areas in which failures are likely to initiate and probable modes of failure can be defined.

The example analyses to be presented demonstrate that this approach to slope stability analysis, applied to steep slopes in cemented soils, provides valuable and qualitatively consistent results. The static and the dynamic results are discussed separately so that their individual merits can be examined. Also, a separate section is given to the material characteristics and the failure criteria employed since they obviously strongly affect the outcome of the analyses.

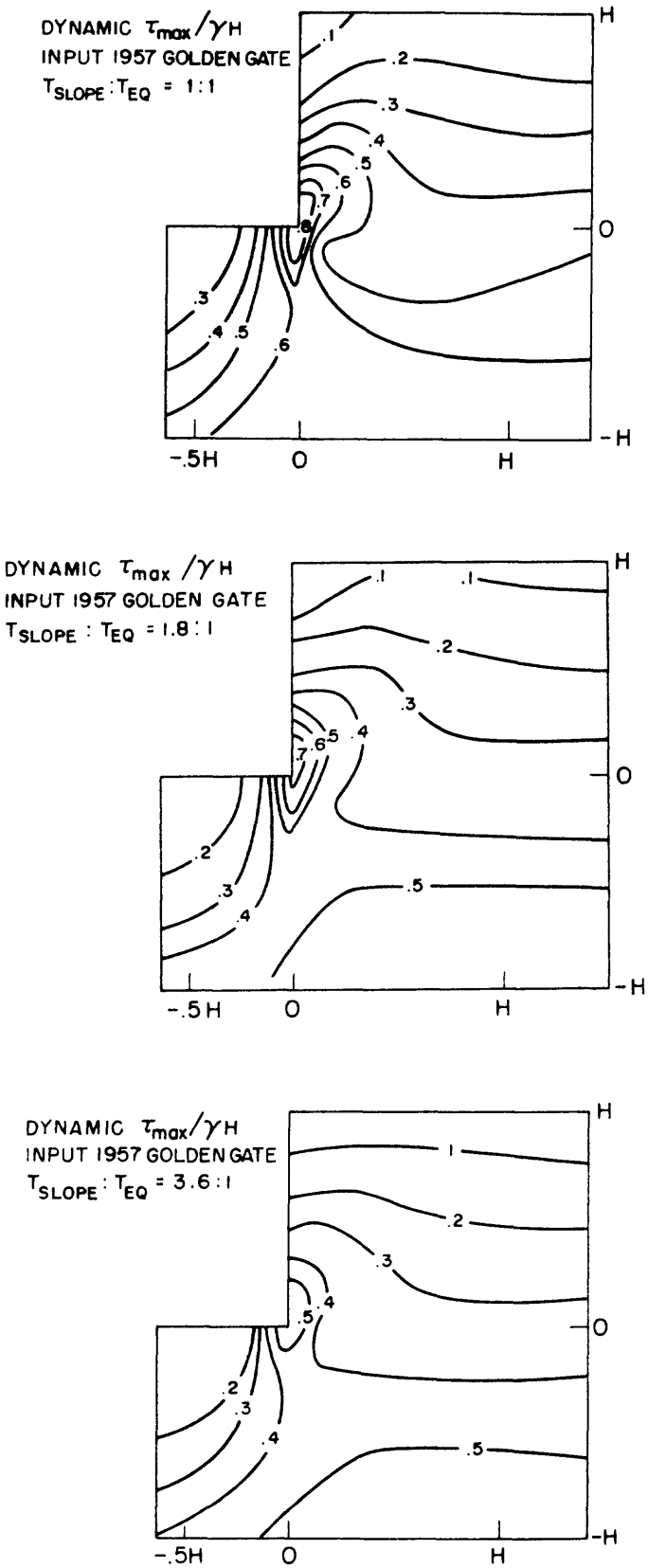

Figure 7-21 DISTRIBUTION OF MAXIMUM, $\tau_{max}/\gamma H$ IN A VERTICAL SLOPE SUBJECTED TO THE 1957 SAN FRANCISCO EARTHQUAKE, H = 25 m, γ = 16.8 kN/m^3.

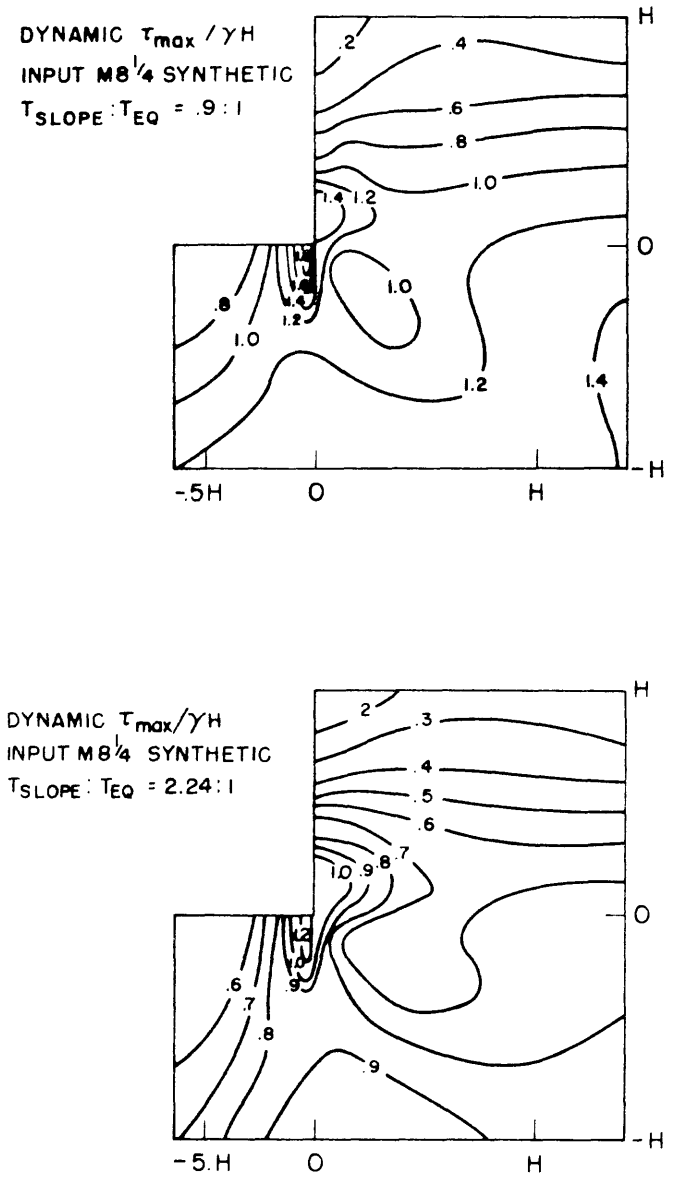

Figure 7-22 DISTRIBUTION OF MAXIMUM $\tau_{max}/\gamma H$ IN A VERTICAL SLOPE SUBJECTED TO A MAGNITUDE 8-1/4 SYNTHETIC EARTHQUAKE, H = 25 m, γ = 16.8 kN/m^3.

7.5.1 Soil Characteristics and Failure Criteria

The material characteristics considered in the example slope stability analyses are mainly those of the artificially cemented sand with 4% cement. However, references are also made to the artificially cemented sand with 2% cement, the naturally cemented sand from Pacifica (Bachus, 1978), and the naturally cemented sand from SLAC (Alfi, 1978) which have similar characteristics. The naturally cemented sands are described in Chapter II (Table 2-1) and the artificially cemented sands are described in detail in Chapter IV (Table 2-1). For convenience, their properties pertinent to this discussion are presented in Table 7-3. All the soils show a strong frictional component of strength represented by the angle of internal friction, Φ, ranging from 34 to 48 degrees. The cohesion, c, ranges from 34.5 kN/m^2 for the sand from Pacifica to 1036 kN/m^2 for the sand from SLAC. The Coulomb failure criterion (equation (3), Chapter IV) is used to define failure under static loading in the compressive stress region. In the tensile stress region, on the other hand, failure is assumed to occur when the minor principal stress decreases to the point where it exceeds the tensile strength of the soil.

Table 7-3

PROPERTIES OF CEMENTED SANDS

Material Type	c [kN/m^2]	Φ [degrees]	σ_T [kN/m^2]	γ_d [kN/m^2]
4% cement	143	35	69	15.8
2% cement	46	34	20	15.5
Pacifica (Bachus, 1978)	34.5	39	N.A.	17.1
SLAC (Alfi, 1978)	1036	48	N.A.	17.8

In Chapter IV it was found that the average dynamic strength of the artificially cemented sand in compression loading (cyclic triaxial tests) is 16 percent higher than its corresponding static strength and that there does not appear to be a unique relationship between the number of cycles to failure and the stress at failure (Figure 7-9). In general, in the dynamic tests in which the stress exceeds the equivalent static stress at failure by more than 16 percent, 64 percent of the samples fail in less than 30 cycles and 45 percent fail in less than 6 cycles of loading. For the purposes of the slope stability analyses, it was assumed that in compression a failure is likely to occur whenever at least one cycle of loading exceeds the equivalent static strength of the soil by more than 16 percent which is a conservative assumption.

In cyclic Brazilian tension tests the strength of the soil decreases rapidly with the number of cycles (Table 7-10). Therefore, in the tensile stress region, the method of expressing the cyclic loading by an equivalent number of uniform cycles (Lee and Chan, 1972) is used to determine whether a failure could occur. The 1957 San Francisco earthquake theoretically produces 6 cycles at an average stress level of 0.65 of the maximum. For the magnitude 8.25 synthetic earthquake, the number of the equivalent uniform cycles, equal to 0.65 of the maximum stress, increases to 29.

7.5.2 Static Slope Response

The static slope response of a vertical slope was evaluated by a conventional limiting equilibrium slope stability technique and the finite element method. The limiting equilibrium approach employed assumes a shear type failure mechanism and does not account for the possibility

of tensile failure. Also, the assumed failure mechanism is not particularly consistent with that usually observed for cemented soil slopes (see Figure 7-23). However, the results of this approach are useful to provide a frame of reference for those of the finite element analysis. The results of the finite element analysis give information as to the possibility of tensile splitting and progressive failure.

Limiting Equilibrium Analysis

Assuming the Coulomb failure criterion applies, the limiting equilibrium analysis reduces to an evaluation of a factor of safety, F_s, which is a ratio of the driving force, D, and the resisting force, R, along a potential shear failure plane inclined at an angle of $45 - \Phi/2$ from vertical (see Figure 7-23). The expression for F_s is:

$$F_s = \frac{R}{D} = \frac{4c}{\gamma H \sin (90 - \Phi)} + \tan (45 - \Phi/2) \tan \Phi \qquad (11)$$

where c is the cohesion, γ is the unit wieght, H is the height of the slope, and Φ is the angle of internal friction.

If the factor of safety from the limiting equilibrium analysis is exactly one, the height of the slope is called the critical height, H_{crit}. The relationship between H_{crit}, γ, and c as given by equation (11) is illustrated in Figure 7-24. It is seen that the amount of cohesion strongly influences the critical height of the slope and that decreasing the unit weight increases the critical height of the slope. For example, the H_{crit} of a slope in sand cemented by 2% cement would be 20.8 m, whereas in sand cemented by 4% cement it would be 64.7 m.

An interesting use of Figure 7-24 is to consider the height of an observed slope in cemented soil and from that deduce the probable cohesion

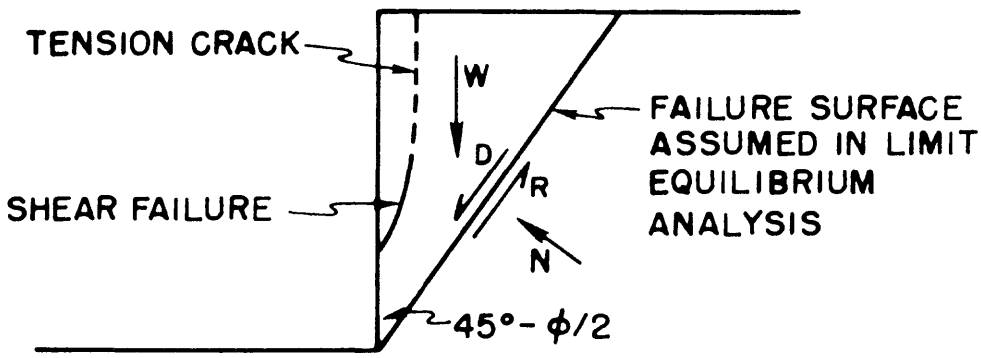

Figure 7-23 GEOMETRY AND FORCES INVOLVED IN A STATIC LIMITING EQUILIBRIUM ANALYSIS OF A VERTICAL SLOPE AND THE OBSERVED FAILURE MODE.

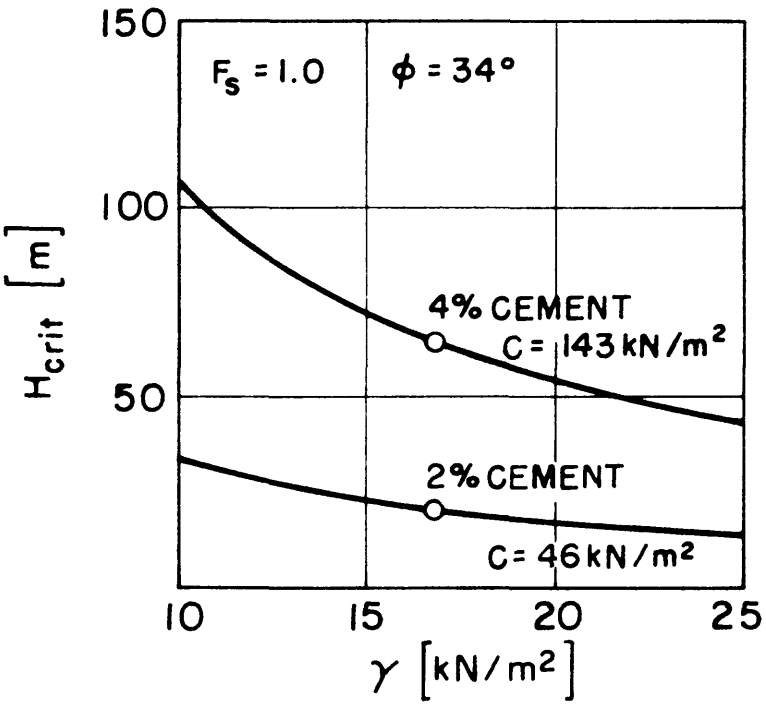

Figure 7-24 CRITICAL HEIGHT, H_{crit}, VERSUS UNIT WEIGHT, γ, FOR A VERTICAL SLOPE IN CEMENTED SOIL.

of the soil. For instance, the slopes in Pacifica are about 50 m high, yet a weak cemented sand unit tested by Bachus (1978) had strength even lower than the sand cemented with 2% cement (see Table 7-3). Thus, these data imply that the other units comprising the slope must have a cohesive strength at least as high as the sand cemented with 4% cement, if not higher.

The effect of unit weight on the critical height of a slope in cemented soil is best demonstrated by considering the volcanic ash soils in Guatemala which have a unit weight of about 10 kN/m^3. If their strength is assumed to be the same as that of the sand cemented with 2% cement, the equivalent critical height of a vertical slope would be 34.6 m as compared to 20.8 m for the cemented sand. Thus, it is apparent that the height of a vertical slope in cemented soil is prominently influenced by its unit weight as well as its strength. Interestingly, vertical road cuts up to 30 m high are observed in the volcanic ash soils in Guatemala.

Unfortunately, although the results obtained by the limiting equilibrium approach provide some interesting insights into the static response of vertical slopes in cemented soil, the shear failure mechanism assumed in this type of analysis has not been observed in the field. The commonly observed failures of very steep slopes in cemented soil are initiated by tensile splitting in the upper part of the slope followed either by toppling or by shearing of the soil in the lower part of the slope (Figure 7-23 and also Figure 2-3). The finite element analyses can be used to address this behavior.

Finite Element Analysis

The nondimensionalized stresses from a static finite element analysis are presented in Figure 7-9. These show that a zone of tension can exist in the upper part of the slope and a high concentration of shear stress is found at the toe. The effect of these stresses must be considered relative to the shear strength of the soil which in the case of cemented soil depends on the confining pressure. Though there is a high concentration of shear stresses at the toe of the slope, the lateral stresses are also quite high and provide the soil with a high level of shear resistance. In fact, until the slope reaches H_{crit}, as defined in the limit equilibrium analysis, the soil in this zone does not fail. On the other hand, there is a concentration of tensile stresses at the slope face, about one third of the way up from the toe. The tensile and shear stresses in this zone exceed the strength of the soil before the height of the slope reaches H_{crit} which indicates that a static failure of a vertical slope in cemented soil could be initiated in this manner. This observation, combined with the facts that the soil fails in a brittle mode and the tensile stresses along the upper part of the slope are likely to be expressed in the form of tensile stress fractures, seems to satisfactorily explain the observed static failures of steep slopes in cemented soils (see Figure 7-22).

7.5.3 Dynamic Slope Response

The example results of the dynamic slope stability analyses presented here are intended to demonstrate the effect of period ratio, slope height, soil strength, and earthquake magnitude on the predicted extent of potential failure zones and, in the process, to define the probable mode of

failure of steep slopes in cemented soils. The following discussion first states the criteria for determining the potential failure zones and then describes the individual results.

Criteria for Determining the Potential Failure Zones

The zones of potential failure within a slope are identified by comparing the dynamic stresses predicted from the finite element analyses (see Section 7.4.3) to the expected soil strength at different points within the slope. The minimum value of the minor principal stress, σ_3, plays an important role in this process. If the value of σ_3 is tensile, the possibility of tensile failure is determined by using the failure criteria given earlier in this chapter (see Section 7.5.1). If, on the other hand, σ_3 is compressive or not sufficiently low to cause a tensile failure, its minimum value is used to determine the expected minimum static shear strength of the soil, which is then compared to the appropriate computed value of maximum shear stress, τ_{max}.

The choice of the value of τ_{max} depends on the particular location in the slope because the maxima and minima of σ_3 and τ_{max} may occur in phase (Figure 7-18) or 90 degrees out of phase (Figure 7-17). It is fairly obvious that in the case where the stresses are out of phase, as in element 139 (Figure 7-17), they are most critical when σ_3 is at its minimum and τ_{max} is at its maximum. It is much less apparent, however, that in the case where the stresses are in phase, as in element 140 (Figure 7-18), the most critical stresses occur at the time when both σ_3 and τ_{max} are at their minima. Thus, in evaluating the potential for shear failure the expected minimum shear strength of the soil is compared to the maximum predicted value of τ_{max} in the zone above the zero

contour of σ_x/σ_y (Figure 7-9) and to the minimum predicted value of τ_{max} in the rest of the slope. The previously discussed failure criteria (see Section 7.5.1) are applied to determine the possibility of shear failure at each given point.

Effect of Period Ratio

Predicted potential failure zones for a 50 m high vertical slope assumed to be composed of sand cemented with 4% cement and subjected to the 1957 San Francisco earthquake are presented in Figures 7-25 and 7-26 for 1:1 and 1.8:1 period ratios, respectively. In the case of the 1:1 period ratio (Figure 7-25), there are three areas in which tensile failure could initiate: at the top of the slope with the maximum stress concentration located about one half of the slope height, 25 m, from the slope face; at the base of the slope with the maximum stress concentration at the break in the slope; and, about one third of the way up from the toe, at the slope face. An area of potential shear failure is found extending from the mid height to just below the toe of the slope.

It has been already shown that as the period ratio increases the magnitude of the dynamic stresses decreases. Correspondingly, the extent of the predicted potential failure zones also decreases. Therefore, the areas of the potential failure zones for the 1.8:1 period ratio (Figure 7-26) are smaller than those for the 1:1 period ratio (Figure 7-25). The zone of potential shear failure no longer extends all the way to the toe and the zone of the potential tensile failure at the toe of the slope is completely absent. If the period ratio were to increase to 3.6:1 (not illustrated), only the zone of potential tensile failure at the mid height of the slope would still remain.

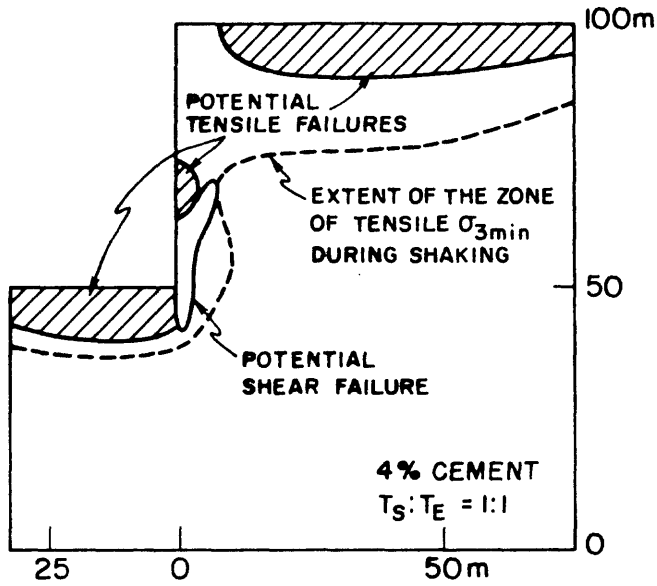

Figure 7-25 DISTRIBUTION OF POTENTIAL FAILURE ZONES IN A 50 m SLOPE OF SAND CEMENTED WITH 4% CEMENT; 1957 SAN FRANCISCO EARTHQUAKE; 1:1 PERIOD RATIO.

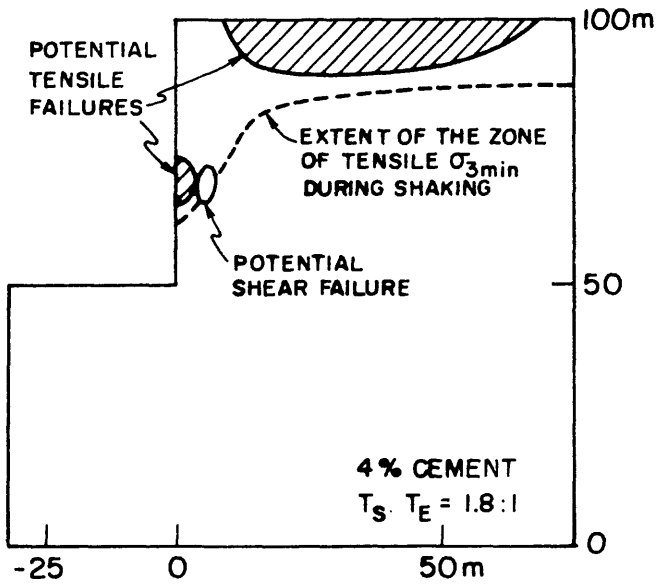

Figure 7-26 DISTRIBUTION OF POTENTIAL FAILURE ZONES IN a 50 m SLOPE OF SAND CEMENTED WITH 4% CEMENT; 1957 SAN FRANCISCO EARTHQUAKE; 1.8:1 PERIOD RATIO.

Effect of Slope Height

The effect of the slope height on the predicted response of the slope can be seen by comparing the potential failure zones in 25 and 50 m slopes to each other (Figures 7-27 and 7-25, respectively) for a period ratio of 1:1. In the 25 m slope the zones of predicted tensile failure are smaller than in the 50 m slope, and there is no possibility of shear failure anywhere within the 25 m slope. This result is consistent with the fact that the initial static stresses in the 50 m slope are already twice as high as those in the 25 m slope and, assuming linear elastic soil response, the dynamic stresses also differ by the factor of two. In general, a change in the slope height results in a corresponding change in the static and dynamic stresses and in the predicted extent of the potential failure zones.

Effect of Soil Strength

The influence of soil strength on the dynamic slope response is demonstrated by assuming that the 25 m slope in Figure 7-28 is composed of weaker soil with characteristics obtained by averaging the properties of sands cemented with 2 and 4 percent cement. This slope has a static factor of safety of 1.45 as compared to 2.0 for a slope of the same height in sand cemented with 4 percent cement. A comparison of the results of the slope response analyses for the slope in 4 percent cement material (Figure 7-27) and for the slope in the weaker material (Figure 7-28), at the same period ratio of 1:1, shows that the zones of potential tensile failure at the top and the toe of the slope are more extensive in the weaker material. Also, in the weaker soil, there is a zone of potential shear failure just below the mid height of the slope which does not occur in the slope composed of 4 percent cement material.

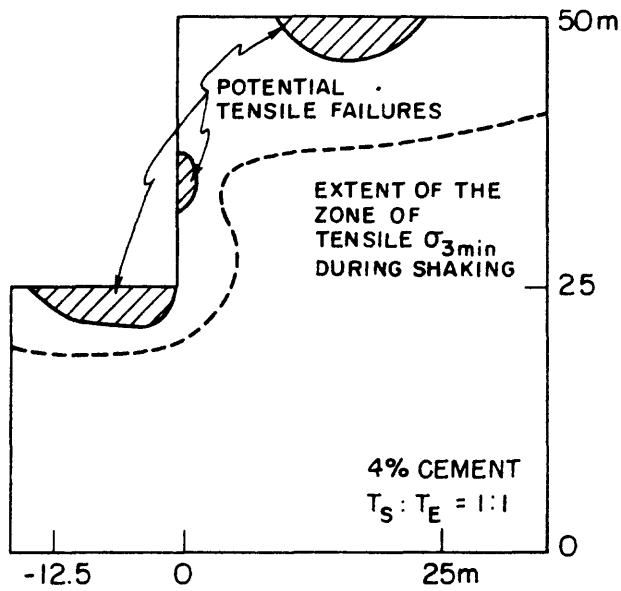

Figure 7-27 DISTRIBUTION OF POTENTIAL FAILURE ZONES IN A 25 m SLOPE OF SAND CEMENTED WITH 4% CEMENT; 1957 SAN FRANCISCO EARTHQUAKE; 1:1 PERIOD RATIO.

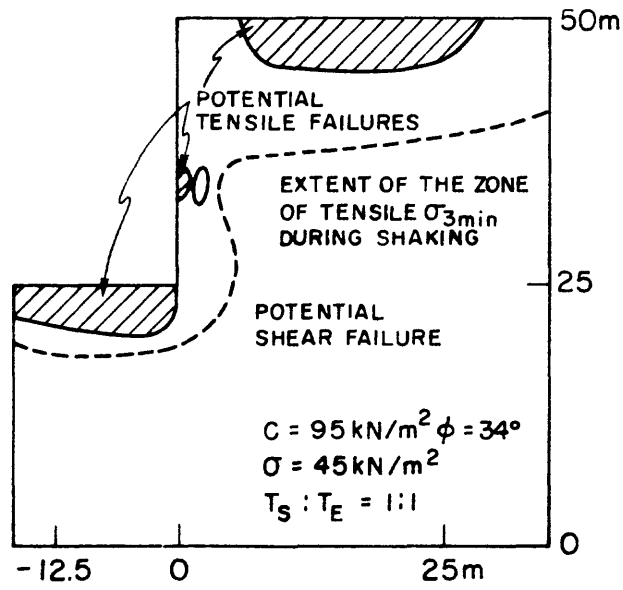

Figure 7-28 DISTRIBUTION OF POTENTIAL FAILURE ZONES IN A 25 m SLOPE OF SOIL WITH AVERAGE PROPERTIES OF THE CEMENTED SANDS: 1957 SAN FRANCISCO EARTHQUAKE; 1:1 PERIOD RATIO.

Effect of Earthquake Magnitude

The dynamic stress distributions presented in Section 7.4.3 show that an increase in the magnitude of the input motion results in an increased magnitude of the dynamic stresses. The extent of the potential failure zones is similarly influenced. In fact, the extent of the potential failure zones determined using the magnitude 8.25 synthetic earthquake is such that massive failures of the entire 25 m high slopes, composed of any of the cemented soils tested (Table 7-3), are predicted. This is a rather surprising result especially considering that, for example, 50 m high slopes in Pacifica have survived the 1906 San Francisco earthquake with relatively little damage. However, it can be explained in terms of the assumptions used in the analyses.

As previously discussed, the linear elastic analyses used herein model neither the development of a progressive failure nor the gradual decrease in shear modulus and the corresponding increase in damping ratio during cyclic loading. Also, it seems unlikely that a natural slope would remain near resonance long enough to develop the magnitude of stresses shown. Therefore, it is most probable that the stresses and the extent of the zones of potential failure initiation presented in this study are exaggerated, especially when period ratios near resonance are assumed. In this respect, it is then inappropriate to directly extend the quantitative results presented thus far to the problem of dynamic slope stability in natural slopes. In order to achieve this goal, the nonlinear aspect of the soil behavior and a careful choice of the initial period ratio should be considered in future research.

On the other hand, a qualitative interpretation of the results of the dynamic slope response analyses provides valuable information about the influence of the various parameters on predicted slope response and also gives a good indication of the probable mode of failure of steep slopes in cemented soil as discussed next.

Mode of Failure

The examples presented in Figures 7-25 through 7-28 demonstrate that the development and extent of the potential failure zones in a slope of cemented soil subjected to dynamic loading are strongly influenced by the period ratio, the slope height, and the strength of the soil. However, though the size of these zones varies depending on the magnitude of the stresses involved, their location and nature remain the same and the order in which they develop with increasing stress level is predictable. The first to develop, at relatively low stress levels, is a zone of potential tensile failure located just below the mid height of the slope. As the stress levels increase, it is followed by the development of a zone of potential tensile failure at the top of the slope, a zone of potential tensile failure at the toe, and a zone of potential shear failure just below the mid height of the slope.

In general, the results of the slope response analyses suggest that steep slopes in cemented soils subjected to dynamic loading most probably fail in tension, with the failure originating in the area below the mid height of the slope. Also, the extent of the potential failure zones near the slope face indicates that the failures should be shallow. These conclusions agree well with the field observations which indicate that failures of steep slopes in cemented soils occur by tensile splitting and that they are usually quite shallow.

Another aspect of the slope response analyses concerns the fact that in all the examples a zone of potential tensile failure at the top of the slope was identified. If this indeed exists, tensile fractures could form a rather large distance from the slope. However, there is no danger of immediate slope failure since the cemented soil beneath the tensile zone away from the slope face is not overstressed. It is interesting that eyewitness accounts of the appearance of the top of the slope in cemented soil immediately following an earthquake often include comments on tensile fractures well behind the slope face (Harp and others, 1978).

Thus, the qualitative interpretation of the dynamic slope response analyses yields results that are quite compatible with the field observations. In addition, the conclusion that the main mode of failure in steep slopes of cemented soil is intension means that slope stability analyses which assume the presence of a shear failure surface are not applicable.

7.6 Summary

Finite element analyses of vertical slopes in linear elastic medium were performed in order to investigate the magnitude of ground accelerations and the nature of the dynamic stress distribution for different types of earthquake loading and different soil properties. The results of these analyses were then used to define the potential failure mode of steep slopes in cemented soils.

Two accelerograms, the S 80° E component of the Golden Gate record from the 1957 San Francisco earthquake and a magnitude 8.25 synthetic earthquake developed by Seed and Idriss (1969), were used in the dynamic

analyses. The modelled soil deposit was 400 m long, 25 m high on the left and 50 m high on the right, with a 25 m high vertical slope in the middle. The material was assumed to be linear elastic with a Poisson's ratio of 0.3 and a damping ratio of 10 percent. A total of five different dynamic finite element analyses, three using the 1957 San Francisco earthquake and two using the magnitude 8.25 synthetic earthquake, were performed assuming a range of shear wave velocities from 250 to 900 m/sec. The different shear wave velocities were used in order to evaluate the influence of the period ratio on the dynamic slope response. (The period ratio is defined as the ratio of the natural period of the soil deposit to the dominant period of the earthquake.)

The results of the dynamic analyses consisted of accelerations at the ground surface and dynamic stresses generated within the slopes. The ground accelerations were interpreted to provide information about the amplification of input earthquake motion due to the presence of the slope and due to the natural period of soil deposit. The dynamic stresses were used to identify the potential failure modes in steep slopes of cemented soil. The main conclusions of these analyses are:

1. Near the slope face the horizontal accelerations are somewhat amplified relative to free field.

2. Significant vertical accelerations may occur near the slope face and may account for some of the increased damage observed in the vicinity of slopes.

3. The amplification of the input acceleration is strongly dependent on the period ratio. At period ratios near resonance the amount of amplification in free field may by far exceed the amplification due to any topographic effects.

4. The magnitude of the dynamic stresses is strongly dependent on the period ratio and earthquake magnitude.

5. For a given period ratio, the pattern of the dynamic stress distribution in a slope of linear elastic material is the same regardless of the earthquake magnitude. Thus, the dynamic stress distributions can be nondimensionalized and the magnitude of the stresses scaled to any peak input acceleration.

6. A seismic event can generate significant levels of tension in steep slopes. Example analyses of dynamic slope response indicate that seismically induced failures in slopes of weakly cemented soil will most probably occur in tension. Also, a zone of tensile cracking at the top of the slope is possible. These results are in good agreement with field observations of slope failures in steep slopes of cemented soil.

7. The linear elastic analyses yield qualitatively consistent results which are compatible with field observations.

CHAPTER VIII

Summary and Conclusions

8.1 Summary

This study represents an initial part of a comprehensive investigation of slope behavior in cemented soils, and its specific objectives are: (1) documenting of the behavior of natural slopes in weakly cemented soils; (2) defining the engineering response of weakly cemented soils under static and dynamic loading; (3) establishing the stress conditions in steep slopes during static and dynamic loading and (4) developing guidelines for evaluation of seismic stability of slopes in cemented soils.

Field observations of slope behavior in the weakly cemented soils have been conducted in Guatemala and in California, along the Pacific Coast between San Francisco and Santa Cruz. The soils in Guatemala are composed mainly of sand and silt size volcanic ash and derive their strength from the interlocking of very angular volcanic glass fragments. In California, the soils are medium to fine grained sands which are usually cemented with clays, iron oxides, and silica.

Testing for the investigation was done using both samples of naturally occurring cemented soils and artificially cemented soils fabricated in the laboratory. The artificially prepared samples were used to circumvent the difficulty of obtaining undisturbed specimens of the sensitive natural soils, and to allow study of a material with characteristics which could be varied as desired. Natural materials were always block sampled, the only procedure considered reliable enough to avoid disturbance. Even so, the

block sampling was a time-consuming process, and the logistics of transporting the weak cemented sands often posed problems.

The artificially prepared laboratory specimens were made of a mix of sand, portland cement and water. Several mixtures were used to model different degrees of cementation. Also, the void ratio of the specimens was varied to investigate the effect of this parameter. The behavior of the artificially cemented sands was found to fall nicely within the ranges of behavior observed for the naturally cemented soils tested.

Static and dynamic laboratory tests were performed to determine the strength and stress-strain response of cemented sands under compression and tension. Over 200 triaxial compression, Brazilian tension and simple shear tests were conducted. In addition, numerous classification tests were carried out to define basic material characteristics. Three different naturally cemented soils and five different artificially cemented soils were included in the investigation.

After a careful consideration of available methods for slope stability analyses, the finite element procedure was selected for the analyses of the static and dynamic slope response. This method is essentially the only one which can be used to determine the stress distribution in the entire slope and thus allow prediction of conditions leading to the precipitate failure of a cemented soil slope. Because the laboratory test results showed cemented soil to behave in essentially a linear fashion prior to failure, the finite element analyses were performed using assumed elastic behavior for the slope materials.

Using this approach, it was possible to isolate the effects of the individual variables: slope height, natural period of the soil deposit, and soil strength on the predicted slope response. Specifically, the magnitude of ground accelerations and nature of the dynamic stress distribution were investigated. The results of these analyses were then used to define the potential failure mode of steep slopes in cemented soils.

8.2 Results and Conclusions

The most important results and conclusions of this study are:

1. Field observations show that the failures of steep slopes greater than 60 degrees) in cemented soils are apparently initiated by tensile splitting in the upper parts of the slopes. The initial tensile failure is then followed either by toppling of the upper blocks or by shear failure of the lower part of the slope. Both types of failure are relatively shallow rarely involving more than 2 to 5 m of soil.

2. Of the three naturally cemented sands tested, two are very similar in strength and physical properties, while the third is very much stronger and denser. Qualitatively, all the sands behave basically as frictional materials with a cohesion or cementation intercept in the Mohr envelope and a small tensile strength. The stronger sand contains 20 percent fines to zero percent fines for the weaker soils, and the grains of the stronger sand show a high degree of interparticle penetration. It is postulated that the fines contribute to the cementation of the stronger sand while the interparticle penetration gives it a high friction angle (48 degrees). The natural and artificial cemented sands are brittle at low confining pressure, but their ductility increases substantially with confining pressure. Under cyclic loading in the compression regime (cyclic triaxial test) the strength of a cemented soil is about 16 percent higher than its equivalent static strength, and there does not appear to be any relationship between the number of cycles to failure and the stress at failure. On the other hand, in cyclic Brazilian tension tests and cyclic simple shear tests in which the minor principal stress is tensile, the strength of a cemented soil decreases with the number of loading cycles. Thus, the tensile cyclic loading seems to have a much more destructive effect on the strength of a cemented soil than the

compressive cyclic loading. This conclusion is very important to cemented soil slope behavior since the principal mode of failure in these slopes is believed to be in tension.

3. The amplification of input acceleration and the magnitude of dynamic stresses in the soil deposit is strongly influenced by the ratio of the fundamental period of the soil deposit to the dominant period of the earthquake. The closer this ratio is to 1 (resonance) the greater the amplification of the input motion and the greater the magnitude of the stresses.

4. Near a vertical slope the horizontal accelerations are only slightly amplified. However, significant vertical accelerations may occur which may account for some of the increased damage observed in the velocity of slopes.

5. For a given period ratio, the pattern of the dynamic stress distribution in a slope of linear elastic material is the same regardless of the earthquake magnitude. Thus, the dynamic stress distributions for a particular slope geometry can be nondimensionalized and the magnitude of the stresses scaled to any peak input acceleration.

6. A seismic event can generate significant levels of tension in steep slopes. Example analyses of dynamic slope response indicate that seismically induced failures in slopes of weakly cemented soil will most probably occur in tension. Also, a zone of tensile cracking at the top of the slope is possible. These results are in good agreement with field observations of slope failures in steep slopes of cemented soil.

7. It was demonstrated that the dynamic linear elastic analyses of vertical slopes yield consistent results that are qualitatively compatible with field observations of behavior of steep slopes.

REFERENCES

1. A. A. S. Alfi, "Experimental Study of a Strongly Cemented Sand," unpublished engineer's thesis, Department of Civil Engineering, Stanford University, Stanford, Calif., 1978.

2. N. N. Ambraseys, "The Seismic Stability of Earth Dams," Proc. of the Second World Conference on Earthquake Engineering, Vol. II, Japan, Jul 1960, pp. 1345-1363.

3. N. N. Ambraseys and S. K. Sarma, "The Response of Earth Dams to Strong Earthquakes," Geotechnique, No. 3, Vol. 17, Sep 1967, pp. 181-213.

4. I. Arango, Y. Moriwaki, and F. Brown, "In-Situ and Laboratory Shear Velocity and Modulus," Proc. of the ASCE Geotechnical Engineering Division Specialty Conference on Earthquake Engineering and Soil Dynamics, Pasadena, Calif., 1978, pp. 198-212.

5. I. Arango and H. B. Seed, "Seismic Stability and Deformation of Clay Slopes," J. of the Geotechnical Engineering Division, ASCE, Vol. 100, No. GT2, Feb 1974, pp. 139-156.

6. R. C. Bachus, "Cemented Sands from Pacifica and SLAC," unpublished internal report, Department of Civil Engineering, Stanford University, Stanford, Calif., 1978.

7. M. G. Bonilla, "Geologic Observations in the Epicentral Area of the San Francisco Earthquake of March 22, 1957," in Special Report 57, California Division of Mines, 1959, pp. 25-37.

8. D. M. Boore, "A Note on the Effect of Simple Topography on Seismic SH Wares," Bulletin of the Seismological Society of America, Vol. 62, No. 1, 1972.

9. C. K. Chan and J. P. Mulilis, "Pneumatic Sinusoidal Loading System," J. of the Geotechnical Division, No. GT 3, Mar 1976, pp. 277-282.

10. G. B. Cleveland, "Landsliding in Marine Terrace Terrain, California," Special Report 119, California Division of Mines and Geology, 1975.

11. U. Close and E. McCormick, "Where the Mountains Walked," National Geographic, V. 41, No. 5, pp. 445-472.

12. R. W. Clough and A. K. Chopra, "Earthquake Stress Analysis in Earth Dams," J. of the Engineering Mechanics Division, ASCE, Vol. 92, No. EM2, 1966, pp. 197-211.

13. Dames & Moore, Geotechnical Investigation, Proposed Positron-Electron Project, Stanford Linear Accelerator Center, Stanford, Calif., Lab. No. 0651-130, Jun 1977.

14. R. Dobry, I. Oweis, and A. Urzua, "Simplified Procedures for Estimating the Fundamental Period of a Soil Profile," Bulletin of the Seismological Society of America, Vol. 66, No. 4, Aug 1976, pp. 1293-1321.

15. J. M. Duncan and Y-Y. Chang, "Nonlinear Analysis of Stress and Strain in Soils," J. of the Soil Mechanics and Foundations Division, ASCE, Vol. 96, No. SM5, Sep 1970.

16. W. D. L. Finn, "Earthquake Stability of Cohesive Slopes," J. of the Soil Mechanics and Foundations Division, ASCE, Vol. 92, No. SM1, Jan 1966, pp. 1-11.

17. W. D. L. Finn, G. R. Martin, and M. K. W. Lee, "Comparison of Dynamic Analyses for Saturated Sands," Proc. of the ASCE Geotechnical Engineering Division Specialty Conference on Earthquake Engineering and Soil Dynamics, Pasadena, Calif., 1978, pp. 472-491.

18. W. D. L. Finn and R. I. S. Miller, "Dynamic Analysis of Plane Non-Linear Earth Structures," Proc. of the Fifth World Conference on Earthquake Engineering, Italy, 1974, pp. 360-369.

19. R. E. Goodman and H. B. Seed, "Earthquake-Induced Displacements in Sand Embankments," J. of the Soil Mechanics and Foundations Division, ASCE, Vol. 92, No. SM2, Mar 1966, pp. 125-146.

20. L. A. Hansen, Ph.D. thesis in preparation, Department of Civil Engineering, Stanford University, Stanford, Calif., 1979.

21. B. O. Hardin, "The Nature of Stress-Strain Behavior for Soils," Proc. of the ASCE Geotechnical Engineering Division Specialty Conference on Earthquake Engineering and Soil Dynamics, Pasadena, Calif., 1978, pp. 3-90.

22. E. L. Harp, R. C. Wilson, G. F. Wieczorek, and D. K. Keefer, "Landslides from the February 4, 1976 Guatemala Earthquake: Implications for Seismic Hazard Reduction in the Guatemala City Area," Proc. Second International Conference on Microzonation, San Francisco, Calif., 1978.

23. J. N. Hutchinson, "Field and Laboratory Studies of a Fall in Upper Chalk Cliffs at Loss Bay, Isle of Thanet,"in Stress Strain Behavior of Soils, Proc. of Roscoe Memorial Symposium, Cambridge, 1971.

24. I. M. Idriss, "Finite Element Analysis for the Seismic Response of Earth Banks," J. of the Soil Mechanics and Foundations Division, ASCE, Vol. 94, No. SM3, May 1968, pp. 617-636.

25. I. M. Idriss, R. Dobry, and R. D. Singh, "Nonlinear Behavior of Soft Clays during Cyclic Loading," J. of the Geotechnical Engineering Division, ASCE, Vol. 104, No. GT12, Dec 1978, pp. 1427-1447.

26. I. M. Idriss and H. B. Seed, "Response of Earth Banks during Earthquakes," J. of the Soil Mechanics and Foundations Division, ASCE, Vol. 93, No. SM3, May 1967, pp. 61-82.

27. I. M. Idriss, H. B. Seed, and N. Serff, "Seismic Response by Variable Damping Finite Elements," J. of the Geotechnical Engineering Division, ASCE, Vol. 100, No. GT1, Jan 1974, pp. 1-13.

28. L. S. Jacobsen, "Steady Forced Vibrations as Influenced by Damping," Transactions ASME, Vol. 51, 1930, p. 227.

29. J. C. Jaeger and N. G. W. Cook, Fundamentals of Rock Mechanics, 2nd Edition, Halsted Press, New York, 1976.

30. G. E. Korbin and T. L. Brekke, "A Model Study of Spilling Reinforcement in Underground Openings," Tech. Rep. MRD-2-75, Missouri River Division, Corps of Engineers, Omaha, Apr 1975; also in Interim Report, Department of Civil Engineering, University of Calif., Berkeley, Calif., Feb 1975.

31. W. D. Kovacs, H. B. Seed, and I. M. Idriss, "Studies of Seismic Response of Clay Banks," J. of the Soil Mechanics and Foundations Division, ASCE, Vol. 97, No. SM2, Feb 1971, pp. 441-455.

32. D. P. Krynine and W. R. Judd, Principles of Engineering Geology and Geotechnics, McGraw-Hill, New York, 1957.

33. A. C. Lawson and others, "California Earthquake of April 18, 1906," Report of the State Earthquake Investigation Commission, Carnegie Institution of Washington, Publication No. 87, 1908.

34. K. L. Lee and K. Chan, "Number of Equivalent Significant Cycles in Strong Motion Earthquakes," Proc. of the International Conference on Microzonation for Safer Construction Research and Application, Seattle, Wash., 1972.

35. R. J. Lutton, "Fractures and Failure Mechanics in Loess and Applications to Rock Mechanics," Research Report S-69-1, U. S. Army Engineer Waterways Experiment Station, Corps of Engineers, Vicksburg, Miss., 1969.

36. J. Lysmer, T. Udaka, C. F. Tsai, and H. B. Seed, "FLUSH a Computer Program for Approximate 3-D Analysis of Soil-Structure Interaction Proglems," EERC, Report No. EERC 75-30, University of Calif., Berkeley, Calif., Nov 1975.

37. F. I. Makdisi, H. B. Seed, and I. M. Idriss, "Analysis of Chabot Dam during the 1906 Earthquake," Proc. of the ASCE Geotechnical Engineering Division Specialty Conference on Earthquake Engineering and Soil Dynamics, Vol. II, Pasadena, Calif., Jun 1978, pp. 569-587.

38. F. I. Makdisi and H. B. Seed, "Simplified Procedure for Estimating Dam and Embankment Earthquake-Induced Deformations," J. of the Geotechnical Engineering Division, ASCE, Vol. 104, GT7, Jul 1978, pp. 849-867.

39. P. A. Maljian and J. L. Van Beneren, "Tied-Back Deep Excavations in Los Angeles Area," J. of the Construction Division, ASCE, Vol. 100, Sep 1974, pp. 337-356.

40. J. K. Mitchell, "The Properties of Cement-Stabilized Soils," paper prepared for Workshop on Materials and Methods for Low Cost Road, Rail, and Reclamation Work, Leura, Australia, 6-10 Sep 1976.

41. J. K. Mitchell, personal communication, 1977.

42. N. M. Newmark, "Effects of Earthquakes on Dams and Embankments," Fifth Rankine Lecture, Geotechnique, No. 2, Vol. 15, Jun 1965, pp. 139-160.

43. L. A. Salomone, H. Singh, and J. A. Fischer, "Cyclic Shear Strength of Variably Cemented Sands, in Earthquake Engineering and Soil Dynamics," Proc. of the ASCE Geotechnical Engineering Division Specialty Conference on Earthquake Engineering and Soil Dynamics, Vol. II, Pasadena, Calif., Jun 1978, pp. 819-835.

44. S. K. Saxena and R. M. Lastrico, "Static Properties of Lightly Cemented Sand," J. of the Geotechnical Division, ASCE, Vol. 104, No. GT12, Proc. Paper 14259, Dec 1978, pp. 1449-1464.

45. H. B. Seed, "A Method for Earthquake Resistant Design of Earth Dams," J. of the Soil Mechanics and Foundations Division, ASCE, Vol. 92, No. SM1, Jan 1966, pp. 13-41.

46. H. B. Seed and I. M. Idriss, "Influence of Soil Conditions on Ground Motions during Earthquakes," J. of the Soil Mechanics and Foundations Division, ASCE, Vol. 95, No. S1, Jan 1969, pp. 99-137.

47. H. B. Seed and I. M. Idriss, "Rock Motion Accelerograms for High Magnitude Earthquakes," EERC, University of Calif., Berkeley, Calif., Report No. EERC 69-7, Apr 1969.

48. H. B. Seed and G. R. Martin, "The Seismic Coefficient in Earth Dam Design," J. of the Soil Mechanics and Foundations Division, ASCE, Vol. 92, No. SM3, May 1966, pp. 25-57.

49. G. B. Sowers and G. F. Sowers, Introductory Soil Mechanics and Foundations, 3rd Edition, The MacMillan Company, New York, 1970.

50. R. Sullivan, "Geological Hazards along the Coast South of San Francisco," California Geology, California Division of Mines and Geology, Vol. 28, No. 2, Feb 1975.

51. R. C. Wilson, R. E. Warrick, and M. J. Bennett, "Seismic Velocities of San Francisco Bayshore Sediments," Proc. of the ASCE Geotechnical Engineering Division Specialty Conference on Earthquake Engineering and Soil Dynamics, Pasadena, Calif., 1978, pp. 1007-1023.

52. K. S. Wong and J. M. Duncan, "Hyperbolic Stress-Strain Parameters for Nonlinear Finite Element Analyses of Stresses and Movements in Soil Masses," Report No. TE-74-3, Department of Civil Engineering, University of Calif., Berkeley, Calif., Jul 1974.

53. S. G. Wright, "A Study of Slope Stability and the Undrained Shear Strength of Clay Shales," Ph.D. thesis, University of Calif., Berkeley, Calif., 1969.

54. S. G. Wright, F. H. Kulhavy, and J. M. Duncan, "Accuracy of Equilibrium Slope Stability Analysis," J. of the Soil Mechanics and Foundations Division, ASCE, Vol. 99, No. SM10, Oct 1973, pp. 783-791.

55. T. L. Youd and S. N. Hoose, "1978, Historic Ground Failures in Northern California Triggered by Earthquakes," U. S. Geological Survey Professional Paper 993, p. 177.

56. O. C. Zienkiewicz, The Finite Element Method in Engineering Science, Mc Graw-Hill Book Co., London, England, 1971.

APPENDIX A

Procedure for Preparation of Artificially Cemented Samples

Following procedure was used for preparation of samples containing 4 percent cement.

1. The mold was cleaned and its internal diameter was measured. Because the aluminum base cap made a bond with the mix during curing, it was coated with silicone lubricant before sample compaction. However, in the preparation of the simple shear samples, the base cap was intentionally cleaned to produce a good bond between the cap and the mix.

2. Enough sand for two samples was accurately weighed (1900 g).

3. Dry cement was accurately weighed (76 g for 4 percent mix).

4. The cement was added to the dry sand and thoroughly mixed in by hand. Mechanical mixing devices were found to keep the sand and cement separated.

5. Water (152 ml) was added and the material was thoroughly mixed by hand.

6. Immediately after mixing was completed, the mixture was compacted in the molds. The samples were compacted in five layers 27.7 mm high using a 35.6 mm tamper. The top of each layer was scarified to a depth of about 3 mm before the following layer was placed. The compaction of two samples usually took about 45 minutes.

7. The molds with the samples were carefully sealed in plastic bags and placed in a curing room as soon as possible after compaction.

8. The samples were carefully extruded from the molds after curing was complete and immediately prior to testing. The samples were also weighed and measured at that time. Moisture content determinations were made after testing.

APPENDIX B

Stress-Strain Curves Obtained from Static Triaxial Tests

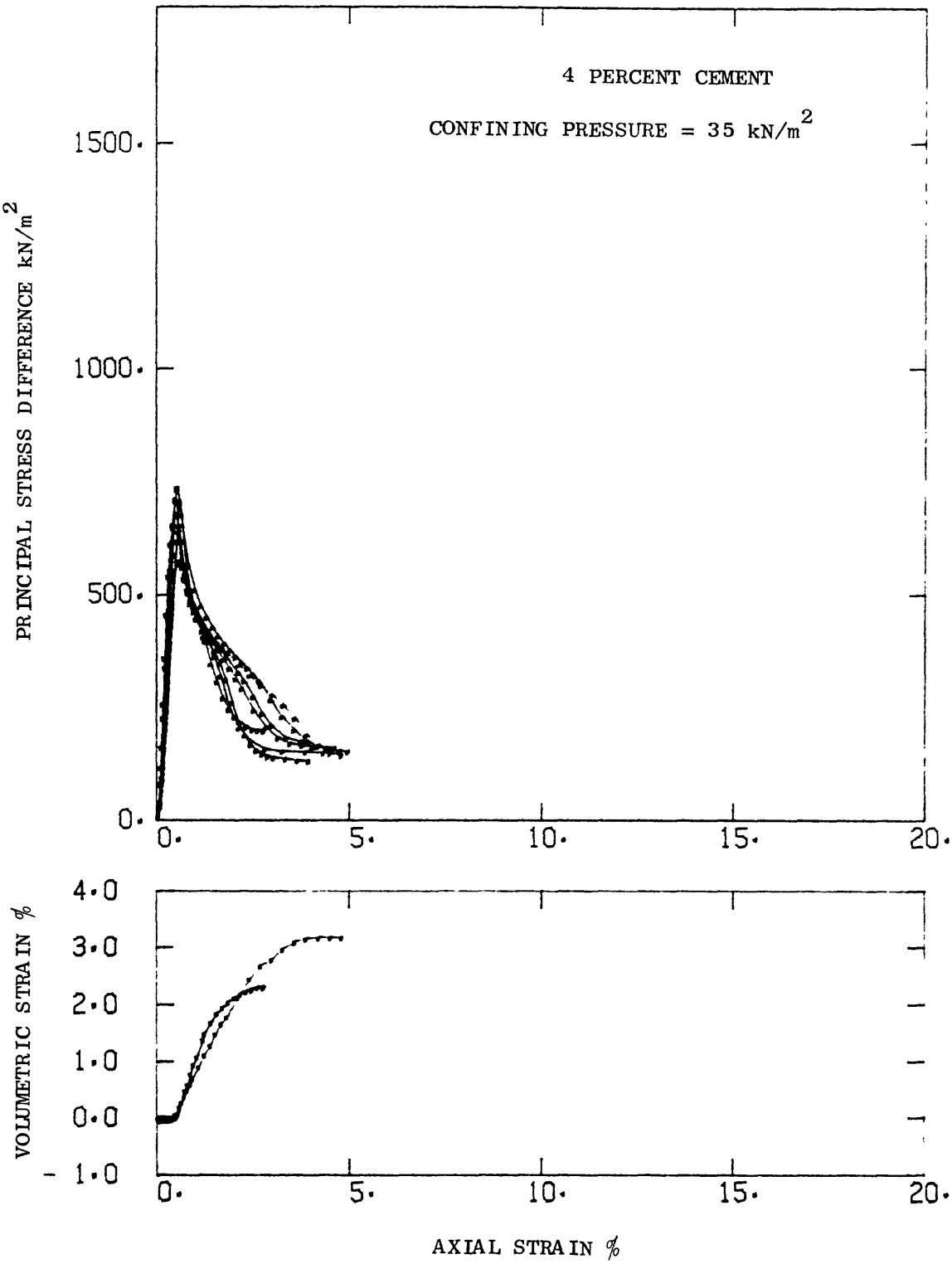

Figure B-1 TRIAXIAL STRESS-STRAIN CURVES FOR SAND CEMENTED WITH 4 PERCENT CEMENT; CONFINING PRESSURE = 35 kN/m^2.

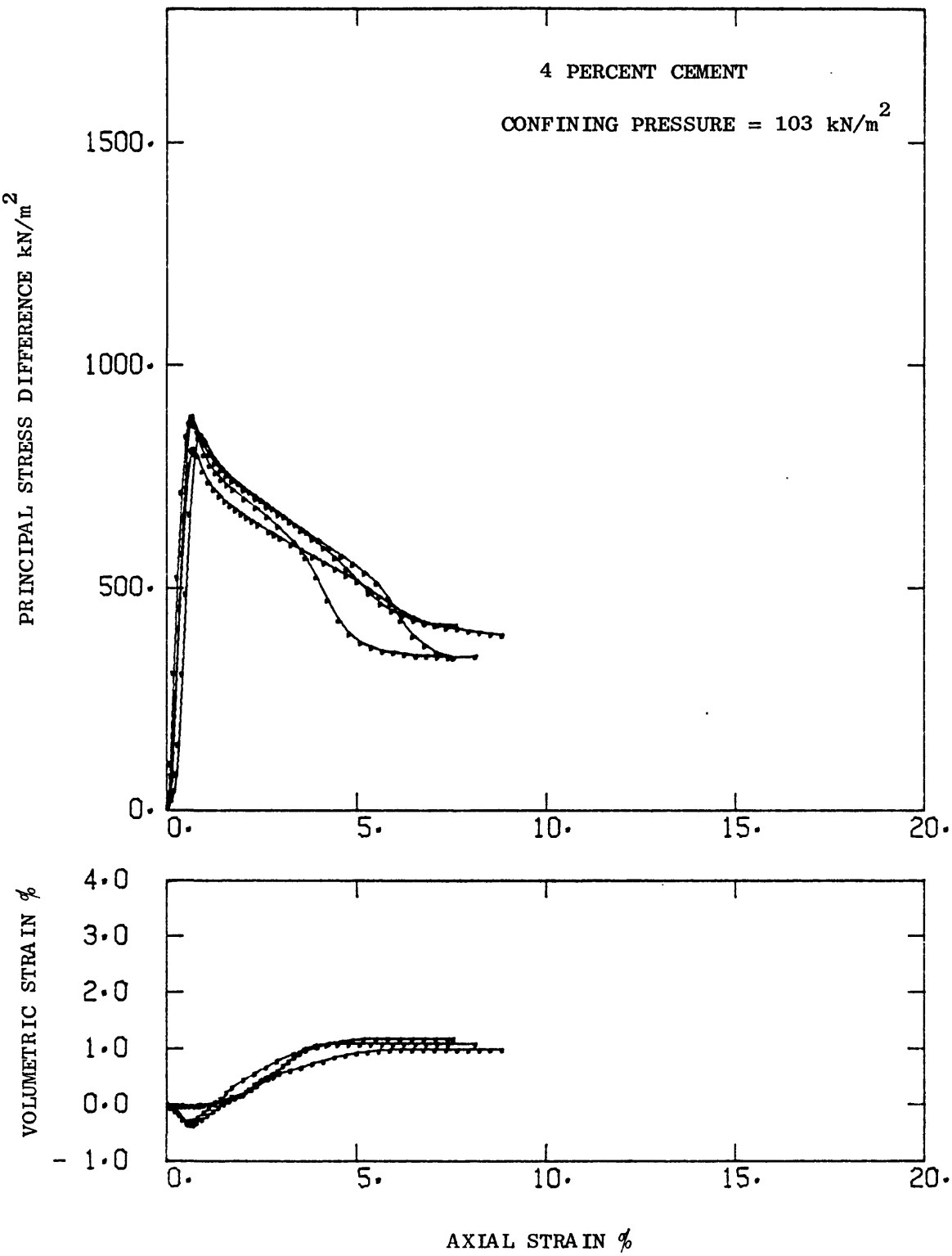

Figure B-2 TRIAXIAL STRESS-STRAIN CURVES FOR SAND CEMENTED WITH 4 PERCENT CEMENT; CONFINING PRESSURE = 103 kN/m^2.

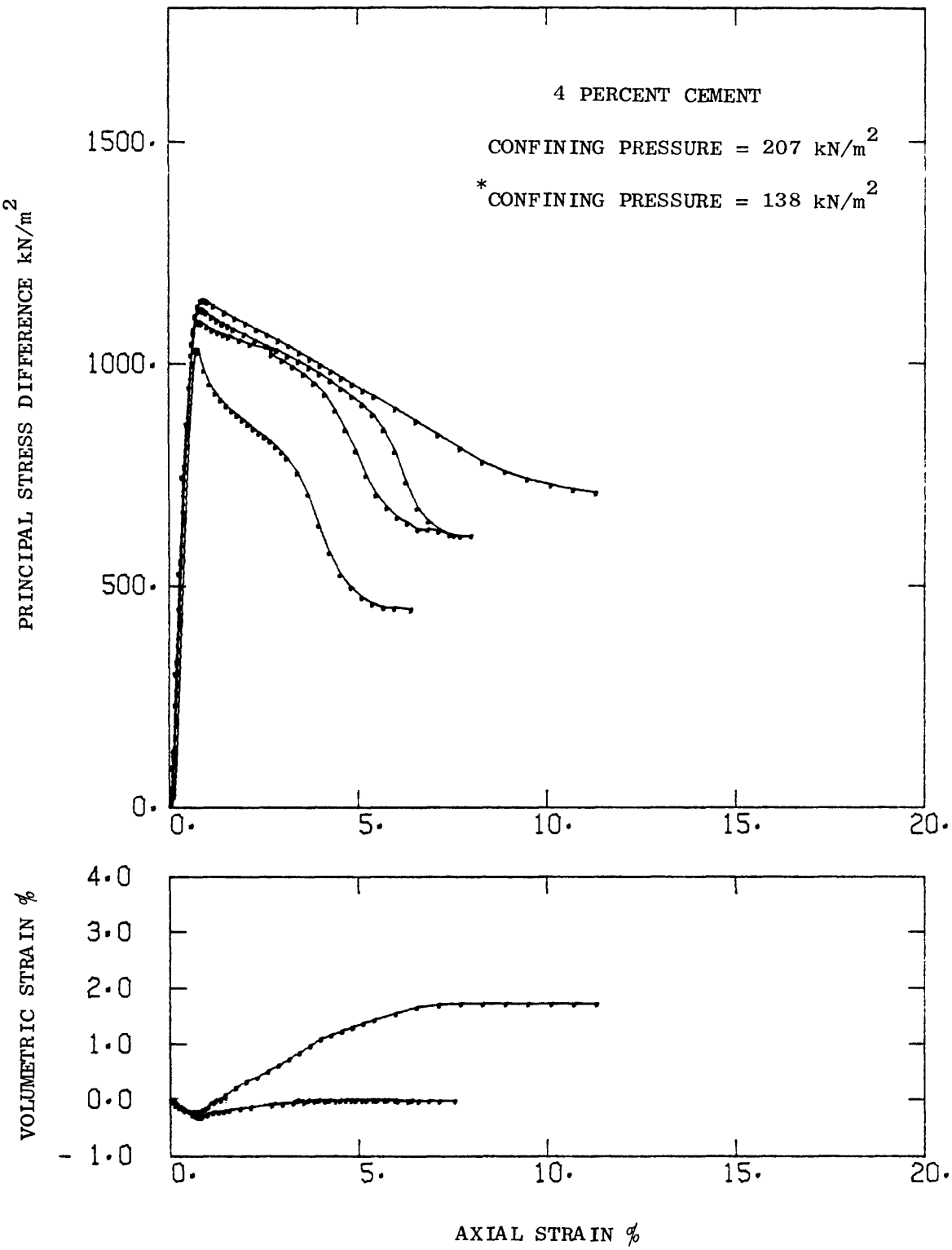

Figure B-3 TRIAXIAL STRESS-STRAIN CURVES FOR SAND CEMENTED WITH 4 PERCENT CEMENT; CONFINING PRESSURE = 138 AND 207 kN/m^2.

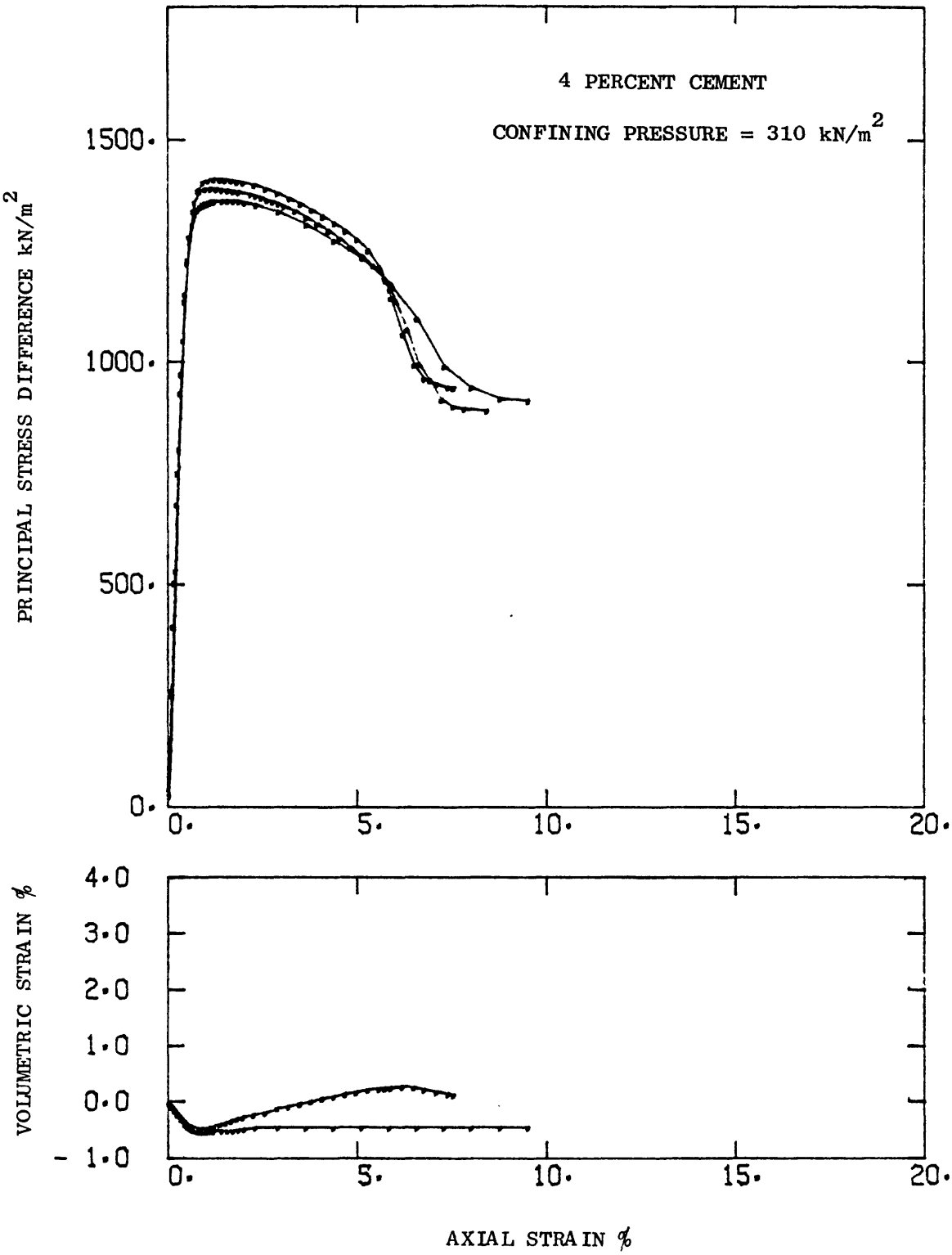

Figure B-4 TRIAXIAL STRESS-STRAIN CURVES FOR SAND CEMENTED WITH 4 PERCENT CEMENT; CONFINING PRESSURE = 310 kN/m^2.

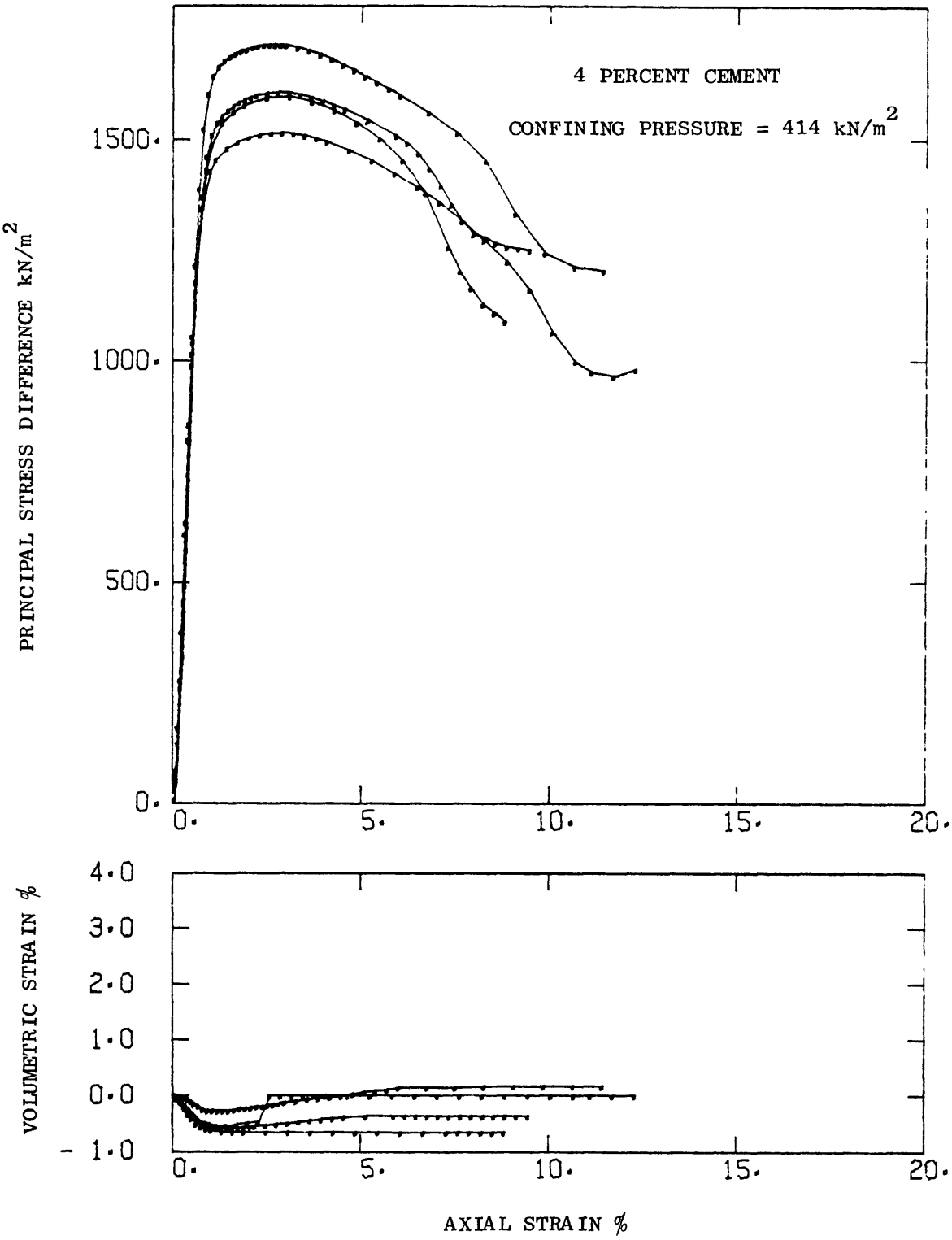

Figure B-5 TRIAXIAL STRESS-STRAIN CURVES FOR SAND CEMENTED WITH 4 PERCENT CEMENT; CONFINING PRESSURE = 414 kN/m^2.

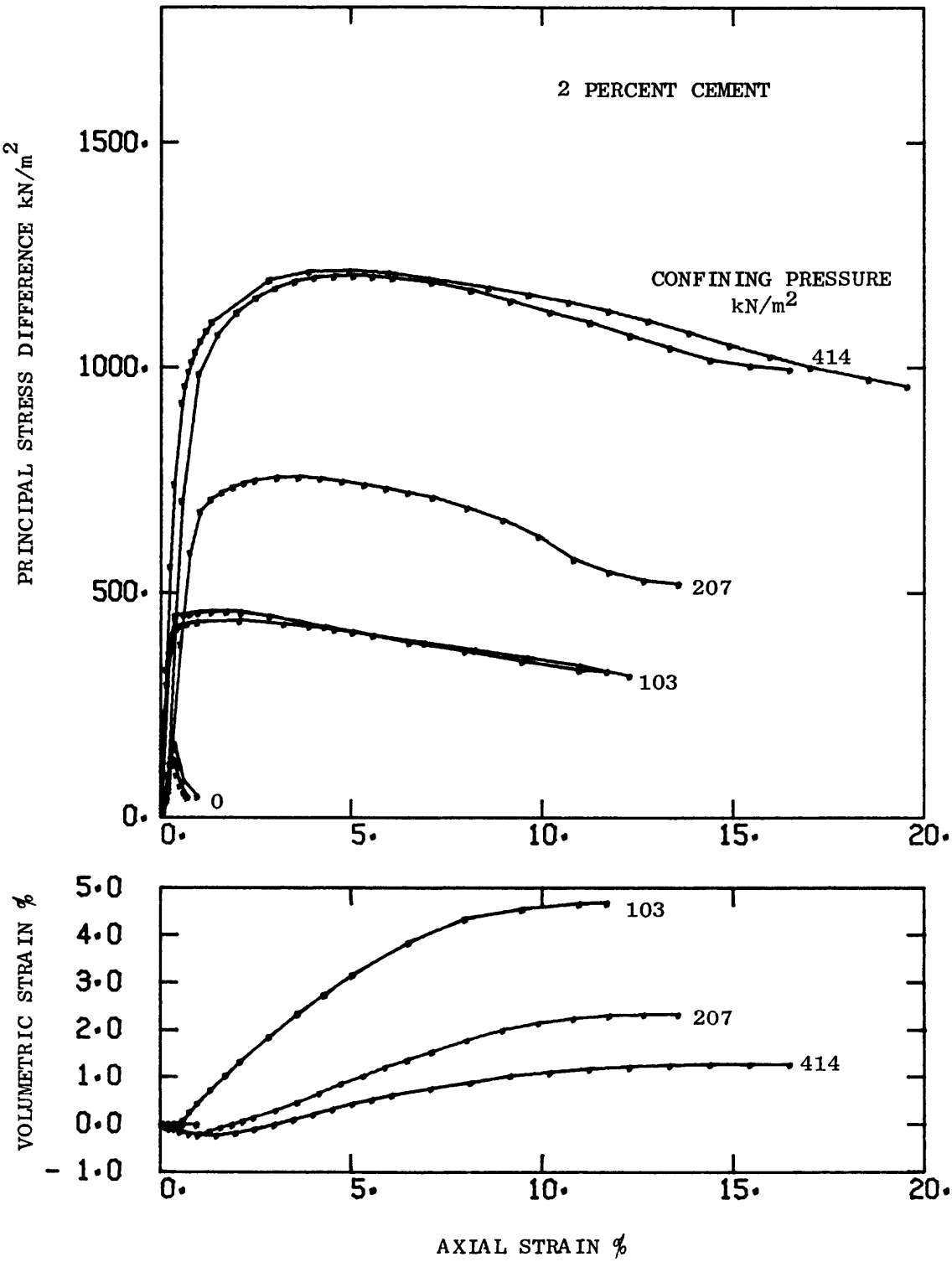

Figure B-6 TRIAXIAL STRESS-STRAIN CURVES FOR SAND CEMENTED WITH 2 PERCENT CEMENT.

APPENDIX C

Analysis of the Initial Stress Distribution in the Unconfined Simple Shear Test

As described in Chapter IV, cylindrical specimens of cemented sand approximately 70mm in diameter and 27.7mm high were used in the unconfined simple shear tests in this study. The ends of the specimens were firmly bonded to the end plattens and the sides were unrestrained. Because of the absence of the lateral restraint which is provided in a standard simple shear test by a steel reinforced membrane, there was a question about the stress distribution within the specimens after the initial axial load was applied. The finite element analysis described here was carried out in order to provide an understanding of the stress distribution in the specimens and to provide a basis for the interpretation of the test results.

The analysis was performed using a finite element program capable of axisymmetric analysis of symmetrically loaded structures which was developed by Hansen (1979). A finite element mesh consisting of 126 rectangular elements approximately 2mm wide and 4.5mm high was used to model the test sample. Boundary conditions were chosen to represent the actual test conditions as closely as possible. The bottom of the mesh representing the contact between the cemented sand and the capping compound was assumed to be rigid. At the top, the aluminum plate was modelled by the first row of elements. The nodes on the upper boundary were free to move in axial direction and fixed against radial movement. In this manner, it was possible to model the uniform axial displacement of the upper platten in response to applied axial loading. Both the aluminum and the cemented sand, were assumed to be linear elastic and

the cemented sand was given a modulus of 134,000 kN/m^2 and a Poisson's ratio of .3.

The results of the finite element analysis are presented in the form of the ratio of the radial stress to the axial stress, or k_o, in Figure C-1 and the ratio of the shear stress on the horizontal plane to the axial stress in Figure C-2. As expected, the contours of k_o plotted in Figure C-1 show that the initial radial stress distribution is non-uniform and that the radial stress increases towards the center of the sample. Obviously, the magnitude of the radial stress at the center of the specimen is a function of its thickness, radius, and the Poisson's ratio of the material. In this case, given the sample geometry and assuming a Poisson's ratio $\nu = .3$, the maximum k_o is about .28 - .3 at the center of the specimen.

The contours of the initial shear stress on the horizontal plane in Figure C-2 indicate that although the applied load is strictly axial, a shear stress is produced adjacent to the end plattens. This induced shear stress is at its maximum near the outer boundary of the specimen and decreases to zero at the center. Therefore, the purely compressive initial applied stress which is assumed in the interpretation of the test data in Chapter V occurs only at the center of the specimen.

The fact that the stress distribution within a simple shear specimen is nonuniform is well recognized, however, most of the researchers agree that the errors introduced by assuming that the state of stress at the center is representative of the whole specimen are minimal (Duncan and Dunlop, 1969; Prevost and Hoeg, 1976; Shen and others, 1978). A more

rigorous interpretation of the test data would be possible only after performing a true 3-D finite element analysis taking into account the nonlinear nature of the soil which is beyond the scope of the present study.

In conclusion, it is felt that the interpretation of the simple shear test data as presented in Chapter V is consistent with the results of the finite element analysis presented here.

References

J. M. Duncan and P. Dunlop, "Behavior of Soils in Simple Shear Tests," Proc. of the 7th International Conference in Soil Mechanics and Found. Eng., Mexico City, Vol. I, 1969, pp. 101-109.

J. H. Prevost and K. Hoeg, "Reanalysis of Simple Shear Soil Testing," Canadian Geotechnical Journal, Vol. 13, 1976.

C. K. Shen, L. R. Herrmann, and K. Sadigh, "Analysis of Cyclic Simple Shear Test Data," Proc. of the ASCE Geotechnical Engineering Division Specialty Conference on Earthquake Engineering and Soil Dynamics, Vol. II, Pasadena, California, June 1978, pp. 864-874.

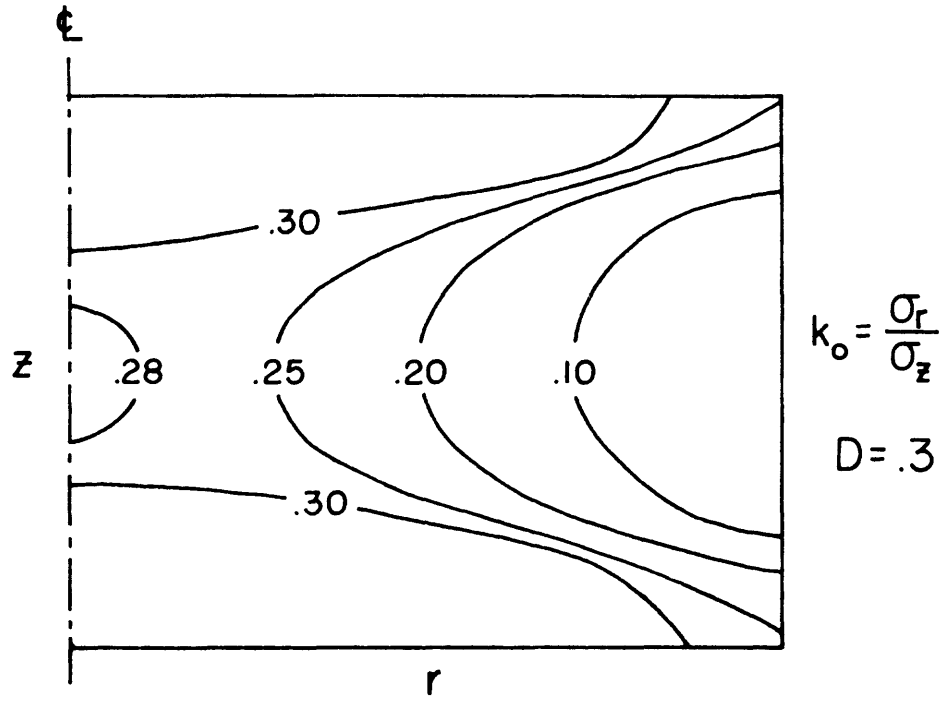

Figure C-1 DISTRIBUTION OF $K_o = \sigma_r/\sigma_z$ IN AN UNCONFINED SIMPLE SHEAR SPECIMEN AS A RESULT OF APPLIED AXIAL STRESS σ_z.

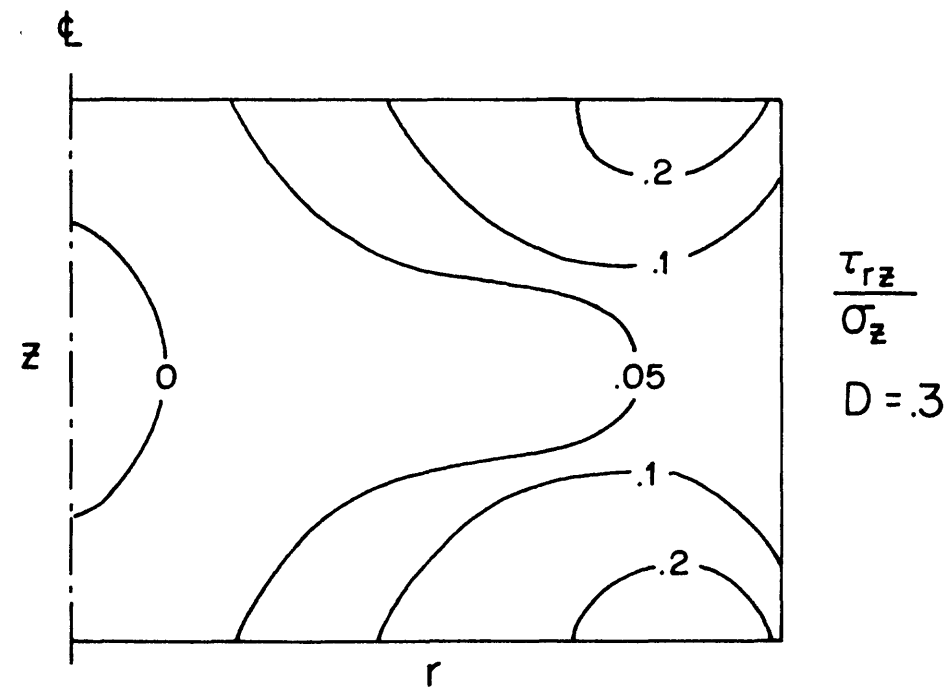

Figure C-2 DISTRIBUTION OF τ_{rz}/σ_z IN AN INDEPENDENT SIMPLE SHEAR SPECIMEN AS A RESULT OF APPLIED AXIAL STRESS σ_z.